

# A STUDY OF THE RADIO-FREQUENCY RADIATION FROM THE SUN

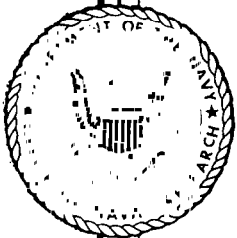
John P. Hagen

July 13, 1949

Approved by:

Dr. John M. Miller, Superintendent, Radio Division I

---



**NAVAL RESEARCH LABORATORY**

CAPTAIN F. R. FURTH, USN, DIRECTOR

**WASHINGTON, D.C.**

CONTENTS

Abstract . . . . . iv

Problem Status . . . . . vi

Authorization . . . . . vi

INTRODUCTION . . . . . 1

THERMAL RADIATION AND ITS MEASUREMENT AT RADIO WAVELENGTHS . . . 16

    Temperature of the Source and Power Density of the Receiver . 19

    Analysis of Receiver Operation. . . . . 20

    The Noise Factor . . . . . 22

    Noise Output of Receiver and Temperature of the Source . . . 25

DESCRIPTION OF THE APPARATUS . . . . . 29

    The Antenna and Mount . . . . . 30

    Method of Calibration of Antenna Pattern and Receiver  
Sensitivity . . . . . 32

    The Receiver . . . . . 33

THE THEORY OF THE RADIATION FROM THE QUIET SUN . . . . . 39

    Electron Concentration and Temperature in the Sun's  
Atmosphere . . . . . 40

    Intensity of Radiation and Coefficient of Absorption. . . . . 46

    The Equivalent Temperature. . . . . 48

    The Optical Depth . . . . . 50

    Refractive Index and Collision Frequency . . . . . 51

    The Absorption Coefficient . . . . . 57

    Variation in the Absorption Coefficient with Height  
and Wavelength . . . . . 58

    Comparison of Theoretical and Observed Equivalent  
Temperatures of the Sun . . . . . 59

THE OBSERVED DATA AT 8.5 MILLIMETERS WAVELENGTH . . . . . 75

    Variation in Emission Across the Surface of the Sun . . . . . 77

    An Example of the Relation of Radio Measurement to Solar  
Activity . . . . . 80

    Possibility of Detecting Other Extra-Terrestrial Objects . . . 89

THE OBSERVATIONS ON THE 20 MAY 1947 TOTAL ECLIPSE OF THE SUN . . 90

    Observed Eclipse Function . . . . . 96

    An Interpretation of the Observed Function . . . . . 98

CONCLUSION

    Penetration for Rays of Different Wavelengths . . . . . 113

    Use of the Results for Determining Conditions in the Sun's  
Atmosphere . . . . . 115

    Suggested Study of the Disturbed Sun . . . . . 118

ACKNOWLEDGMENTS . . . . . 120

REFERENCES . . . . . 121

## ABSTRACT

The monochromatic equivalent temperature of the quiet sun measured at radio wavelengths varies between the limits of 6700 degrees Kelvin at 8 millimeters to  $10^6$  degrees Kelvin at 200 centimeters wavelength. This is to be expected when the opacity of the sun's atmosphere at radio wavelengths is considered and when a proper temperature distribution for the corona and chromosphere is assigned.

The opacity of the solar atmosphere for the various radio wavelengths was computed, the coefficient of absorption being a function of the electron density, the wavelength, the temperature, and the refractive index of the gas according to the equation:

$$K = \frac{2\sqrt{2} \lambda^2 n_e^2 e^6}{3\sqrt{\pi} \mu c^3 (mkT)^{3/2}} \log_e \left( \frac{4kT}{e^2 \sqrt[3]{2n_e}} \right)^2$$

where  $K$  is the absorption coefficient,  $\lambda$  the wavelength,  $n_e$  the electron density,  $e$  the charge on the electron,  $c$  the velocity of light,  $\mu$  the refractive index,  $m$  the mass of electron,  $k$  Boltzmann's constant, and  $T$  the temperature in degrees Kelvin. Following Martyn, the analysis of Lorentz, and Chapman and Cowling was employed. The electron density distribution in the corona proposed by Baumbach and modified by Allen and Van de Hulst was used. In the chromosphere the electron density distribution is that proposed by Wildt. The temperature distribution used in the corona was that of Alfven. The equivalent

## ABSTRACT (Cont.)

temperature for any ray is shown to be

$$T_e = \sum_{r=1}^n (1 - e^{-K_r \Delta h_r}) T_r e^{-\sum_{s=r+1}^n K_s \Delta h_s} .$$

For the purposes of the computation, the atmosphere is divided into layers where  $K_r$ ,  $\Delta h_r$ , and  $T_r$  are the absorption coefficient, the thickness, and the temperature of the  $r^{\text{th}}$  layer. Equivalent temperatures were computed in this manner for rays emerging at various positions from the center of the limb.

In order to obtain a fit with the experimental data on the equivalent temperature of the sun as a function of wavelength, it is necessary to assign a new temperature distribution for the lower part of the sun's atmosphere. A good fit with the experimental data is obtained if the temperature is assumed to rise slowly from the boundary temperature of 4830 degrees Kelvin at the photosphere to 10,000 degrees at a height of 10,000 kilometers, and then to rise exponentially to a maximum temperature of  $10^8$  degrees at a height of 25,000 kilometers. This set of conditions in the solar atmosphere adequately explains the behavior of the quiet sun at short radio wavelengths.

The observations at a wavelength of 3.2 centimeters of a total solar eclipse are described. At this wavelength there was a residual radiation of 4 percent at the time of totality. One-fourth of the 4 percent was due to thermal radiation from the moon and the remainder was due to thermal radiation from the corona.

**PROBLEM STATUS**

**This is an interim report; work on the problem is continuing.**

**AUTHORIZATION**

**NRL Problem R11-09R  
(NR 535-009)**

## A STUDY OF THE RADIO-FREQUENCY RADIATION FROM THE SUN

### INTRODUCTION

To detect the radio signals coming to the earth from extraterrestrial sources, a directive antenna and highly sensitive radio receiver must be used. The improvements in the directivity of radio antennas and in the sensitivity of receivers have been two of the projects on which radio engineers have been engaged since the beginning of radio, but it is only in recent years that these improvements have been carried to the point where the comparatively weak radio-frequency radiation from extra-terrestrial sources can be quantitatively measured. The discovery of a radio-frequency radiation which could be attributed to our galaxy as a source was made in 1932 and was followed by many investigations.<sup>\*1,2,3</sup> Later when further improvements were made in the operation of receivers, solar emission was detected, and it in turn is being intensively investigated.<sup>4,5,6</sup> The improvement in the efficiency and the directivity of antennas has been achieved through a process of learning how to put together and how to phase properly large arrays of dipole antennas at the longer wavelengths, and how to properly illuminate parabolic reflectors at the shorter wavelengths.

The gain and directivity of an antenna are related to the physical size of the antenna in much the same fashion as the resolving power of a telescope is determined by its aperture. The same considerations hold for the tolerances on the surface of the antenna as hold in the design of the lens or the reflector of a telescope. In the radio case, rather than to use resolving power, it is more customary to refer to the beamwidth between half-power points. This is determined by the equation

$$B.W. = \frac{1.2\lambda}{D} \quad (1)$$

---

\*References will appear at the end of this report.

where B.W.=the beamwidth in radians  
 $\lambda$ =the wavelength  
 D=the diameter of the aperture

the two latter being expressed in the same units.

The gain of the antenna determines the increase in the intensity\*\* of the received signal over that which would be received were an isotropic radiator used as an antenna. Under these conditions, the gain is determined by the equation

$$G = 0.65 \left( \frac{\pi D}{\lambda} \right)^2 = 8.17 \frac{A}{\lambda^2} \quad (2)$$

where A and  $\lambda$  are in the same units. Similarly,

$$G = 8.17A$$

if A is expressed in square wavelengths. The beamwidth is seen to increase linearly with wavelength and inversely with diameter, whereas the gain increases linearly with the area and inversely with the square of the wavelength. The radiation pattern and the gain of the antenna are susceptible to accurate measurement, and since, as will be shown later, they enter directly into the reduction of the data, it is essential that these measurements be made with great care. In interpreting the results of various observers, it is well to bear in mind the dimensions involved. An antenna ten feet in diameter would have a beamwidth varying between  $0.2^\circ$  at 8.5 millimeters and approximately  $35^\circ$  at 1.5 meters. The beamwidth of a fifty-foot diameter antenna on the other hand would vary between  $0.04^\circ$  at 8.5 millimeters and  $7^\circ$  at 1.5 meters. These relations are shown in Figure 1.

The antennas used in this work have been mounted in various fashions, depending upon the resources of the observer, the geometry of the antenna, and the purpose for which the work is done. In some cases the antennas are mounted in a stationary position and the objects in the sky are allowed to drift through the field. In other cases, a simple alt-azimuth mount has been used, and the pointing has been done in both coordinates. The more practical mounts have, of course, been equatorial. Figure 2 shows a ten-foot diameter parabola mounted on an alt-azimuth mount, where the training in azimuth and elevation is done by hand.

---

\*\* Throughout this report "intensity" means "power intensity."

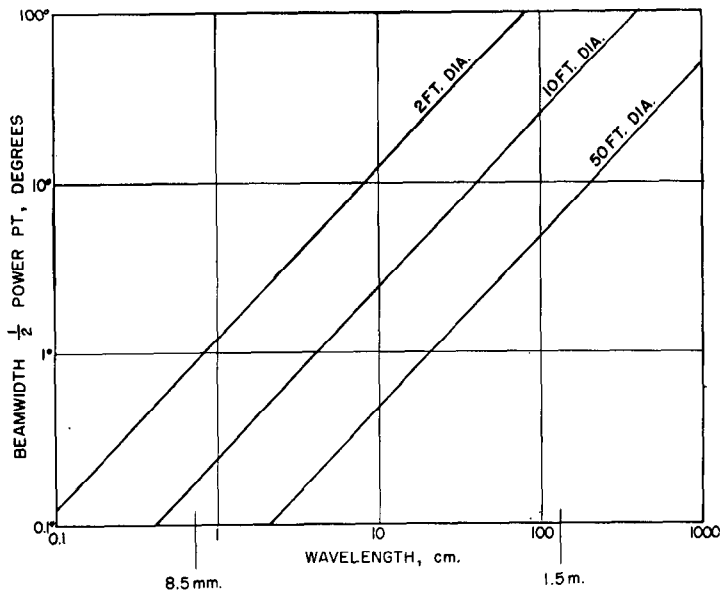


*Figure 1 - Beamwidth between half-power points as a function of wavelength for antennas of various diameters*

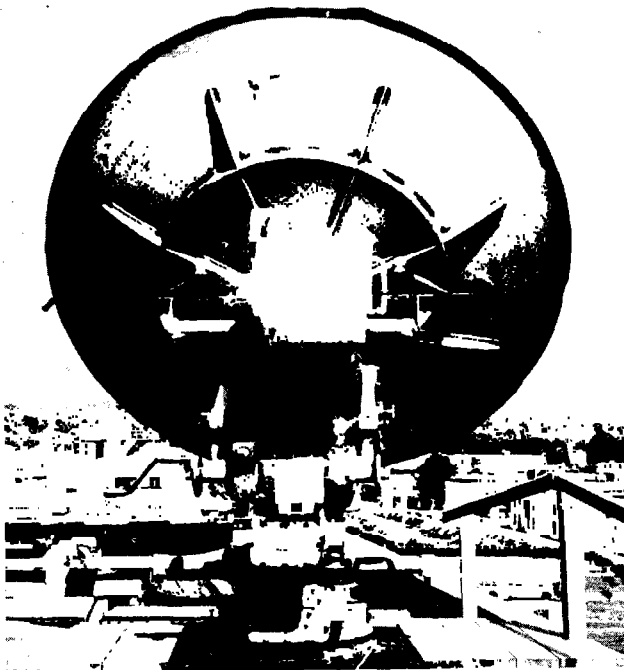


*Figure 2 - Three-centimeter radiometer—rear view showing the mount and box containing the radiometer*

Figure 3 shows a similar parabola mounted on an equatorial mount driven by clockwork in much the same fashion as a telescope. The radiation falling on the parabolic antenna is brought to focus by the parabola, and at the focal point there is a much smaller and therefore

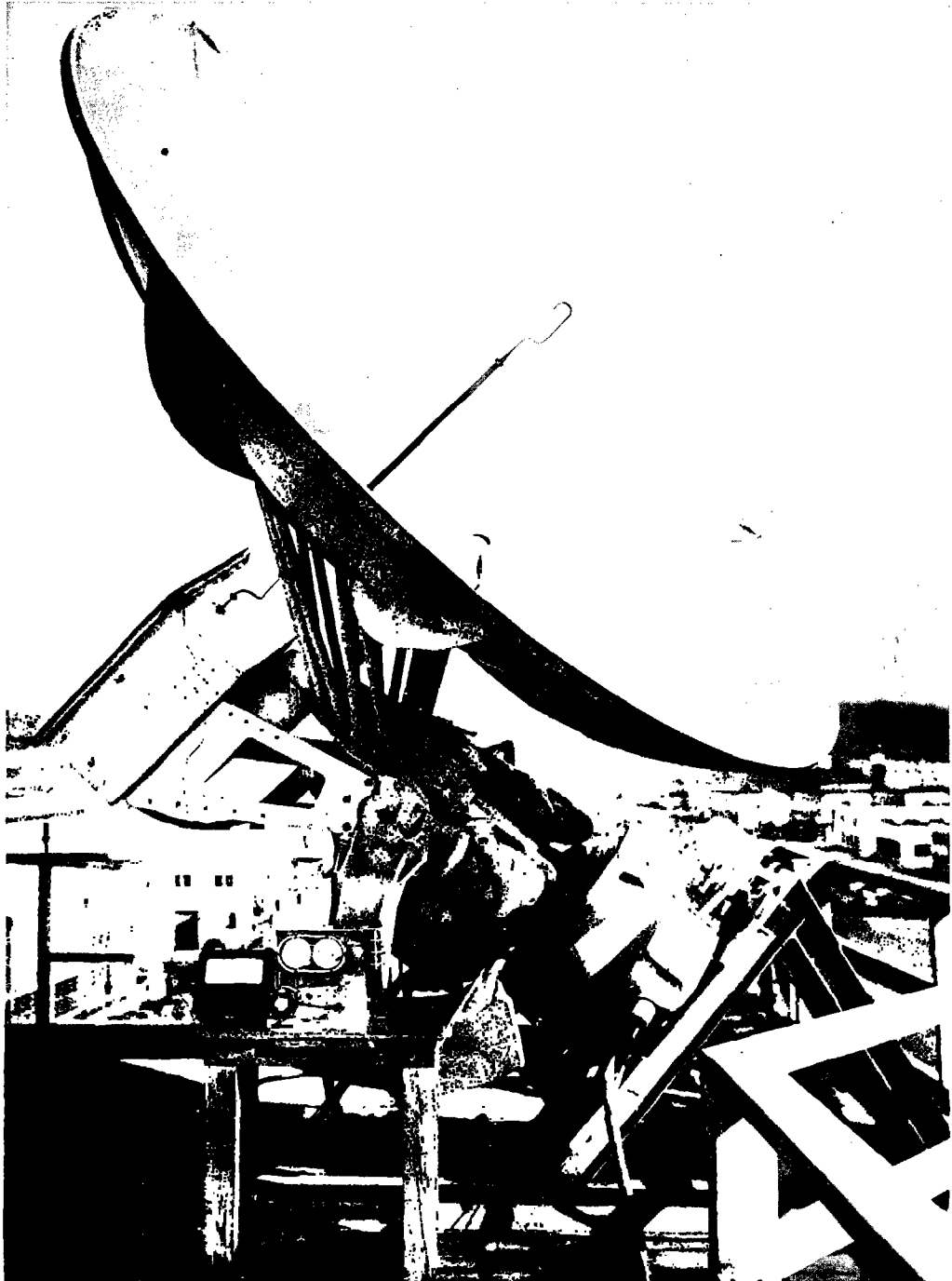


*Figure 3 - Ten-foot diameter parabolic antenna with 8.5-millimeter feed horn*

less directive antenna connected to a transmission line or waveguide, which usually is carried back of the reflector and is there connected to the receiver. When a multi-element array of dipoles is used, the dipoles are arranged in a regular pattern and so phased by separately adjusting their spatial and electrical separation that the voltage appearing at the terminals of the entire antenna due to the effect of any one dipole is in phase with the voltage due to any other dipole when a plane wave is normally incident on the array.

If the antenna could be placed inside a large absorptive enclosure, or black body, at a uniform temperature  $T^{\circ}$  Kelvin, it would be in equilibrium with the thermal or black body radiation at this temperature. It will be shown that at the terminals of the antenna there would appear a voltage equivalent to the thermal agitation noise generated in a resistance equal to the radiation resistance of the antenna at a temperature  $T^{\circ}$  Kelvin.

$$p = kT\Delta f \quad (3)$$

where  $p$  is the available power at the input to the receiver,  $k$  is Boltzmann's constant,  $T$  is the temperature of the enclosure in degrees Kelvin, and  $\Delta f$  is the bandwidth of the receiver.<sup>7</sup> Therefore even if a receiver could be produced which had no internal sources of noise whatever, noise would still be introduced into the system from the antenna. If the receiver does introduce additional noise, then the noise signal entering by way of the antenna must be a significant fraction of the set noise to be measurable, since the character of the two is the same. These concepts may be made quantitative by use of the quantity called noise figure or noise factor of the receiver. The noise figure of a receiver may be defined as the ratio of the noise-to-signal ratio at the output terminals to the noise-to-signal ratio at the input terminals. That is:

$$F = \frac{\frac{N}{S}}{\frac{n}{s}} \quad (4)$$

where

$F$  = noise figure  
 $N$  = noise level at output  
 $S$  = signal level at output  
 $n$  = noise at input  
 $s$  = signal at input.

The better receivers have lower noise figures. It will be shown that if all parts of the receiver are at room temperature  $T_0$ ° Kelvin, then the output power  $N$  is:

$$N = k T_0 \Delta f F G \quad (5)$$

where

$k$  = Boltzmann's constant  
 $T_0$  = room temperature  
 $\Delta f$  = bandwidth  
 $G$  = gain of receiver.

This equation effectively defines  $F$ .

When the antenna is pointed at a source of radiation whose angular diameter is small compared with the beamwidth of the antenna pattern the equivalent temperature at the input terminals of the receiver will be shown to be

$$t_s = \frac{G}{4} T_s \left( \frac{r}{R} \right)^2, \quad (6)$$

where

$t_s$  = equivalent temperature at input to receiver  
 $T_s$  = temperature of source  
 $r$  = diameter of source  
 $R$  = distance of source  
 $G$  = gain of the antenna over an isotropic radiator.

If the antenna beamwidth is smaller than the source, then the equivalent temperature at the input terminals of the receiver is that of the source.

$$t_s = T_s \quad (7)$$

Intermediate cases are dealt with later in this report.

In December, 1932, Karl G. Jansky reported<sup>1</sup> that, in the course of some studies on radio interference at a wavelength of 14.6 meters, he had observed a type of interference which varied in a quite uniform

manner with respect to time. His observations were made with a rotatable directional antenna so that the azimuth of the source of interference could be determined with some accuracy. The radiation pattern of the antenna is shown in Figure 4. Observations of the time of coincidence of the direction of the signal arrival with the observer's meridian when plotted with time of day as abscissa and day of the year as ordinate fell on a straight line, as is seen in Figure 5.

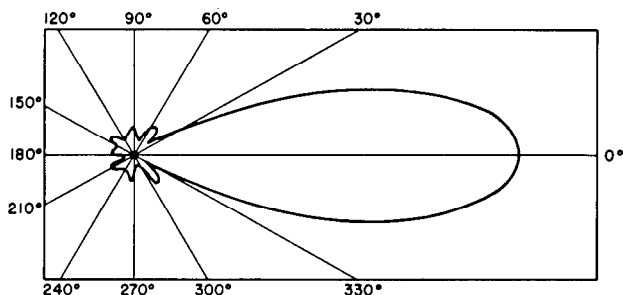


Figure 4 - Directional characteristic of antenna array at 14.6 meters as used by Jansky

Jansky noted that this could be explained if the source of interference were fixed in a position on the celestial sphere with a right ascension of eighteen hours. He was able also to assign a declination of approximately  $-10^{\circ}$  to the source. His measurement of declination was not nearly so accurate as right ascension.

The work of Jansky was followed by Reber,<sup>8,9</sup> who repeated the observations using a more highly directive antenna and a shorter wavelength. Reber's wavelength was 187 centimeters. His antenna was a thirty-one foot diameter parabolic reflector so mounted that its motion corresponded to that of a meridian circle, making it possible to determine the elevation of the signal as the source crossed the meridian. Reber's data were taken in sufficient detail to enable him to construct constant intensity contour charts showing the distribution of the source of noise on the celestial sphere. This is shown in Figure 6. From Figure 6 it is clear that the direction of arrival of the noise coincides with the plane of the galaxy. Williamson et al<sup>10</sup> have analyzed the available data to show that the coordinates of the galactic pole determined by this method are, in equatorial coordinates: Right Ascension  $12^h, 37^m.7$ , Declination  $28^{\circ}.1$ . These figures are the average for the data taken at 84 and 188 centimeter wavelength. Both Reber and Jansky looked for but did not find radiation from the sun. In

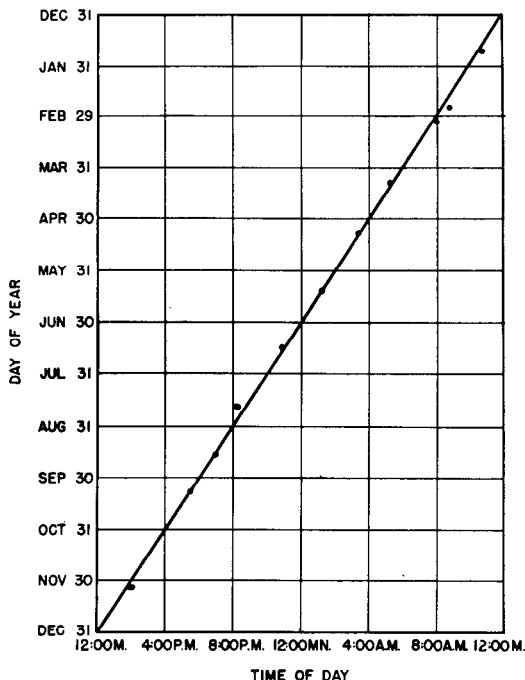


Figure 5 - Time of passage of position of maximum intensity of galactic noise across meridian

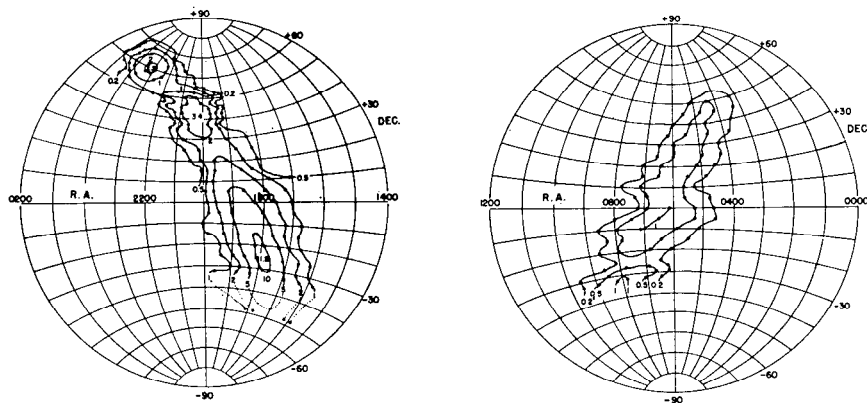


Figure 6 - Constant intensity contours in Right Ascension and declination for galactic noise at 187 centimeters

1945 Southworth<sup>4</sup> reported observations he and his associates had made on the microwave radiation from the sun at three wavelengths in the region between 1 and 10 centimeters. The wavelengths were approximately 1 centimeter, 3 centimeters, and 10 centimeters. Southworth showed that the intensity of the signal received from the sun was such that it could be attributed to black body radiation. A discussion of the correspondence between the observed temperature and the photospheric temperature will be left until some of the later and more refined experiments are taken up. It should be mentioned that about this time Reber also reported detecting a signal from the sun.

All of the early observers noted that the signal received either from the galaxy or the sun sounded in headphones and appeared on an oscilloscope no different from the random noise inherent in the operation of the receiver, so they referred to the signal as galactic or solar noise. Johnson<sup>11</sup> and Nyquist,<sup>12</sup> in studying the thermal agitation of electrical charge in conductors, arrived at the conclusion that a conductor radiates an amount of energy which is proportional to its temperature and the bandwidth of the device measuring the signal. In 1941 Burgess<sup>7</sup> pointed out that the expression for the so-called Johnson noise was the one-dimensional equivalent of the Rayleigh-Jeans formula for radiation from a hot body. The Rayleigh-Jeans expression is in turn an approximation of Planck's radiation law, the approximation being good only when the product  $\lambda T$  is large compared to  $\frac{ch}{k}$  where  $c$  = the velocity of light,  $h$  = Planck's constant, and  $k$  = Boltzmann's constant. The characteristics of the signal, even though it appears as noise in a receiver, are no different from those of the radiation of a hot body in any part of the spectrum, and it is perhaps unfortunate to call the signal by the names "galactic noise" or "solar noise."

Since 1945 there has been much activity in the measurement and interpretation of both solar and galactic radiation. The results of

the measurements to date of solar radiation over the wavelength range 8 millimeters to 375 meters are shown in Figure 7 and Table 1. Over this wavelength range the equivalent temperature of the quiet sun is seen to vary from 7000 degrees Kelvin at the short wavelengths to  $10^6$  degrees Kelvin at the longer wavelengths.

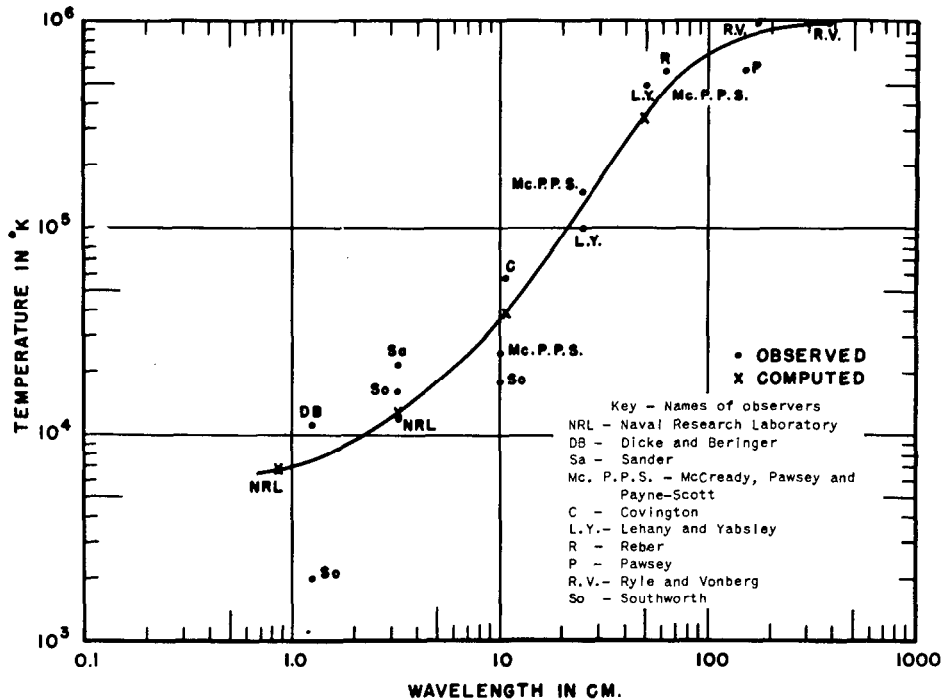


Figure 7 - Variation in the equivalent temperature of the sun with wavelength

In considering these data it should be borne in mind that the accuracy with which the equivalent temperature of the sun can be assigned is, in nearly all cases, quite low. In order to locate this curve properly, most of these measurements will need to be repeated using recent improvements in the techniques of measurement and calibration. A discussion of the methods of measurement and of calibration will be given later.

In Figure 8, the data of Figure 7 are shown with a graph of the computed intensity of the sun as a black body at  $6000^{\circ}$  Kelvin. The radiation from the sun as observed is not constant in amplitude but varies in an irregular and unpredictable fashion. One of the purposes of this work is to correlate these variations with observed variations in solar activity and with meteorological and ionospheric variations. At the shortest wavelength the radiation is most constant. The intensity of the signal varies from day to day as the index of

TABLE 1  
Observed Equivalent Temperature of the Quiet  
Sun at Various Radio Wavelengths

Observer	Wavelength in cm	Effective Temperature in Degrees K
Hagen	0.85	6,740
Southworth	1.25	2,000
Dicke and Beringer	1.25	11,000
Naval Research Laboratory	3.15	12,000
Southworth	3.2	16,000
Sander	3.2	22,000
McCready, Pawsey and Payne-Scott	10	25,000
Southworth	10	18,000
Covington	10.6	58,000
Lehany and Yabsley	25	100,000
McCready, Pawsey and Payne-Scott	25	150,000
Lehany and Yabsley	50	500,000
McCready, Pawsey and Payne-Scott	50	500,000
Reber	62.5	590,000
Pawsey	150	600,000
Ryle and Vonberg	172	ca. $10^6$
Ryle and Vonberg	375	ca. $10^6$

solar activity varies. The correlation between the intensity of the signal and solar activity is poor at the shortest wavelengths and improves to a maximum in the middle (about 10 cm) wavelength range. As the wavelength of observation increases the variations in the received signal become more erratic and more abrupt. Even at the longer wavelengths, though, the intensity decreases at times to some low level below which it never appears to go. This low level of intensity is characterized by a smooth, steady signal and is accompanied by a low state of activity on the sun. It is the equivalent temperature associated with this quiet state which was used in preparing Figure 7 and Table 1.

Superimposed upon this steady state are three types of variation. The first is not distinguishable from the steady state by any characteristic other than amplitude. It is the day-to-day variation which is common to all wavelengths and which is in some way associated with the increase in the solar activity. The second type of variation occurring at times of increased solar activity is that of short bursts of intensity whose duration does not exceed 30 seconds and might be as

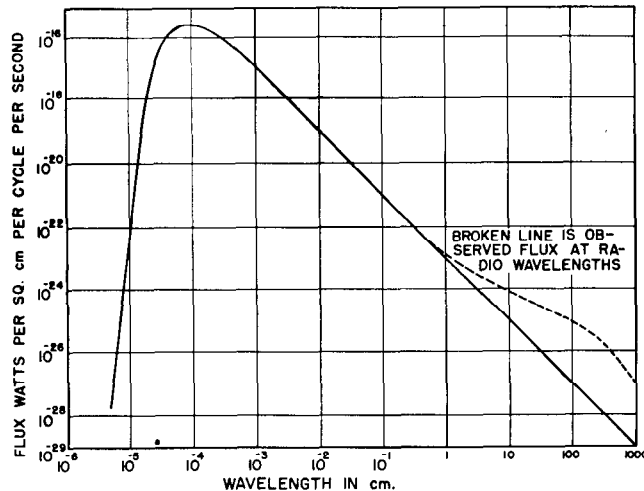


Figure 8 - The total monochromatic flux of radiation from the sun as a black body at  $6000^{\circ} K$  received at the distance of the earth, with the measured radio flux shown dotted

short as 2 or 3 seconds. These bursts, so-called, occur at random and may be more or less frequent depending upon the circumstances. The intensity of the bursts decreases as the wavelength of observation decreases, so that in the centimeter region they are not observed at all. The third and most spectacular type of variation is one in which the intensity suddenly increases to many times its quiet level, then falls exponentially, returning to the quiet level in from twenty minutes to two hours. This type of variation is referred to as an outburst and occurs at all wavelengths, although the intensity is again lower at the shorter wavelengths.<sup>16</sup> The occurrence of an outburst seems always to be coincident with the appearance of a solar flare and with a consequent sudden ionospheric disturbance on the earth. When the same outburst has been observed at various wavelengths under circumstances where the relative times of occurrence could be measured it was observed that the outburst was seen first at the shorter wavelengths and later at the longer. Since, as will be shown later, the shorter wavelength radiation originates in deeper layers of the sun's atmosphere than the longer. The outburst is caused by a disturbance in the flare which moves outward from the surface of the sun.

The radiation from the sun in the radio-frequency spectrum is frequently circularly polarized.<sup>13</sup> At longer wavelengths the degree of polarization may at times be as high as 90%. At the shorter wavelengths the degree of polarization is much less, being on the order of 3% at 10 centimeters<sup>14</sup> and of negligible magnitude at 3 centimeters.<sup>15</sup>

REPRODUCTION

In general, the beamwidths of the antennas used to look at the sun have all been larger in diameter than the sun itself. The two exceptions are, first, the interference-type used by Ryle and Vonberg,<sup>17</sup> where a two-antenna system which operates as a Michelson type interferometer was used to produce a pattern made up of several fringes within the main antenna pattern, the angular width of the fringe being determined by the linear separation of the two antennas. A similar experiment was performed by Pawsey and his co-workers.<sup>18</sup> Instead of using two antennas a single antenna was mounted on a cliff overlooking the sea, where the signal from the antenna interfered with the signal from its image. This, of course, is similar to the well known Lloyd's mirror experiment. The interference pattern of Ryle and Vonberg is shown in Figure 9. Here the two antennas were separated by about ten

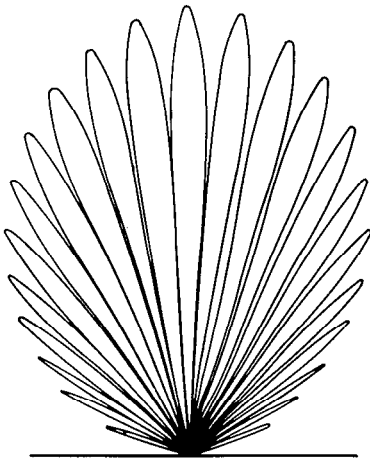


*Figure 9 - Interference pattern in the plane which includes the line joining the two antennas and the axis of the beams produced by two aerials separated by 10 wavelengths*

wavelengths and situated on a line running east and west. They thereby obtained an interference pattern having minima separated by about  $6^\circ$ . In order to resolve detail on the surface of the sun, separations greater than this were required, and the authors made observations with spacings of 25, 90, and 140 wavelengths. The wider separations result, of course, in a larger number of narrower fringes. Using the separation of 140 wavelengths, they concluded that the source of intense radiation occurring at a time of high solar activity subtended an angle in the east-west plane not greater than 10 minutes of arc. This measurement indicated that at a wavelength of 170 centimeters the equivalent temperature of the source was at least  $2 \times 10^9$  degrees Kelvin. The Australian group, using the Lloyd's mirror technique, arrived at a value of 6.5 minutes of arc as the diameter of a disturbed area at 150 centimeters. The second example of high resolution is the ten-foot diameter parabola used at 8 millimeter wavelength in the investigation which is the subject of this report. Here the beamwidth between half-power points is 0.2 degrees, so that some resolution is obtained in crossing the sun's disc. It has been

possible to draw contour curves of the intensity of the radiation from the sun and with the resolution available under favorable circumstances to follow the activity of a spot across the surface of the sun.

The most powerful tool in analyzing the distribution of the emission from the surface of the sun that has appeared to date has been the analysis of the variation of the sun's emission in the course of a total eclipse. The eclipse of May 20, 1947, described later in this report was observed at 3-centimeter wavelength.<sup>18</sup> At the same eclipse a Russian group<sup>20</sup> observed the emissions at a wavelength of 150 centimeters. The 3-centimeter experiment showed that there was residual radiation from the corona but that this radiation originated in the lower part of the corona. That part of the corona which was uncovered at mid-totality radiated an amount of energy which was 3% of the energy radiated by the uncovered sun. One percent of the radiation was due to the moon, from 30% to 40% due to sunspots, and the remainder was steady background. The Russians found that the residual intensity at totality was 40% that of the uncovered sun. This, coupled with the shape of their eclipse curve, indicates that at this long wavelength the effective diameter of the sun is almost twice normal, which is consistent with the theory of the generation of radiation at these wavelengths in the sun's atmosphere.

To determine the minimum detectable change in temperature of a source whose angular dimension is that of the sun, it is necessary to consider the beamwidth and the gain of the antenna used, the noise figure or the efficiency of the receiver, and the stability of the amplifiers. On the assumption that the amplifiers are sufficiently stable to measure a 0.3% change in amplifier current (this is easily realizable) the minimum source temperature,  $T_s$ , observable for several wavelengths using a ten-foot diameter antenna is calculated and the results show in Table 2. It is shown later that the equivalent waveguide temperature is

$$t_s = T_s G \frac{1}{4} \left( \frac{r}{R} \right)^2, \quad (6)$$

where  $t_s$  is the waveguide temperature,  $T_s$  is the temperature of the source,  $G$  is the gain of the antenna,  $r$  is the radius of the source, and  $R$  is the distance of the source from the earth. This equation holds when the angular diameter of the source is less than the beamwidth. When the angular diameter of the source is larger than the beamwidth, then equation (6) becomes

$$t_s = T_s. \quad (7)$$

TABLE 2

Minimum Observable Temperature at Various Wavelengths  
Using a Ten-Foot Diameter Antenna and a Source  
Having the Sun's Diameter

Wave-length (cm)	NF (db)	Min. $t_s$ ° K	Antenna Gain over an Iso- tropic Radiator	Beam Width <sup>o</sup>	Min. Obser- vable $T_s$ Calculated ° K	$T_s$ (sun) ° K from Fig. 7
0.85	20	100	$8.3 \times 10^5$	0.2	100	7,000
1.25	15	40	$3.8 \times 10^5$	0.28	40	9,000
3.2	12	15	59,000	0.72	47	17,000
10.0	10	10	60,000	2.25	310	50,000
25.0	10	10	960	5.63	1930	100,000
50.0	6	4	240	11.3	3100	250,000
150.	4	2.5	26.6	33.8	18,000	700,000
200.	3	2	15.0	45.0	25,000	900,000

The noise figures used in constructing Table 2 are those consistent with good practice today. Under ideal circumstances these noise figures could be improved upon somewhat. It is thus seen that with a ten-foot diameter antenna the sun should be easily measurable over this wavelength range.

Several workers<sup>21,22,23,24,25,26,27</sup> discuss the mechanism for the production of this radiation in the atmosphere of the sun. Two approaches have been used: a macroscopic one based on the theory derived for the analysis of our ionosphere, where an absorption coefficient due to Lorenz is derived, and a microscopic approach based on the assumption of free-free transitions between the electron gas and ionized hydrogen atoms, where an absorption coefficient due to Kramers<sup>28</sup> and later modified by Gaunt<sup>29</sup> and Menzel and Pekeris<sup>30</sup> is derived. The result of the theoretical investigations shows that the longer wavelength radiation cannot penetrate very deeply into the corona, whereas the very short wavelength radiations can penetrate well into the chromosphere. This is consistent with the experimental results when the kinetic temperatures of the gases in the chromosphere and corona are considered.

While this approach gives a reasonable explanation of the effective temperature as measured at radio wavelengths for the quiet sun, it is in no way satisfactory for an explanation of the radiation from the disturbed sun. The equivalent temperature of small areas on the surface of the sun as measured at the longer wavelengths may rise

to values as high as  $10^9$  degrees to  $10^{10}$  degrees Kelvin. It is not reasonable to presume then that these radiations are thermal in origin, since they always occur in conjunction with an active area near a sunspot. They must in some way be connected with the clouds of hot gases and electrons ejected from layers deep in the sun.

The work on the measurement of galactic noise has been hampered by the fact that the resolution obtainable with the antennas available and at the wavelengths used has not been sufficiently sharp to define properly the structure of the radiation. Both Reber and Hey and his co-workers<sup>8,9,11,12,13</sup> have published charts of the distribution of galactic noise in the sky, and these have been discussed in a recent paper by Williamson.<sup>10</sup> In this paper Williamson points out that the direction of the galactic pole as determined by the radio measurements is consistent with that determined from star counts. Williamson's analysis is predicated on the basis that the source of galactic radiation is the interstellar gas and that the gas is most heavily concentrated in the plane of the galaxy. The mechanism for the radiation is generally presumed to be that of free-free transitions of an electron with an ionized hydrogen atom,<sup>3,3,3,4,3,5,3,6</sup> although there are present indications that this may not be so and that the source may be more complex in origin.

There has been insufficient quantitative data taken as yet on galactic radiation to define its wavelength distribution. All the published measurements of galactic radiation have been made at wavelengths longer than 60 centimeters, but plans are underway to search for galactic radiation using very large antennas at 30 centimeters and shorter wavelengths. If the radiation is found at these shorter wavelengths then the consequent higher resolution will allow more detailed space distributions to be obtained.

The scope of this report is to discuss the results of the measurement of the intensity of the sun's radiation at short wavelengths. A discussion of the theory behind the measurements and of the method used will be given. The operation of the receiver, the measurement of the antenna characteristics, and the calibration of the over-all device is described. The results of the measurements are given, followed by an interpretation of the distribution of the radiation on the sun. There is a description and analysis of the work on the May 20, 1947 eclipse and its analysis. This is followed by a discussion of the impact of these measurements on the interpretation of the condition of the sun's atmosphere. In conclusion, the future plans for the work are discussed and suggestions made as to the proper direction for other investigations in this field.

THERMAL RADIATION AND ITS MEASUREMENT  
AT RADIO WAVELENGTHS

The relations that exist between the temperature of the source, the wavelength of the radiation considered, the energy density of the radiation and the emissive power of a surface are well known, and the theory of this radiation can be found in standard texts.<sup>37,38</sup> A consideration of Planck's radiation law

$$\psi_{\lambda} d\lambda = 8\pi ch \frac{\lambda^{-5} d\lambda}{e^{\frac{ch}{\lambda kT}} - 1} \text{ ergs/cm}^3 \quad (8)$$

where

- $\psi_{\lambda}$  = the monochromatic energy density
- $\psi_{\lambda} d\lambda$  = the amount of radiant energy per unit volume in a wavelength range  $d\lambda$  at a wavelength  $\lambda$
- $c = 3 \times 10^{10}$  cm/sec = the velocity of light
- $h = 6.624 \times 10^{-27}$  erg.sec = Planck's constant
- $\lambda$  = the wavelength in centimeters
- $e$  = the base of the Napierian logarithms
- $k = 1.380 \times 10^{-16}$  erg/deg = Boltzmann's constant.

shows that the radiation from a black body at a temperature  $T$  extends over the entire electromagnetic spectrum. The intensity will be at a maximum at a wavelength which is inversely proportional to the temperature and will fall off rapidly on each side. Nevertheless for the special conditions under consideration here, that is, where  $T \approx 6,000^{\circ}$  Kelvin and for a body of the size and distance of our sun, there will be a measurable radiation over most of the radio-frequency spectrum (see Figure 7 and Table 2). The development of extremely sensitive radio receivers and highly efficient receiving antennas has made it possible in recent years to detect and measure this "thermal" radiation from the sun in the radio-frequency spectrum.

The derivation to be given here is made on the assumption that the sun radiates as a quasi-black body. It will be shown that while the character of the emission measured is that of black body radiation, the equivalent temperatures derived from the measured intensities of the emission are in all cases greater than  $6,000^{\circ}$  Kelvin.

It might be pointed out that in measuring the intensity of the emission from the sun, and hence its equivalent temperature, there are three sets of circumstances which affect the interpretation of the result. In the first and ideal case the radiation pattern of the

antenna is sufficiently narrow so that the entire beam is smaller in diameter than the sun. In this case the effective antenna temperature is the same as the equivalent temperature of the sun. The second condition would be that in which the antenna pattern is so broad that the gain of the antenna does not vary within the angle subtended by the sun. In this case, while the effective antenna temperature will be less than the equivalent temperature of the sun by an amount determined by the gain of the antenna, nevertheless, the equivalent temperature of the sun as a source can be calculated by well known and rigorous expressions. The third case is that where the beamwidth of the antenna lies between the two previous cases and is commensurate with the angular diameter of the sun. Here when the axis of the beam is directed at the center of the sun, the gain varies across the disc of the sun, and therefore to compute the equivalent temperature of the sun from the measured intensity of the emission an integration involving a detailed knowledge of the pattern of the antenna must be performed.

In equation (8) the exponent in the denominator,  $\frac{ch}{\lambda kT}$ , will become quite small for large values of  $\lambda$  and  $T$ . In this case we may expand the denominator of equation (8) by means of the series

$$e^{\alpha} = 1 + \alpha + \frac{\alpha^2}{2} \dots$$

obtaining:

$$e^{\frac{ch}{\lambda kT}} - 1 = \frac{ch}{\lambda kT} + \frac{c^2 h^2}{2\lambda^2 k^2 T^2} \dots$$

If  $\lambda T$  is large compared to  $\frac{ch}{k}$  then only the first term to the right need be kept. When this substitution is made, equation (8) becomes

$$\Psi_{\lambda} d\lambda = \frac{8\pi kT}{\lambda^4} d\lambda \text{ ergs/cm}^3 \quad (9)$$

which is the Rayleigh-Jeans formula. Since in the radio-frequency region  $\lambda T \gg \frac{ch}{k}$ , Rayleigh-Jeans' formula will be used in this discussion.

Let  $i_{\lambda}$  be the intensity of monochromatic radiation at wavelength  $\lambda$  in a given direction from an element of surface of a hot body, and

assume that  $i_\lambda$  is the same in all directions. To determine  $e_\lambda$ , the total rate of monochromatic flux per unit area, refer to Figure 10,

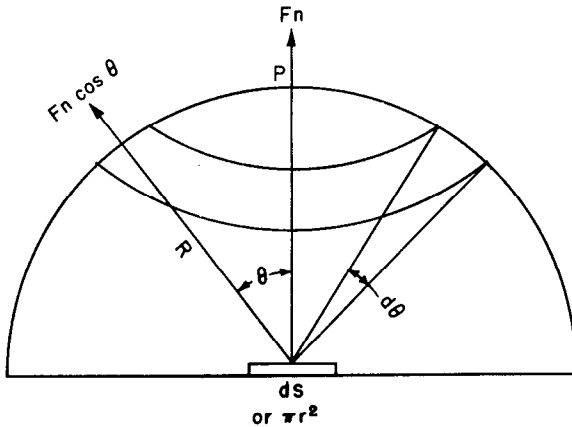


Figure 10 - Construction for computing the flux per unit area

area of the emitting surface,  $dS \cos \theta$ , the area of the receiving surface  $2\pi R^2 \sin \theta d\theta$  and inversely with the square of the distance between the two surfaces  $R^2$ . The total flow of monochromatic radiation through the ring is

$$i_\lambda dS \cos \theta \frac{2\pi R^2 \sin \theta d\theta}{R^2} = 2\pi i_\lambda dS \cos \theta \sin \theta d\theta.$$

When this is integrated over the hemisphere, the total flux through the hemisphere and therefore the total flux out of the surface  $dS$  is obtained.

$$\text{Total flux} = 2\pi i_\lambda dS \int_0^{\frac{\pi}{2}} \cos \theta \sin \theta d\theta = \pi i_\lambda dS. \quad (10)$$

This is the total monochromatic flux out of the surface  $dS$ . By definition  $e_\lambda$  is the total rate of monochromatic flux per unit area.

$$e_\lambda = \frac{\text{total flux}}{dS} = \pi i_\lambda \text{ ergs/sec/cm}^2. \quad (11)$$

Temperature of the Source and Power Density of the Receiver

Consider a pill box of surface area  $dS$  and thickness  $dx$  placed within an enclosure having perfectly reflecting walls. The total flux out of each surface is  $\pi i_\lambda dS$ . Therefore the total flux out of the pill box is  $2\pi i_\lambda dS$ . If the enclosure is in equilibrium, then the total flux into the box will be  $2\pi i_\lambda dS$ . The volume of the box is  $dS dx$ . The total energy in the box is equal to the total flux times the time of transit across the box  $\frac{dx}{c}$ . Therefore the total energy equals  $\frac{4\pi i_\lambda dS dx}{c}$ . The monochromatic energy density of radiation,  $\psi_\lambda$  is

$$\psi_\lambda = \frac{\text{total energy}}{\text{volume}} = \frac{4\pi i_\lambda}{c} \quad \text{therefore } \psi_\lambda = \frac{4e_\lambda}{c} \text{ ergs/cm}^3. \quad (12)$$

From equations (11) and (12) it is seen that within the enclosure  $i_\lambda = \frac{c\psi_\lambda}{4\pi}$ . Using the Rayleigh-Jeans law, equation (9) to eliminate  $\psi_\lambda$ ,

$$i_\lambda = \frac{2ckT}{\lambda^4} \text{ ergs/sec/cm}^2/\text{unit solid angle}. \quad (13)$$

To compute the power absorbed by an isotropic radiator in a spherical enclosure of radius  $R$  whose walls are at a temperature  $T$ , consider an element of emitting area on the surface of the enclosure  $dA$ . The power absorbed from this element by the isotropic radiator, whose effective area<sup>39</sup> is  $\frac{\lambda^2}{4\pi}$ , is

$$dP = i_\lambda d\lambda \cdot dA \cdot \frac{\lambda^2}{4\pi R^2} \text{ erg/sec.} \quad (14)$$

When this is integrated over the whole enclosure

$$P = i_\lambda d\lambda \cdot 4\pi R^2 \cdot \frac{\lambda^2}{R^2} \\ = i_\lambda \lambda^2 d\lambda.$$

When only one polarization is accepted then

$$P = \frac{1}{2} i_{\lambda} \lambda^2 d\lambda. \quad (15)$$

Substituting from equation (13) for  $i_{\lambda}$  and remembering that  $df = \frac{cd\lambda}{\lambda^2}$ :

$$P = kTdf. \quad (16)$$

This was first derived by Burgess<sup>7</sup> and is the same expression as that obtained by Johnson<sup>11</sup> and Nyquist<sup>12</sup> for the available power across a two-terminal network which is at temperature T.

#### Analysis of Receiver Operation

To determine the flux per unit area at the earth due to radiation from the sun, assume that the cosine law holds and that the sun may be replaced by a disc normal to the line joining the earth and the sun. When equation (14) is integrated over the surface of the sun and with the factor 1/2 included to take care of linear polarization then

$$P_s = \frac{1}{2} i_{\lambda} d\lambda \cdot \pi r^2 \cdot \frac{\lambda^2}{4\pi R^2}.$$

where  $r$  is the radius of the sun. Substituting for  $i_{\lambda}$  from equation (13) and writing  $df = c d\lambda / \lambda^2$ :

$$P_s = \frac{1}{4} kT_s df \frac{r^2}{R^2} \quad (17)$$

where  $T_s$  is the equivalent temperature of the sun. Suppose a directive antenna having a gain  $G$  over an isotropic radiator is used. If the antenna beamwidth is sufficiently greater than the angle subtended by the sun so that there is little variation in gain across the surface of the sun, then

$$P_s = \frac{G}{4} kT_s df \frac{r^2}{R^2} \text{ ergs/sec.} \quad (18)$$

If a resistive termination at the input to the receiver is substituted for the antenna and the temperature of the termination is raised to a value  $t_s$  such that the output from the receiver is equal to that obtained when the antenna is pointed at the sun, then

$$P_s = k t_s df \text{ ergs/sec.} \quad (19)$$

$t_s$  will be referred to as the effective antenna temperature. Substituting from above,

$$T_s = \frac{4t_s}{G \frac{r^2}{R^2}} \text{ degrees Kelvin.} \quad (20)$$

It should be pointed out that this equation holds when the angular diameter of the sun is much less than the beamwidth of the antenna.

When the angular diameter of the sun is sufficiently greater than the beamwidth so that the entire antenna pattern falls on the sun, the preceding analysis must be modified.

Let  $dA$  be an element of area on the solar disc. Then from equation (14) the power received at the antenna due to radiation by this element of area is

$$dP = i_\lambda d\lambda \cdot dA \cdot \frac{\frac{\lambda^2}{4\pi}}{R^2} \cdot G$$

where  $G$  is the gain of the antenna over an isotropic radiator. Introducing the factor  $1/2$  to take care of linear polarization and substituting from  $i_\lambda$  as before:

$$dP = \frac{1}{4\pi} \cdot k T_s df \cdot G \cdot \frac{dA}{R^2},$$

but  $\frac{dA}{R^2} = d\omega$ . Make this substitution and integrate over all space. Since all of the beam falls on the sun,  $\int G d\omega = 4\pi^{3\theta}$   
and

$$P_s = k T_s df \text{ erg/sec.} \quad (21)$$

and since from equation (19)

$$P_s = k t_s df \text{ erg/sec.},$$

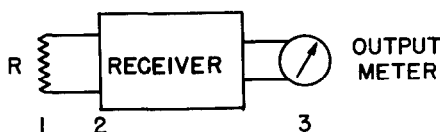
then

$$T_s = t_s \quad (22)$$

This equation holds for the case where the angular diameter of the sun is larger than the antenna beamwidth and is of particular interest in the work described here.

### The Noise Factor

To interpret the variations in the noise output of the receiver caused by the signals from the antenna, which have the characteristics of noise, it is necessary to analyze the behavior of the receiver with respect to noise. Figure 11 is a schematic diagram of the receiver.



EQUIVALENT CIRCUIT OF RECEIVER

Figure 11 - Equivalent circuit of receiver

The resistance  $R$  represents the impedance connected across the input terminals of the receiver, and in all cases it will be assumed that there is an impedance match. When the receiver is in its most sensitive condition the gain control will be advanced until first-circuit noise appears at the output. The meter shown in the figure is connected to the second detector in the

receiver and measures the noise power at the output of the receiver. In use the efficiency of the receiver will be determined by the ability of the receiver to present at the output a maximum signal-to-noise ratio. The noise figure,  $F$ , of a receiver is defined<sup>40</sup> as the

ratio of the available noise-to-signal ratio at the output terminals to the noise-to-signal ratio at the input terminals. Therefore

$$F = \frac{\frac{N}{S}}{\frac{n}{s}}, \quad (23)$$

where

$N$  = the output noise power when the receiver network is at ambient temperature,  $T_0$

$S$  = the output signal power

$n$  = the available noise power at the input terminals

$s$  = the available signal power at the input terminals.

In this fashion  $F$  is a pure number. In referring to receivers in practice it is usually convenient to refer to the value of  $F$  in decibels, in which case the expression noise factor ( $NF$ ) is used.

$$NF = 10 \log_{10} F \text{ decibels.} \quad (24)$$

It has been shown that the available noise power at the input terminals of the receiver due to thermal noise in the resistor  $R$  will be

$$n = kT_0 df,$$

where  $T_0$  is the ambient temperature and  $k$  and  $df$  are as previously defined. Rewriting equation (23) to obtain an expression for  $N$ :

$$N = FG_r kT_0 df, \quad (25)$$

where  $G_r = \frac{S}{s}$  and is the gain of the receiver. By definition the portion of the output noise due to thermal noise in  $R$  at  $T_0$  is

$$N_i = G_r kT_0 df. \quad (26)$$

Therefore the contribution of the network is

$$N_r = N - N_i = (F-1)G_r k T_0 df . \quad (27)$$

Consider what takes place at the output terminals of the receiver when the input signal is derived from a noise generator connected to the input terminals. Such a noise generator could be a resistive termination which is raised to some high temperature, or it may be the sun. In the work described here a superheterodyne receiver is used, and the radiation from the sun is accepted at both signal frequency and image frequency. Under normal circumstances when a superheterodyne receiver is used, it is customary to accept signals at signal frequency but not at image frequency, and so for purposes of completeness the analysis of both conditions will be included.

First consider the case where the noise generator contributes a signal at signal frequency but not at image frequency nor at any other frequency such as harmonics, at which the receiver may be sensitive. The output power when the network is held at  $T_0$  and the resistor  $R$  at  $T$  is from equations (26) and (27)

$$N_T = N_i + N_r = G_r k T df + (F-1)G_r k T_0 df . \quad (28)$$

Then from (25) and (28)

$$\frac{N_T}{N} = \frac{T + (F-1)T_0}{FT_0} .$$

Solving for  $F$  :

$$F = \frac{T - T_0}{T_0} \cdot \frac{N}{N_T - N} . \quad (29)$$

This is equivalent to equation (23). If  $T$  is adjusted to double the output power measured when  $R$  and the network are at  $T_0$ , where  $N$  is the output power at  $T_0$  and  $N_T$  is the output power at  $T$ , then

$$F = \frac{T - T_0}{T_0} = \frac{T}{T_0} - 1. \quad (30)$$

This last equation indicates the method used for calibrating the receiver and thereby determining the noise figure.

Now take the case where the generator contributes a signal at both the signal and image frequencies but at no others. Proceeding as before:

$$N = FG_r k T_0 df. \quad (25)$$

It is well to note that network noise and the contribution to the output noise by the input termination at the temperature of the receiver network is customarily and usually implicitly assumed to pass both through the signal and the image channel; whereas the signal per se should pass through only the signal channel. Contributing to  $N_T$ , the output power when the network is held at  $T_0$  and the resistor at  $T$ , there are: (1) the network noise, equation (27); (2) noise from the receiver up to the temperature  $T_0$ , equation (26); (3) noise from the resistor in the range  $T_0$  to  $T$ . In other words, in computing the available noise signal power from a source with a wide frequency distribution, since both signal and image contribute, the power will be

$$p = 2k(T - T_0) df;$$

thus

$$N_T = 2G_r k (T - T_0) df + G_r k T_0 df + (F - 1)G_r k T_0 df,$$

where the first term to the right is the contribution from the resistor above the temperature  $T_0$  and includes both signal and image. The second

term is that part of the set noise arising in the input termination, and the last term is that part of the set noise originating in the network, all at  $T_0$ . Simplifying:

$$N_T = 2G_r k(T - T_0)df + FG_r kT_0df. \quad (31)$$

The ratio can be expressed as:

$$\frac{N_T}{N} = \frac{2(T - T_0)}{FT_0} + 1. \quad (\text{Using (31) and (25)})$$

Therefore

$$F = 2 \frac{(T - T_0)}{T_0} \cdot \frac{N}{N_T - N}. \quad (32)$$

As before if the temperature of the termination is adjusted to double the noise output then

$$F = 2 \frac{(T - T_0)}{T_0} = 2 \left( \frac{T}{T_0} - 1 \right). \quad (33)$$

#### Noise Output of Receiver and Temperature of the Source

In practice it is not always necessary to compute the noise figure of the receiver. If the increase in the output of the receiver due to the radiation from the sun is measured and then the increase in output due to a known increase in temperature in a resistive termination at the input of the receiver is measured, the equivalent temperature of the sun can be computed directly. Rearranging equation (31) using equation (25):

$$N_T = 2G_r k(T - T_0)df + N.$$

If  $N_T$  for the sun is measured and called  $N_{T_s}$  and  $N_T$  for the hot load called  $N_{T_l}$ , then

$$N_s = N_{T_s} - N = 2G_r k (t_s - T_o) df, \quad (34)$$

and

$$N_l = N_{T_l} - N = 2G_r k (T_l - T_o) df \quad (35)$$

where  $N_s$  is the increment in noise due to the sun and  $N_l$  the increment due to the load. From the two equations above

$$\frac{N_s}{N_l} = \frac{t_s - T_o}{T_l - T_o}. \quad (36)$$

The ratios of the temperatures of the sun and the load above ambient temperature are equal to the ratio of the increments in the output of the receiver due to the sun and the hot load. From  $t_s$  obtained in this fashion the equivalent temperature of the sun  $T_s$  can be computed from equation (20) or (22).

The foregoing describes the method of calibration used in this report. It should be pointed out that if one were to obtain a value for the noise figure of the receiver by the hot load method or any other method, such as with a signal generator, then the equivalent temperature of the source could be computed from the equation for the noise figure. Referring back to equations (20) and (22), it is seen that when the antenna beamwidth is narrower than the angle subtended by the sun, antenna temperature measured in this way is the equivalent temperature of the sun; whereas when the antenna beamwidth is greater than the angle subtended by the sun, the equivalent temperature of the sun must be computed from the antenna temperature, the gain of the antenna, and the solid angle subtended by the sun.

Since the signal contributed by the solar radiation is random noise and is identical in constitution with the locally generated

CONFIDENTIAL

receiver noise, the stability of the output of the receiver determines the accuracy with which measurements of the intensity of the signal from the sun can be made. Therefore in the design of the receiver every consideration is given to increasing the stability of the output reading since the input signal and the locally generated noise have the characteristics of random noise.

In a given time the number of rectified noise pulses in the output of the receiver is determined by the bandwidth of the i-f amplifier. An amplifier having a bandwidth of 1 megacycle will have approximately  $10^6$  pulses per second; whereas an amplifier having a bandwidth of 10 kilocycles would have approximately  $10^4$  pulses per second. Since the distribution of the pulses is a statistical one, then some of the pulses will be large, others small. The occurrence of a pulse of a given size is in no way affected by the size of the pulse just preceding it; but if in a random variation of this nature, the number of times a pulse of a given amplitude has occurred is considered, then it is known that the chance that number deviates from the number predicted by the distribution is proportional to  $1/\sqrt{n}$ , where  $n$  is the number of pulses in the time considered. It is therefore obvious that in order to smooth out the readings on the output meter, as wide an i-f bandwidth as possible should be used. If the i-f bandwidth is 3 megacycles, then the expected fluctuation is approximately  $(1/3 \times 10^6)^{1/2} \approx 6 \cdot 10^{-4}$ . In the receiver used here, a rise in temperature of  $500^\circ$  Kelvin in a resistor across the input terminals produces a change in output current of about 25 parts in 600. A 1% change in output then corresponds to a rise in temperature of  $120^\circ$  Kelvin. The statistical fluctuation is, then, 6 parts in  $10^4$  or  $7^\circ$  Centigrade. This fluctuation can be reduced by heavily by-passing the output meter with a condenser, which in effect decreases its bandwidth but has the adverse effect of making the motion of the meter more sluggish and thereby increasing the time necessary to make a reading. In the present apparatus the output meter is by-passed so that the fluctuation temperature is less than  $7^\circ$  Centigrade. A more exact expression for the stability is given by Dicke:<sup>41</sup>

$$\frac{\Delta T}{T} = \frac{\pi^{\frac{3}{2}} N}{8} \left( \frac{\alpha}{\Delta \omega} \right)^{\frac{1}{2}} \quad (\text{equation (27) loc. cit.})$$

where  $\Delta T$  = the statistical fluctuation in degrees Kelvin  
 $T$  = the temperature at which the measurement is made  
 $N$  = the noise figure of the receiver  
 $\alpha$  = the bandwidth of the low-pass filter on the output meter  
 $\Delta \omega$  = the bandwidth of the i-f amplifier.

Inserting numerical values pertinent to this receiver:

$$\begin{aligned} N &= 100 \\ \alpha &\approx 0.1 \text{ per second} \\ \Delta \omega &= 2\pi \cdot 3 \cdot 10^6 \text{ per second} \end{aligned}$$

and assume  $T = 300^{\circ}$  Kelvin; then

$$\Delta T \approx 1.5^{\circ} \text{C} .$$

A further refinement of the receiver which tends to remove variations in the output due to fluctuations in the gain of the receiver can be made. There are two methods of doing this presently used.<sup>17,41</sup> In the 8.5 millimeter apparatus, gain variation has been minimized by heavily stabilizing the input voltages to the apparatus. The 3 centimeter equipment on the other hand uses the gain stabilization method of reference (41). This is essentially a bridge method where the signal entering the antenna is compared at a 30 cycle per second rate with the thermal noise from a well matched resistor.

#### DESCRIPTION OF THE APPARATUS

An apparatus for the detection and measurement of emission in the radio-frequency spectrum consists of an antenna to which is coupled a sensitive receiver whose output may be measured on a meter. Extra-terrestrial emission is generally of such low amplitude that high-gain antennas and very sensitive receivers must be used. In the millimeter and centimeter wave region most antennas are quasi-optical in nature; that is, they consist of some form of reflector which focuses the incident radiation and some form of "feed" or pickup device which will collect the focused radiation and transmit it to the input terminals of the receiver.

A photograph of the complete antenna and receiver is shown in Figure 3. The control box for positioning the antenna is on the table in front. The cables leading from the control box and from the base of the pedestal go below to the power source and to the amplidyne and amplifier. At the end of the piece of waveguide projecting through the reflector is the feed horn which is covered with a thin sheet of material and is transparent to these wavelengths. Sealing the feed horn presents a problem since, when the antenna is pointed at the sun it serves to focus not only radiation of an 8-millimeter wavelength but also wavelengths in the infrared. This means of course that any material which is an absorber at infrared wavelengths will become very hot if it is placed on or about the feed. Thin transparent polystyrene tape seems to work very well in sealing the horn.

## NAVAL RESEARCH LABORATORY

Between the reflector and the feed horn the waveguide is encased in a one-inch pipe in order to obtain mechanical rigidity. This pipe is held in position with the help of three taut wires. From the back of the reflector the waveguide continues on into the receiver box. Referring to Figure 12 the waveguide enters the top of the box and continues over to the i-f strip on the left. The crystal mixer is directly above the i-f strip. The local oscillator and the waveguide filter are in the center of the box and are connected into the waveguide leading to the receiver in a T junction.

For calibration purposes the hot load, which is in the box on the lower right-hand side of the receiver box, is connected to the receiver in place of the antenna, as shown in Figure 13. This is done by breaking the waveguide run to the antenna and inserting in its place a piece of waveguide which includes a variable attenuator. During the calibration procedure the variable attenuator is set for either full attenuation or no attenuation. Full attenuation in this case corresponds to a loss of 20 decibels. During calibration, then, the waveguide leading to the receiver is terminated by either the hot load at a known elevated temperature or by the attenuator at ambient temperature.

The necessary meters for monitoring the operation of the receiver are mounted in the top left side of the box. The connections going to the power supplies for the receiver are in cables leading out of the bottom of the box. When the cover is placed on the box with a rubber gasket, the whole container including the waveguide run is water tight.

#### The Antenna and Mount

As shown in Figure 3, the antenna used with the 8.5-millimeter receiver consists of a parabolic reflector ten feet in diameter and a feed horn connected by means of waveguide to the receiver. The paraboloid is constructed of cast aluminum which has its front surface machined in the form of a paraboloid of revolution to as close tolerances as possible. When measured with a template after being mounted in position it was found that no part of the surface deviated from a true paraboloid by more than 0.005 inches. Thus the surface is true to within 0.1 wavelength through the millimeter wavelength band, and one would expect the pattern and the gain of the antenna to



be as computed for this band of wavelengths. The F/d ratio for the parabola is 0.3. At the focus of the parabola a feed horn is located which has directional characteristics such that the parabola has a tapered illumination. The parabola and feed horn are rigidly secured together and are mounted on a pedestal in much the same way as an astronomical telescope is mounted. The mount is so inclined that one axis of revolution is aligned with the earth's axis. The second axis of revolution is at right angles to the first. This results in a motion of the antenna in right ascension and in declination.

There are two methods used for controlling the position of the antenna in right ascension. In the first method a synchronous motor in the pedestal is so geared to the axis of rotation that the antenna follows a fixed position on the celestial sphere. In the second method the synchronous motor is disengaged, and a direct-current motor driven by an amplidyne and servo-control unit keeps the antenna pointed in a direction determined by the position of the shaft of a selsyn generator located in a separate control box. The position of the shaft of the selsyn-control unit may be changed by turning a small hand crank, or it in turn may be geared to a small synchronous motor and be made to turn in synchronism with the earth's rotation. Motion in declination is at present obtained by means of a hand crank geared directly to the declination axis.

A guiding telescope is rigidly attached to the framework supporting the antenna reflector and looks through a hole cut in the reflector. Things are so arranged that the operator can control the position of the antenna in right ascension and declination through the electro-mechanical control mechanism while guiding with the telescope. On the reticule of the telescope there is a grid formed by the intersection of five vertical and five horizontal lines. The reticule is adjusted so that the lines forming the grid are aligned with the right ascension and declination circles. The separation of the lines is such that when the intersection of the two center lines coincides with the center of the sun, the outside lines are tangent to the limb. This makes it possible, by setting the sun's limb tangent to the various lines, to move the antenna beam across the sun in nine equally spaced steps in right ascension for each of nine steps in declination. Each step is eight minutes in width for a sun thirty-two minutes in diameter.

#### Method of Calibration of Antenna Pattern and Receiver Sensitivity

The beam pattern of the antenna was measured in two planes, (Figure 14 and Table 3). This measurement was accomplished by setting

up a generator of 8.5-millimeter waves on a hill about one mile from the position of the antenna and measuring the output of the receiver as a function of antenna position. The antenna position was determined by means of the reticule in the telescope. It is seen that the beamwidth at half-power points is  $0.2^\circ$  in the H plane and  $0.18^\circ$  in the E plane and that the entire pattern is within a circle less than 32 minutes in diameter. Since the antenna pattern is smaller than the diameter of the sun, the gain of the antenna over the gain of an isotropic radiator was not measured inasmuch as this figure is not needed for the reduction of the data. If needed, the gain may be computed from the pattern and is about  $8.2 \times 10^5$  times that of an isotropic radiator.

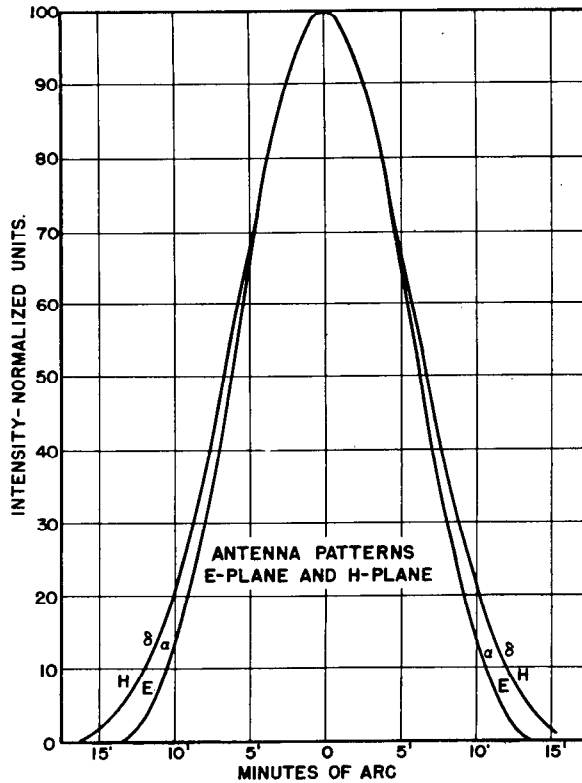


Figure 14 - Beam pattern for 8.5-millimeter antenna

### The Receiver

A superheterodyne receiver is used which has an i-f amplifier having a high gain and a bandwidth of 3 megacycles centered at 30 megacycles per second. The gain of the i-f amplifier is sufficiently high so that set noise generated in the mixer and in the first stages of the i-f amplifier appears in the output. This amplifier is followed by a linear second detector and an output meter.

The 8-millimeter local oscillator generates such high noise sidebands that the sensitivity of the receiver is seriously affected. To correct for this and obtain a receiver sufficiently sensitive to be useful for this work it is necessary to insert a narrow band filter, tuned to the local oscillator frequency, between the local oscillator and the crystal detector. The passband of the filter is such that noise components separated from the local oscillator frequency by as much as the i-f frequency are heavily attenuated. The receiver is

TABLE 3  
 Beam Pattern for Ten-Foot Diameter Antenna  
 at 8.5-Millimeter Wavelength

E Plane		H Plane	
Angle from Arbitrary Zero in Minutes of Arc	Intensity Relative Power	Angle from Arbitrary Zero in Minutes of Arc	Intensity Relative Power
0	1.0	0	1.5
1	3.0		
2	3.0	2.5	4.0
3	4.0		
4	6.0	5.0	5.0
5	8.0		
6	10.0	7.5	15.0
7	15.0		
8	16.5	10.0	19.0
9	19.0		
10	20.0	12.5	21.0
11	21.0		
12	23.0	15.0	19.0
13	22.0		
14	22.0	17.5	14.0
15	21.0		
16	18.0	20.0	9.0
17	17.0		
18	12.0	22.5	4.5
19	11.0		
20	9.0	25.0	1.5
21	5.5		
22	3.0		
23	0.5		

assembled as shown in Figure 15. In addition to the components named, the hot load used for calibration purposes and the cavity wavemeter, which serves the dual purpose of determining the wavelength to which the receiver is tuned and also filtering out unwanted noise from the local oscillator tube, are shown in the diagram.

The over-all characteristics of the receiver are such that readings of the output meter are directly proportional to the power of the input signal, and therefore the readings are directly proportional to

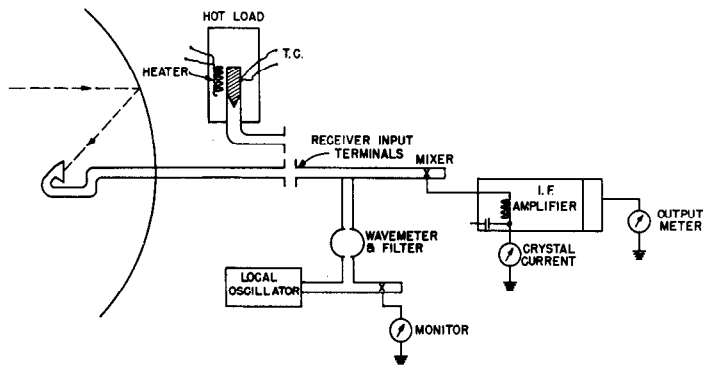


Figure 15 - Block diagram of receiver

the temperature of the source when the antenna is pointed at a hot body such as the sun.

To calibrate the receiver the hot load is substituted for the antenna and the output current measured as the temperature of the load is changed. A copper constantan thermocouple is soldered to the waveguide containing the load to measure the temperature. The calibration curve for the thermocouple is given in Figure 16.

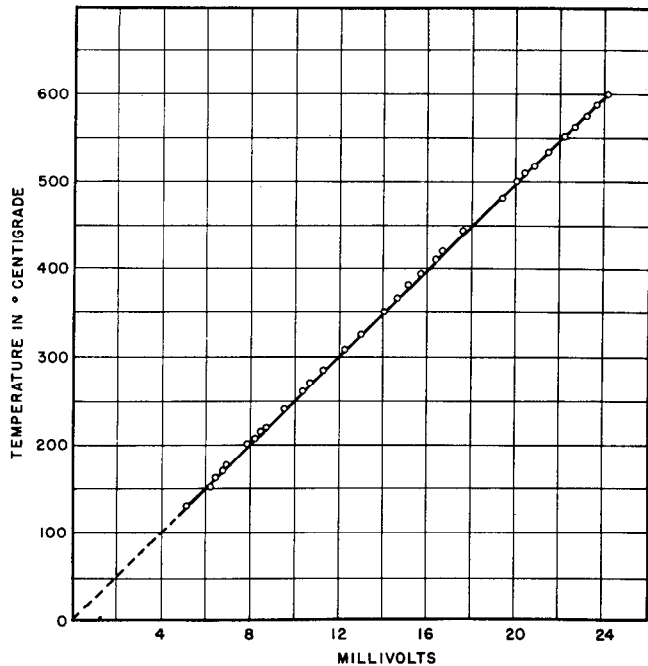


Figure 16 - Calibration of the copper-constantan thermocouple

TABLE 4  
Calibration of Receiver

Date	Ambient Temperature ° Kelvin	Thermo-couple Scale Divisions	T ° K	$\Delta I$ $\mu a$	I $\mu a$	$\Delta I/I$
2/5/49	278	20.2	508	26	557	0.0467
		19.4	489	26		0.0467
		18.8	474	24		0.0431
		16.4	413	21.0		0.0377
		16.2	409	20.0		0.0359
		14.4	363	20.0		0.0359
		14.0	353	19.0		0.0341
		10.4	264	13.5		0.0242
		10.1	257	10.5		0.0188
		10.0	248	12		0.0215
		7.4	188	9		0.0162
		7.4	188	9		0.0162
		4.0	102	3		0.0054
		3.9	99	8		0.0144
		3.7	94	7		0.0126
		2.4	62	6.3		0.0113
		23.3	587	31		0.0557
		20.5	517	25		0.0448
		19.8	498	27.5		0.0494
		19.0	478	24.5		0.0440
2/8/49	283	18.5	467	25	557	0.0448
		20.5	515	24.5		0.0440
		19.03	480	22.5		0.0404
		18.0	455	23.5		0.0415
2/25/49	283	15.3	387	15.0	569	0.0264
		15.0	378	18.0		0.0322
		14.4	363	16.0		0.0281
		14.0	353	14.0		0.0246
		13.6	343	14.0		0.0246
		13.1	332	13.0		0.0228
		12.8	323	15.0		0.0264
		7.6	193	8.0		0.0140
		7.5	190	7.0		0.0123
		7.3	185	10.0		0.0176
		7.2	182	9.0		0.0158
		7.2	182	8.0		0.0140
		3.2	82	4.0		0.0070
		3.2	82	4.0		0.0070
		3.2	82	2.0		0.0035
		3/12/49	275	20.5		515
18.0	455			19	0.0323	
17.5	440			18	0.0307	
16.0	405			19	0.0324	
15.5	390			16	0.0272	
13.5	340			16	0.0272	
10.0	255			8	0.0136	
10.0	255			9	0.0153	
7.0	175			3	0.0051	
5.0	130			0	0.0000	
3/14/49	283	20.5	515	25	647	0.0387
		19.8	500	26		0.0402
		19.0	480	22.5		0.0348
		18.5	465	27		0.0418
		17.5	440	22		0.0340
		17.1	432	21		0.0325
		16.5	417	23		0.0356
		16.0	404	22		0.0340
		10.2	260	8		0.0123
		9.8	250	10		0.0154
		9.6	245	7		0.0108
		9.6	245	9.5		0.0147
		9.5	242	10.5		0.0162
			Average of 7 readings	128		5.9

The fractional change in the output current  $\frac{\Delta I}{I}$  was computed for each measurement and was plotted against the increase in the temperature of the load above ambient temperature. The data are shown in Table 4. All the data of Table 4 are plotted in Figure 17. From Figure 17 it is seen that a change in load temperature of 500° Centigrade corresponds to a value of  $\frac{\Delta I}{I}$ , of 0.0403. To compute the receiver sensitivity equation (32) is used. The ambient temperature during the period of these measurements averaged 280° Kelvin.

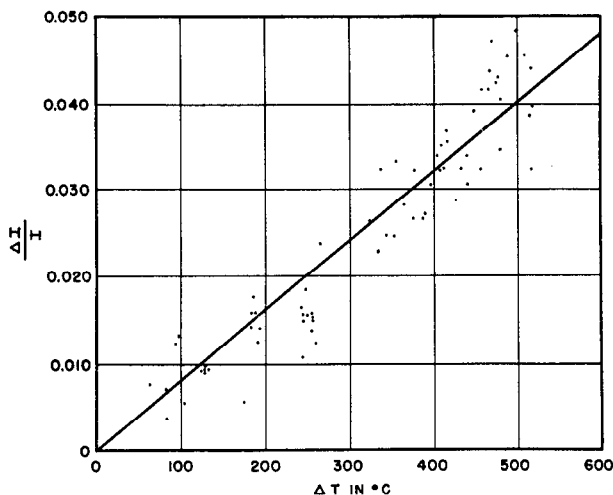


Figure 17 - Calibration of the 8.5-millimeter receiver using a hot load

Substituting values,

$$F = 2 \frac{\Delta T}{T_0} \cdot \frac{I}{\Delta I} = \frac{2 \cdot 500}{280 \cdot 0.0403} = 88.5,$$

and

$$NF = 10 \log_{10} F = 19.5 \text{ db.}$$

For the 8.5-millimeters wavelength this is a reasonable figure. To improve the sensitivity further work has to be done on improving the

crystal detector and reducing the noise of the local oscillator. To use the receiver calibration of Figure 17 to obtain the equivalent temperature of the sun it is not necessary to make the intermediate step of calculating the noise figure. The waveguide temperature is required to obtain the equivalent temperature of the sun from equations (6) or (7). From Equation (36) and the definition of the terms involved

$$t_s = \frac{\Delta I_s}{I} \frac{\Delta T_L}{\frac{\Delta I_L}{I_L}}, \quad (37)$$

where  $I$  = receiver current with antenna pointed at sky,

$\Delta I_s$  = increase in current when antenna is pointed at sun,  
 $\Delta T_L, \Delta I_L, I_L$  refer to Figure 17.

The second term on the right of (37) may be given a numerical value using Figure 17. The equation then becomes

$$t_s = 1.24 \cdot 10^4 \frac{\Delta I_s}{I} .$$

It should be observed that this procedure gives the temperature of the sun above sky temperature. While it has not been feasible to measure the sky temperature at 8.5-millimeters, it has been measured at 3.14 centimeters and found to be less than 50° Kelvin. It is reasonable to assume that at 8.5-millimeters the value will be not greater than this and will perhaps be less. The sky temperature is contributed to by two factors: thermal radiation by the earth's atmosphere and cosmic noise. Since the attenuation in the atmosphere is about 0.5 decibels, which corresponds to a reduction in signal of 11%, then the atmosphere should have an equivalent temperature of about 30 degrees Kelvin. The intensity of cosmic noise decreases with wavelength and corresponds to a temperature of not over 20° at 3 centimeters wavelength.

Lack of stability in the receiver due to variations in the gain of the receiver is caused principally by temperature or humidity changes or by changes in the line voltage. This lack of stability can in a large measure be avoided by carefully regulating the various power supplies for the equipment and by avoiding large

changes in temperature and humidity at the receiver. Such an approach is used to obtain stability in the operation of the 8.5-millimeter receiver. In the 3-centimeter receiver a more elaborate arrangement is used.

The output of the i-f amplifier is applied to a detector. The rectified current from this detector is then a function of the amplitude of the signal in the i-f amplifier and is proportional to the signal power absorbed by the antenna and applied to the input terminals of the receiver. To interpret the reading of the output meter in terms of the equivalent temperature of the source of radiation, it is necessary to consider the pattern and gain of the antenna, the noise factor of the receiver, and the loss in the waveguide. If the emissive power of the source in, say, watts per square centimeter per frequency interval is to be given instead of its equivalent temperature, then the bandwidth of the receiver must be known. Some of these characteristics are relatively constant; others vary from day to day. It is therefore necessary to measure initially all of these characteristics quite carefully and then use a calibration procedure to monitor more frequently the more variable of the characteristics. The antenna characteristics and the loss in the waveguide will be relatively constant; whereas the noise factor of the receiver is apt to vary from day to day.

The sensitivity of the receiver is best measured by substituting in place of the antenna a source of emission whose intensity can be calculated on the basis of well established physical principles once some parameter such as temperature has been measured. As was shown earlier, if a resistive termination is used, then the effective power radiated by this termination is the product of the temperature, the bandwidth, and Boltzmann's constant. A resistive termination can be made by filling the waveguide with some material that has moderately high absorptive power, taking the precaution to make the transition from the unfilled guide to the guide filled with the absorbing material a gradual one. Carbon serves as a satisfactory absorbing material, and if the transition from air to carbon is made over a range of several wavelengths in the guide, then the termination will be a good one, and the carbon block will serve as a satisfactory hot load generating the amount of available power predicted by radiation theory.

#### THE THEORY OF THE RADIATION FROM THE QUIET SUN

In an earlier part of the report, observed facts concerning the radiation from the quiet sun were presented and the similarity

of the radiation to thermal radiation stressed. Then the method of measurement was described. Next, a theory for the generation of the waves by the tenuous but hot ionized atmosphere of the sun will be presented. Measurements at 8.5-millimeters wavelength are also given and shown to be consistent with the theory. There is good agreement when the theory is later used to interpret the data taken at the 20 May, 1947 eclipse. The entire process depends upon the initial choice of an electron distribution and the assignment of a temperature distribution that provides the best fit in the analysis of the data, yet is reasonably consistent with the results of other workers.

The treatment that follows applies only to the quiet sun. The effect of the general magnetic field of the sun is neglected since there is now reasonable doubt as to its magnitude,<sup>42,43</sup> and in any case, since its estimated maximum value is less than 50 gauss, its effect on these shorter wavelength radiations would be negligible. The magnitude of the emission from disturbed areas on the sun is such that a process other than thermal must be postulated. This is a subject for further work.

### Electron Concentration and Temperature in the Sun's Atmosphere

In the visible spectrum the sun radiates as a nearly black body with an effective temperature of about 6,000° Kelvin. The radiation coming from the middle of the disc is more intense than that from the limb, and this effect is more evident in the violet than in the red. This limb darkening can be attributed to the fact that the radiation in the central ray originates from deeper and hotter layers than the radiation originating at the limb since the radiation from the limb must pass at an oblique angle through the atmosphere of the sun.

The sun's surface consists of an intensely hot gas which is opaque in the visible part of the spectrum. The density and pressure of the gas immediately outside the photosphere decreases exponentially. The variation in opacity with height is so rapid that the gas above the photosphere appears quite transparent and the sun appears to have a sharply defined limb. The light that we receive from the sun originates then in the region called the photosphere as a continuous spectrum and has superimposed upon it the absorption lines due to the passage of the light through the more rarified and somewhat cooler gases immediately outside the photosphere. It is the analysis of these

absorption lines originating in this narrow region which has in the past yielded most of the information on the physical nature of the sun.

Photographs of the emission spectrum of the atmosphere of the sun taken during the few short minutes available at the time of total eclipse have yielded to date what is known of the structure of the sun's sun's lower atmosphere. Many authors, most recently Wildt,<sup>44</sup> have derived relationships between the pressure, temperature, and abundance of the various elements with height above the photosphere using this method. It is clear that the abundance of the various elements in the atmosphere other than hydrogen decreases rapidly with height so that in the higher chromosphere, and above the atmosphere of the sun is almost pure hydrogen. For the purposes of this report the atmosphere of the sun is considered to be a highly ionized yet electrically neutral rarified gas. The ions present in the atmosphere are predominately hydrogen with a slight admixture of other elements; principally helium in the corona, and the heavier elements in the chromosphere. The concentration of hydrogen is so great that it can be assumed the entire atmosphere consists of ionized hydrogen atoms and electrons and that the number density of the two is the same, resulting in an electrically neutral gas.

The shape and the extent of the corona varies with the sunspot cycle. For the present the idealized atmosphere used is obtained by taking an average of the distributions at various times in the sunspot cycle and by assuming that the corona is uniformly distributed around the disc. This assumption, as can be seen later, does not affect the interpretation of the observations at centimeter wavelengths to any great extent since the corona is nearly transparent at these wavelengths. In any discussion of observations at meter wavelengths the asymmetrical shape of the corona should be considered.

The problem of determining the depth from which radiation which is generated by a gas of this nature originates has been previously solved. As Milne<sup>45</sup> has shown, the radiation may be considered to originate at an average optical depth of unity where the optical depth of the medium is defined as the integral of the absorption in the medium along the path of the ray, i.e.,

$$T_{\nu} = \int_0^h K_{\nu} dh \text{ or } dT_{\nu} = K_{\nu} dh,$$

or

where  $K_\nu$  is the absorption coefficient and  $dh$  an element of length along the path traversed by the ray. One has to be careful in applying these relationships to the radio-frequency case, for here under some conditions the index of refraction differs greatly from unity. It will be shown however that, under all conditions discussed, the dielectric constant of the medium never differs from unity by more than a few percent, and thus it will be assumed in this discussion that the dielectric constant is in fact unity. Furthermore, the radiation originating in the cooler regions near the photosphere escapes through the optically thin but hotter outer regions. Under these circumstances it will be seen that the equivalent temperature of the radiation differs somewhat from the temperature of the material at the optical depth of unity.

Baumbach<sup>46</sup> reviewed the observational data on the brightness of the corona and arrived at an expression for the variation of electron density with height. He did not consider scattering by dust particles. More recently, Allen<sup>47</sup> and van de Hulst<sup>48</sup> have reviewed Baumbach's work and have modified his expressions for the electron density, taking into consideration scattering by dust particles. The results of Allen and van de Hulst are not in exact agreement, but both differ from Baumbach's in the same direction and by approximately the same amounts. For the purposes of this work, a value for the electron density in the corona lying between Allen and van de Hulst is taken. The values for the electron density obtained in this way are carried in to a depth corresponding to

$$\rho = 1.03$$

where  $\rho = \frac{R}{R_0}$ ,  $R$  being the distance out from the center of the sun and  $R_0$  being the radius of the sun at the photosphere. To obtain the electron densities from  $\rho = 1.021$  in to  $\rho = 1.0007$ , Wildt<sup>44</sup> is followed. Wildt extrapolates from Baumbach to obtain the first point on his distribution at  $\rho = 1.021$  where  $n_1$ , the number of electrons per cubic centimeter, is taken as  $3.55 \times 10^8$ . At the base of the chromosphere a value of  $n_2 = 1.74 \times 10^{11}$  electrons per cubic centimeter is recommended. This electron density is based upon an interpretation of the Paschen series of the hydrogen spectrum. Wildt shows that the electron pressure in the region between these two data points follows the law

$$\frac{d \log p_e}{dh} = -0.20 \cdot 10^{-8} \text{ cm}^{-1},$$

where

$p_e$  = the electron pressure

$h$  = the height above the photosphere.

To obtain the final distribution used, these two distributions are smoothly joined in the region  $\rho = 1.015$  to  $\rho = 1.05$ . The result is shown as the heavy line in Figure 18, where the data of Wildt, Baumbach, Allen and van de Hulst is also shown. The data are tabulated in Table 5, where the densities chosen for this work are found in the last column.

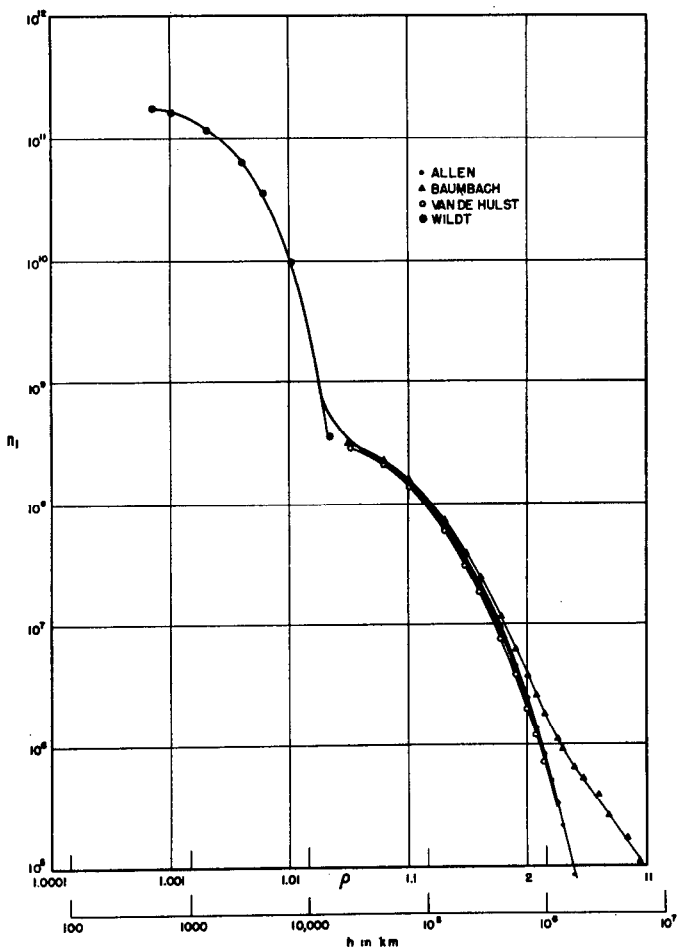


Figure 18 - Electron density,  $n_1$  electrons per CC, in the sun's atmosphere

As the first approximation to the temperature of the corona and chromosphere, the work of Alfvén<sup>49</sup> is used. Alfvén's conclusion was that the temperature of the corona near the base is  $\approx 10^6$  degrees Kelvin. The work of Alfvén was reviewed by Waldmeier,<sup>25</sup> who gives a

TABLE 5  
Corrected Electron Densities

$\rho$	$h_{km}$	$n_1$ - Electrons per cc x $10^{-6}$				Final Smooth $n_1$
		Baumbach	Van de Hulst	Allen	Wildt	
1.0	0	458	430	454		
1.0007	487				174,000	174,000
1.001	6,950					162,000
1.003	20,850					86,000
1.006	41,700					33,300.
1.01	69,500					9,800
1.02	139,000					615
1.021					355	
1.03	208,500	311	290			355
1.06	417,000	229	210			210
1.10	695,000	156	137	154		148
1.20	1,390,000	70.4	58	68.5		65
1.30	2,085,000	38.4	30	36.6		33
1.40	2,780,000	23.8	18	22.0		20
1.60	4,170,000	11.1	7.5	9.3		8.5
1.80	5,560,000	6.13	3.8	4.57		4.0
2.00	6,950,000	3.73	2.0	2.42		2.2
3.00	13,900,000	0.913	0.19	0.213		0.21

somewhat different temperature distribution, but since, as will be shown later, the temperatures so derived are to be considered only as a first approximation to the true temperature distribution and since also for this work we are principally concerned with the shorter radio wavelengths where the penetration is deeper, the temperature in the corona has only a small bearing on the interpretation of the results.

The procedure employed here is to compute the opacity of the sun's atmosphere for several wavelengths using the electron distribution of Figure 18 and an arbitrary temperature distribution whose limiting points are  $10^6$  degrees in the corona and 4830 degrees Kelvin. Since the principal absorption for any one wavelength comes from a rather shallow layer, as can be seen in Figure 25, then the equivalent temperature for each wavelength is associated with the depth at which the principal absorption occurs. The final temperature distribution of Figure 19, 20, and 23 was arrived at by a method of successive approximations in which an allowance was made for limb brightening which becomes excessive at 50 centimeters wavelength.

Figure 19 - The electron density  $n_1$ , the temperature  $T$ , and the absorption coefficient  $\kappa$  for the four wavelengths 8.5 millimeters, 3.14 centimeters, 10.6 centimeters, and 50 centimeters as a function of height above photosphere

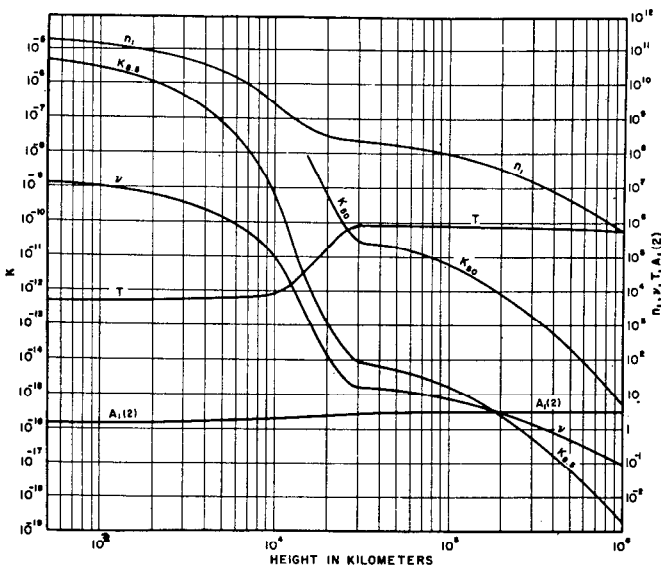
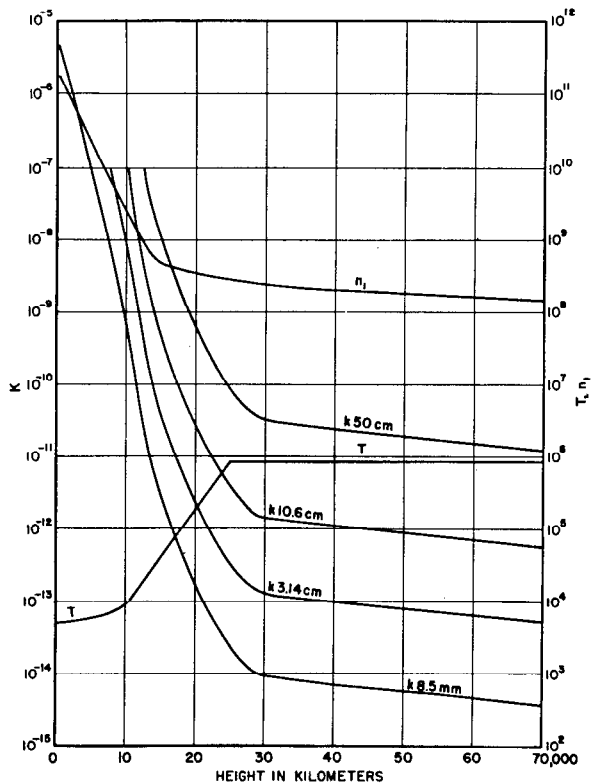


Figure 20 - The electron density  $n_1$ , the collision frequency  $\nu$ , the temperature  $T$ , the factor  $A_1(2)$ , and the absorption coefficient  $\kappa$  for 8.5 millimeters and 50 centimeters as a function of height above the photosphere

## Intensity of Radiation and Coefficient of Absorption

Let the absorption coefficient,  $K_\nu$ , be defined in this manner

$$I_\nu = I_{o_\nu} e^{-K_\nu h}, \quad (38)$$

where  $I_{o_\nu}$  = the intensity at the frequency  $\nu$  of radiation entering a uniform, absorbent slab of thickness  $h$ ;

$I_\nu$  = the intensity of the emergent radiation;

$e$  = the base of Napierian logarithms;

$K_\nu$  = the monochromatic absorption coefficient;

$h$  = the distance along the ray through the medium.

If in equation (38)  $K_\nu$  is constant over the path of the integration, then

$$\tau_\nu = K_\nu h .$$

Thus in equation (38) with the restriction that  $K_\nu$  be constant over the interval considered

$$I_\nu = I_{o_\nu} e^{-K_\nu h} = I_{o_\nu} e^{-\tau_\nu}. \quad (39)$$

The power absorbed in the medium is

$$I_{o_\nu} - I_\nu = I_{o_\nu} (1 - e^{-K_\nu h}) = a_\nu I_{o_\nu}, \quad (40)$$

where  $a_\nu$  is the fractional absorption and varies from 0 to 1

$$a_\nu = 1 - e^{-K_\nu h} = \frac{I_{o_\nu} - I_\nu}{I_{o_\nu}} . \quad (41)$$

Since the entire analysis deals with monochromatic emission and absorption, the subscript  $\nu$  will be dropped and used only where it is necessary to distinguish between the effects at two different wavelengths. The variation in  $K$  through the sun's atmosphere cannot be described by a simple analytic expression, so it is better to sum the absorptions rather than to integrate. This approach will be used to obtain a solution for the transfer equation. Equation (38) without the subscripts is written

$$I = I_0 e^{-Kh}. \tag{42}$$

Figure 21 represents the path of a ray travelling to the right. The path is broken up into elemental units, each  $\Delta h$  long. The elements are numbered successively from 1 through  $n$ , starting at the left. Let  $I_{rs}$  be the intensity of the radiation emitted by the  $r^{\text{th}}$  element

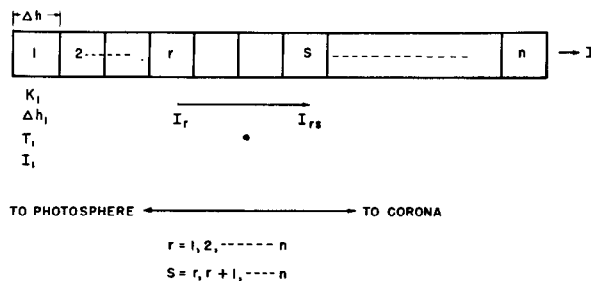


Figure 21 - Construction for analyzing the contributions to the total intensity

measured at the point where it leaves the  $s^{\text{th}}$  element, where  $s > r$ . Then using equation (42),

$$I_{12} = I_1 e^{-K_2 \Delta h_2} \tag{43}$$

where  $K_r$  is the mean absorption in the  $r^{\text{th}}$  element. Hence

$$I_{13} = I_{12} e^{-K_3 \Delta h_3} = I_1 e^{-K_2 \Delta h_2 - K_3 \Delta h_3}, \tag{44}$$

and

$$I_{1n} = I_1 e^{-\sum_{s=2}^n K_s \Delta h_s}. \quad (45)$$

Therefore

$$I_{rn} = I_r e^{-\sum_{s=r+1}^n K_s \Delta h_s}. \quad (46)$$

If  $I$  is written as the sum of the intensities of the emergent radiation of all elements after passing through the  $n^{\text{th}}$  element, then  $I$  is the intensity of the emergent radiation. Then

$$I = \sum_{r=1}^n I_{rn} = \sum_{r=1}^n I_r e^{-\sum_{s=r+1}^n K_s \Delta h_s}. \quad (47)$$

#### The Equivalent Temperature

Kirchoff's law states that, at a given temperature and wavelength  $\frac{E}{a} = e_\lambda$ , a constant independent of the nature of the body.  $E = \pi I$  is the rate of radiation emission in the small wavelength region around  $\lambda$  from unit surface of the hot body, where  $a$  is the absorption for rays of the same wavelength falling on the body and  $e_\lambda$  is the rate of emission from unit surface of a black body at the given temperature and wavelength.

The flux in a given direction and in the wavelength region  $d\lambda$  is  $i_\lambda d\lambda = \frac{e_\lambda}{\pi} d\lambda$ . From equation (13):  $i_\lambda d\lambda = \frac{2ckT}{\lambda^4} d\lambda$ . For each of our elements  $a$  has the value  $1 - e^{-K_r \Delta h_r}$  and using Kirchoff's law, the intensity of the emission from the  $r^{\text{th}}$  element is

$$I_r d\lambda = a_r i_{\lambda_r} d\lambda = (1 - e^{-K_r \Delta h_r}) \frac{2ckT_r}{\lambda^4} d\lambda. \quad (48)$$

By defining the equivalent temperature,  $T_e$ , so that  $T_e$  is the temperature of the equivalent black body radiating with the intensity  $I$ , then

$$I_r = \frac{2ckT_{e_r}}{\lambda^4}. \quad (49)$$

From (48) and (49)

$$T_{e_r} = (1 - e^{-K_r \Delta h_r}) T_r. \quad (50)$$

Making the substitution for  $I_r$  according to equation (48) in equation (47) and writing  $I = \frac{2ckT_e}{\lambda^4}$ , then dividing by the common factor  $\frac{2ck}{\lambda^4}$ :

$$T_e = \sum_{r=1}^n (1 - e^{-K_r \Delta h_r}) T_r e^{-\sum_{s=r+1}^n K_s \Delta h_s}. \quad (51)$$

The equation is used to compute the equivalent temperature.

Referring to the definition of  $a$  in equation (41), this may be written

$$T_e = \sum_{r=1}^n a_r T_r (1 - a_{n_{r+1}}) = \sum_{r=1}^n (a_r T_r - a_r a_{n_{r+1}} T_r), \quad (52)$$

where  $a_{n_{r+1}}$  is the total absorption of the ray after it leaves the  $r^{\text{th}}$  element,  $a_{n_{r+1}}$  could be written as the product of all  $a_s$  for values of  $s$  taken from  $r+1$  to  $n$ . Equation (52) was written out to clarify the meaning of equation (51). In equation (52), for any chosen value of  $r$  the first term on the right is the emission of that element, the second term the absorption in subsequent elements. In the sum, the first term on the right is due to the emission of the column as a whole; the second term is a correcting term and takes into consideration the absorption of each unit of the radiation by the over-lying layers.

Equation (51) may be re-arranged to facilitate computation:

$$\begin{aligned}
 T_e &= \sum_{r=1}^n T_r \left( e^{-\sum_{s=r+1}^n K_s \Delta h_s} - e^{-K_r \Delta h_r} e^{-\sum_{s=r+1}^n K_s \Delta h_s} \right) \\
 &= \sum_{r=1}^n T_r \left( e^{-\sum_{s=r+1}^n K_s \Delta h_s} - e^{-\sum_{s=r}^n K_s \Delta h_s} \right) .
 \end{aligned}
 \tag{53}$$

The two terms in parenthesis are successive terms in one column of the calculations.

To compute the equivalent temperature of the solar atmosphere using these relations, first determine from the computed values of  $K$  that  $h$  for which

$$\sum K_s \Delta h_s \approx 1.$$

This defines approximately the depth of maximum penetration and indicates the region over which the summation is to be performed. For a better solution it will be necessary to carry the summation somewhat deeper than this relation indicates.

### The Optical Depth

To arrive at an expression for the optical depth of the sun's atmosphere, it is necessary to determine how the absorption coefficient  $K$  varies with height in an atmosphere where the number of electrons per cubic centimeter and the kinetic temperature of the electrons vary with height. Since in any region where the absorption is appreciable there are many electrons per cubic wavelength (always greater than  $10^5$  per cubic wavelength in those regions of the corona where there is significant absorption), a macroscopic rather than microscopic approach is indicated. The macroscopic approach follows a method used in the analysis of our ionosphere where an expression for the dielectric constant of the electron gas is developed. See,

for example, Mimno<sup>50</sup>. The microscopic approach follows Kramers,<sup>28</sup> who investigated the continuous absorption to be expected when an electron makes a free-free transition with an ionized molecule. The free-free transition is one in which the electron approaches the ion from a great distance on a hyperbolic orbit and leaves on a second orbit of lower energy; the difference in energy of the approaching and receding orbits being the energy radiated at the collision. Kramer's analysis follows classical mechanics. Gaunt,<sup>29</sup> Menzel and Pekeris,<sup>30</sup> and others have applied quantum mechanics to the analysis and have arrived at an expression for the absorption coefficient which is very similar to that determined by following a non-quantum treatment, as has been demonstrated by Martyn,<sup>21</sup> among others. The derivation of the absorption coefficient on macroscopic grounds presented here follows Martyn. The final expression for the absorption coefficient differs from his equation (8) only because of an obvious typographical error in his work. The equation defining optical depth is

$$T = \int_0^h K dh.$$

It will be shown that the absorption coefficient  $K$  is a function of the number density of the electrons, the kinetic temperature of the electrons, and of the frequency. The frequency is at our disposal, but the number density of the electrons and the temperature are functions of the height. Using summation methods, the expression for the optical depth becomes

$$T = \sum_{i=1}^n K_i \Delta h_i. \quad (54)$$

#### Refractive Index and Collision Frequency

For an electron gas the refractive index is

$$\mu^2 = 1 - \frac{4\pi e^2 n_2}{m(\omega^2 + \nu^2)} \approx 1 - \frac{4\pi e^2 n_2}{m\omega^2}, \quad (55)$$

when  $v^2 \ll \omega^2$

and where  $\mu$  = the refractive index at the angular frequency  
 $e$  = the electronic charge  
 $n_2$  = the number density of the electrons  
 $m$  = the mass of electrons  
 $2\pi f = \omega$  = the angular frequency  
 $\nu$  = the collision frequency.

The refractive index is seen to be a function only of the number density of the electrons and of the frequency, and thus may be calculated for various layers in the sun's atmosphere. Table 6 shows the variation in the refractive index with wavelength over the critical regions. The data of Table 6 are plotted in Figure 22. In the table both the refractive index  $\mu$  and the quantity  $1-\mu^2$  are tabulated. It should be observed from Table 6 and Figure 22 that the dielectric constant is very close to unity for the heights above the photosphere covered in Table 6. These heights are so chosen because,

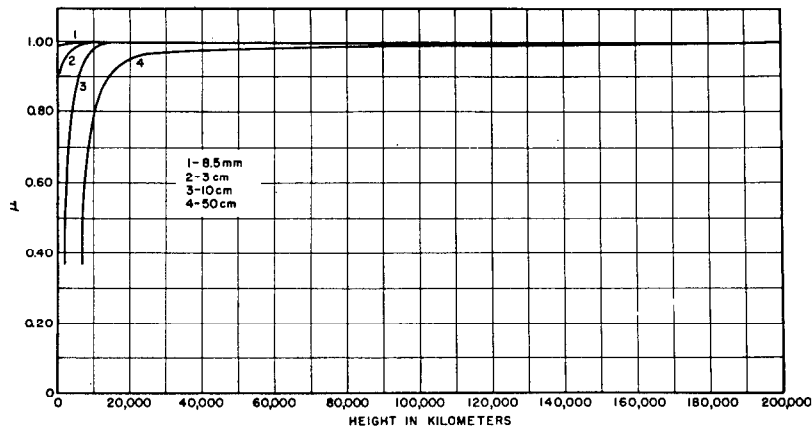


Figure 22 - The index of refraction at four different radio wavelengths plotted against height above the photosphere

as will be demonstrated, it is here that the regions responsible for the emission of radiation at these various wavelengths are located. Thus the approximation can be made, where convenient, in the later equations that, over the region of interest, the dielectric constant is approximately unity.

In order to compute  $\nu$ , the frequency of collisions of electrons with ions, it is necessary first to determine the mean-free

TABLE 6  
Variation of Index of Refraction,  $\mu$ , and  $1-\mu^2$  with  
Wavelength and Height above the Photosphere

$h$ Kilometers	8.5 MM		3.14 CM		10.6 CM		50 CM	
	$1-\mu^2$	$\mu$	$1-\mu^2$	$\mu$	$1-\mu^2$	$\mu$	$1-\mu^2$	$\mu$
500	$1.12 \times 10^{-2}$	0.994	$1.53 \times 10^{-1}$	0.910				
1000	$8.72 \times 10^{-3}$	0.996	$1.19 \times 10^{-1}$	0.939				
2000	$5.5 \times 10^{-3}$	0.997	$7.51 \times 10^{-2}$	0.962	$8.55 \times 10^{-1}$	0.371		
4000	$2.34 \times 10^{-3}$	0.999	$3.19 \times 10^{-2}$	0.984	$3.64 \times 10^{-1}$	0.797		
6000	$9.75 \times 10^{-4}$	1.000	$1.33 \times 10^{-2}$	0.993	$1.52 \times 10^{-1}$	0.911		
10,000	$1.64 \times 10^{-4}$	1.000	$2.24 \times 10^{-3}$	0.999	$2.55 \times 10^{-2}$	0.987	$5.67 \times 10^{-1}$	0.803
20,000	$2.38 \times 10^{-5}$	1.000	$3.25 \times 10^{-4}$	1.000	$3.70 \times 10^{-3}$	0.998	$8.23 \times 10^{-2}$	0.958
28,000	$1.70 \times 10^{-5}$	1.000	$2.32 \times 10^{-4}$	1.000	$2.64 \times 10^{-3}$	0.999	$5.88 \times 10^{-2}$	0.970
30,000	$1.63 \times 10^{-5}$	1.000	$2.22 \times 10^{-4}$	1.000	$2.53 \times 10^{-3}$	0.999	$5.63 \times 10^{-2}$	0.971
70,000	$9.56 \times 10^{-6}$	1.000	$1.30 \times 10^{-4}$	1.000	$1.49 \times 10^{-3}$	0.999	$3.30 \times 10^{-2}$	0.983
139,000	$4.20 \times 10^{-6}$	1.000	$5.73 \times 10^{-5}$	1.000	$6.53 \times 10^{-4}$	1.000	$1.45 \times 10^{-2}$	0.993
278,000	$1.29 \times 10^{-6}$	1.000	$1.76 \times 10^{-5}$	1.000	$2.01 \times 10^{-4}$	1.000	$4.46 \times 10^{-3}$	0.998
417,000	$5.49 \times 10^{-7}$	1.000	$7.49 \times 10^{-6}$	1.000	$8.54 \times 10^{-5}$	1.000	$1.90 \times 10^{-3}$	0.999
695,000	$1.42 \times 10^{-7}$	1.000	$1.94 \times 10^{-6}$	1.000	$2.75 \times 10^{-5}$	1.000	$4.91 \times 10^{-4}$	1.000
1,390,000	$1.36 \times 10^{-8}$	1.000	$1.86 \times 10^{-7}$	1.000	$2.11 \times 10^{-6}$	1.000	$4.70 \times 10^{-5}$	1.000

NAVAL RESEARCH LABORATORY

path of the electron and then the collision cross section of the electron and proton. Fortunately Cowling<sup>51</sup> and Chapman and Cowling<sup>52</sup> have considered this problem in a form applicable to the theory developed here. The situation is complicated by the fact that in terms of our laboratory experience the electrons are relatively slow moving, thus direct experimental determinations of the collision cross section of electrons and protons have not been made. There is a strong attractive force between the electrons and protons which Chapman and Cowling have considered and which leads to a rather large value for the cross section.

Cowling's expression<sup>51</sup> for the effective collision interval in a completely ionized binary gas is given in his equation (35). It is

$$T_{gr} = \frac{m_g m_r (n_g + n_r)}{(\rho_g + \rho_r) k T} D_{gr}, \quad (56)$$

where  $T_{gr}$  is the effective collision interval for the molecules of the  $g^{\text{th}}$  and  $r^{\text{th}}$  gases. This  $T_{gr}$  should not be confused with  $\tau$ , the optical depth used elsewhere in this report.  $T_{gr}$  will be dropped from the equations shortly.  $m_s$  is the mass of a molecule of the  $s^{\text{th}}$  gas.  $n_s$  is the number density of the molecules of the  $s^{\text{th}}$  gas.  $\rho_s$  is the density of the  $s^{\text{th}}$  gas in grams per cubic centimeter.  $D_{gr}$  is the coefficient of mutual diffusion of the  $g^{\text{th}}$  and  $r^{\text{th}}$  gases in the absence of other gases;  $k$  and  $T$  are the Boltzmann constant and the temperature in degrees Kelvin.

Chapman and Cowling<sup>52</sup> evaluated  $D_{gr}$  for a gas, the large proportion of whose molecules are ionized and in which electrostatic forces play a dominant part in the encounters. The attractive force is assumed to satisfy the equation

$$F = \frac{e_1 e_2}{r^2}$$

where  $e_1$  and  $e_2$  are the charges on the two molecules and  $r$  is the distance between them. Under these conditions it is shown that the coefficient of mutual diffusion becomes

$$[D_{12}]_1 = \frac{3}{16n} \left( \frac{2kT}{\pi M_1 M_2 m_0} \right)^{\frac{1}{2}} \cdot \left( \frac{2kT}{e_1 e_2} \right)^2 \frac{1}{A_1(2)}. \quad (57)$$

where  $[ ]_1$  refers to a first approximation  
 $n = \sum \eta_s =$  the total number of molecules per cubic centimeter  
 $k =$  as before  
 $T =$  as before  
 $m_0 = m_1 + m_2.$

where  $m_1$  and  $m_2$  have the same meaning as before,

$$M_1 = \frac{m_1}{m_0}$$

$$M_2 = \frac{m_2}{m_0}$$

$e_1$  and  $e_2 =$  the charge on the individual ions of the two gases,

$$A_1(2) = \log_e \left[ 1 + \left( \frac{4dkT}{e_1 e_2} \right)^2 \right]$$

$d =$  the mean distance between pairs of neighboring molecules.

Hence

$$d \approx n^{-\frac{1}{3}}$$

The number of collisions per molecule per second  $v_{qr}$  will be

$$v_{qr} = \frac{1}{T_{qr}} \tag{58}$$

Putting equation (56) in (58) and substituting for  $D_{12}$  from equation (57), the total expression for the collision frequency  $v_{qr}$  is obtained. Since the gas is a binary gas, we can now dispense with many of the subscripts. Set  $q=1$  and let it refer to the heavy ion of charge  $e_1$ ; and set  $r=2$ , letting it refer to the electron of charge  $e_2$ . Since we are assuming an ionized hydrogen gas, then  $e_1 = -e_2$ , and since the individual charge appears in the equation always in an even power, we may write  $e$  for the charge. Equation (58) then becomes

$$v \equiv v_{12} = \frac{1}{T_{12}} = \frac{(\rho_1 + \rho_2)kT}{m_1 m_2 (n_1 + n_2)} \cdot \frac{16n}{3} \cdot \left( \frac{\pi m_0 M_1 M_2}{2kT} \right)^{\frac{1}{2}} \left( \frac{e^2 e_2}{2kT} \right)^2 \cdot A_1(2). \tag{59}$$

To simplify, consider a part of equation (59):

$$\frac{\rho_1 + \rho_2}{m_1 m_2 (n_1 + n_2)} n (m_0 M_1 M_2)^{\frac{1}{2}} \quad (59a)$$

When the relations

$$\begin{aligned} m_0 &= m_1 + m_2, \\ n &= n_1 + n_2, \\ M_1 M_2 &= \frac{m_1 m_2}{m_0^2}, \\ \rho_s &= m_s n_s \end{aligned}$$

are considered, (59a) becomes

$$\frac{m_1 n_1 + m_2 n_2}{(m_1^2 m_2 + m_1 m_2^2)^{\frac{1}{2}}} \quad (59b)$$

but  $m_2 \ll m_1$ ; therefore (59b) reduces to

$$\frac{n_1}{\sqrt{m_2}} \quad (n_1 = n_2 \text{ since the gas is electrically neutral}). \quad (59c)$$

Equation (59) now becomes, when (59a) is replaced by (59c)

$$V = \frac{n_1}{\sqrt{m_2}} kT \frac{16}{3} \left( \frac{\pi}{2kT} \right)^{\frac{1}{2}} \frac{e^4}{(2kT)^2} A_1(2).$$

Collecting terms:

$$V = \frac{2\sqrt{2\pi} n_1 e^4}{3m_2^{\frac{1}{2}} (kT)^{\frac{3}{2}}} A_1(2). \quad (60)$$

The Absorption Coefficient

The expression for the classical absorption coefficient is

$$K = \frac{\nu}{c\mu} \frac{4\pi n_1 e^2}{m\omega^2}, \quad (61)$$

or using equation (55)

$$K = \frac{\nu}{c} \frac{1-\mu^2}{\mu}. \quad (62)$$

The complete expression for  $K$  becomes upon substituting in equation (61) the value of  $\nu$  given in equation (60),

$$K = \frac{8\sqrt{2} \pi^{\frac{3}{2}} n_1^2 e^6}{3c(mkT)^{\frac{3}{2}} \mu \omega^2} \log_e \left[ 1 + \left( \frac{4dkT}{e^2} \right)^2 \right]. \quad (63)$$

To further simplify this expression:

- (a)  $d$  was defined as being equal to  $n^{-\frac{1}{3}}$ . Since  $n = 2n_1$ , then

$$d = \frac{1}{\sqrt[3]{2n_1}},$$

- (b) The expression in the square brackets under the logarithm in (63) is very much greater than unity,

(c)  $\omega^2 = (2\pi f)^2 = \left( \frac{2\pi c}{\lambda} \right)^2.$

On making these substitutions (63) becomes

$$K = \frac{2\sqrt{2} \lambda^2 n_1^2 e^6}{3\sqrt{\pi} \mu c^3 (mkT)^{\frac{3}{2}}} \log_e \left( \frac{4kT}{e^2 \sqrt[3]{2n_1}} \right)^2. \quad (64)$$

## Variation in the Absorption Coefficient with Height and Wavelength

Since the function  $A_1(z)$  is slowly varying, then it can be said that

$$K = K' \frac{\lambda^2 n_1^2}{\mu T^{\frac{3}{2}}}. \quad (65)$$

Everything in  $K'$  is sensibly constant. It is sufficient then to compute  $K$  for some one wavelength and then correct it in the following manner to obtain the absorption for any other wavelength.

$$K_2 = K_1 \left( \frac{\lambda_2}{\lambda_1} \right)^2 \frac{\mu_1}{\mu_2} \quad (66)$$

where  $K_1$  and  $\mu_1$  are the absorption coefficient and refractive index computed for a wavelength  $\lambda_1$ ,  $K_2$  and  $\mu_2$  correspond to the wavelength  $\lambda_2$ .

For purposes of calculation reassemble the various formulas and re-arrange:

From (55)

$$1 - \mu^2 = \frac{4\pi n_1 e^2}{m\omega^2}, \quad (67)$$

$$\mu = \left( 1 - \frac{4\pi n_1 e^2}{m\omega^2} \right)^{\frac{1}{2}}. \quad (68)$$

From (57)

$$A_1(z) = 2 \log_e \frac{4kT}{e^2 \sqrt{2n_1}} \quad (69)$$

from (60)

$$\nu = \frac{2\sqrt{2}\pi n_1 e^4}{3\sqrt{m_2} (kT)^{\frac{3}{2}}} A_1(2); \quad (70)$$

from (62)

$$K = \frac{\nu}{c} \frac{1-\mu_2}{\mu}. \quad (71)$$

The numerical values of the electron density, the temperature, the refractive index, the factor  $A_1(2)$ , the collision frequency  $\nu$ , and the absorption coefficient, all computed for a wavelength of 8.5 millimeters for the region of interest in the sun's atmosphere, are given in Table 7 and are shown in Figure 20.

#### Comparison of Theoretical and Observed Equivalent Temperatures of the Sun

In computing the values of the various quantities given in Table 7 the values of  $n_1$  for the various heights were taken from Figure 18; the values of  $T$  for heights above 50,000 kilometers were taken from Alfvén.<sup>49</sup> Below 50,000 kilometers the temperature was assumed to decrease exponentially to a value of 4830° Kelvin at the photosphere. A series of calculations was performed following this assumption which led to computed values of  $T_e$  for several wavelengths. These computed values did not agree with the observed equivalent temperatures of Figure 7, being too low for the longer wavelengths and too high for the shorter. The assumed temperature distribution low in the atmosphere was then readjusted through several approximations to that shown in curve "B" of Figure 23. The values of temperature in the third column of Table 7 are taken from Figures 20 and 23.

The absorption coefficients for the four wavelengths 8.5 millimeters, 3.14 centimeters, 10.6 centimeters, and 50 centimeters were computed and are given in Table 8. The coefficient for 8.5 millimeters was computed first using equation (64). The values of  $n_1$  and  $T$  were obtained from Figures 18 and 23. The coefficients for the other wavelengths were computed from the coefficient for 8.5 millimeters using equation (66). These coefficients are shown in Figure 19.

TABLE 7  
The Calculation of the Absorption Coefficient as a Function of Height  
above the Photosphere

h km	$n_1$ per cc	$\sigma^T$ K	$T/\sqrt{2n}$	$A_1(2)$	$n_1/T^2$	$\sqrt{\text{Collisions/}}sec/Molecule$	K 8.5 per cm
500	$1.73 \times 10^{11}$	$5.07 \times 10^3$	$7.23 \times 10^{-1}$	14.92	$4.81 \times 10^5$	$1.30 \times 10^7$	$4.82 \times 10^{-6}$
1,000	$1.35 \times 10^{11}$	$5.13 \times 10^3$	$7.94 \times 10^{-1}$	15.11	$3.69 \times 10^5$	$1.01 \times 10^7$	$2.94 \times 10^{-6}$
2,000	$8.52 \times 10^{10}$	$5.24 \times 10^3$	$9.45 \times 10^{-1}$	15.46	$2.24 \times 10^5$	$6.29 \times 10^6$	$1.15 \times 10^{-6}$
4,000	$3.63 \times 10^{10}$	$5.75 \times 10^3$	$1.38 \times 10^0$	16.21	$8.33 \times 10^4$	$2.45 \times 10^6$	$1.91 \times 10^{-7}$
6,000	$1.51 \times 10^{10}$	$6.14 \times 10^3$	$1.97 \times 10^0$	16.93	$3.12 \times 10^4$	$9.58 \times 10^5$	$3.11 \times 10^{-8}$
10,000	$2.54 \times 10^9$	$8.32 \times 10^3$	$4.84 \times 10^0$	18.90	$3.36 \times 10^3$	$1.14 \times 10^5$	$6.26 \times 10^{-10}$
13,900	$6.20 \times 10^8$	$2.88 \times 10^4$	$2.67 \times 10^1$	22.13	$1.27 \times 10^2$	$5.10 \times 10^3$	$6.88 \times 10^{-12}$
20,000	$3.68 \times 10^8$	$1.80 \times 10^5$	$2.00 \times 10^2$	26.76	$4.82 \times 10^0$	$2.34 \times 10^2$	$1.86 \times 10^{-13}$
28,000	$2.63 \times 10^8$	$8.40 \times 10^5$	$1.04 \times 10^3$	29.46	$3.42 \times 10^{-1}$	$1.83 \times 10^1$	$1.04 \times 10^{-14}$
34,750	$2.30 \times 10^8$	$8.40 \times 10^5$	$1.09 \times 10^3$	29.56	$2.99 \times 10^{-1}$	$1.60 \times 10^1$	$7.94 \times 10^{-15}$
70,000	$1.48 \times 10^8$	$8.40 \times 10^5$	$1.26 \times 10^3$	29.85	$1.92 \times 10^{-1}$	$1.04 \times 10^1$	$3.31 \times 10^{-15}$
139,000	$6.50 \times 10^7$	$8.40 \times 10^5$	$1.66 \times 10^3$	30.39	$8.44 \times 10^{-2}$	$4.65 \times 10^0$	$6.51 \times 10^{-16}$
278,000	$2.00 \times 10^7$	$8.10 \times 10^5$	$2.37 \times 10^3$	31.10	$2.74 \times 10^{-2}$	$1.54 \times 10^0$	$6.62 \times 10^{-17}$
417,000	$8.5 \times 10^6$	$7.30 \times 10^5$	$2.84 \times 10^3$	31.47	$1.37 \times 10^{-2}$	$7.82 \times 10^{-1}$	$1.43 \times 10^{-17}$
695,000	$2.2 \times 10^6$	$6.70 \times 10^5$	$4.08 \times 10^3$	32.19	$4.00 \times 10^{-3}$	$2.33 \times 10^{-1}$	$1.10 \times 10^{-18}$
1,390,000	$2.1 \times 10^5$	$5.60 \times 10^5$	$7.49 \times 10^3$	33.42	$5.00 \times 10^{-4}$	$3.03 \times 10^{-2}$	$1.37 \times 10^{-20}$

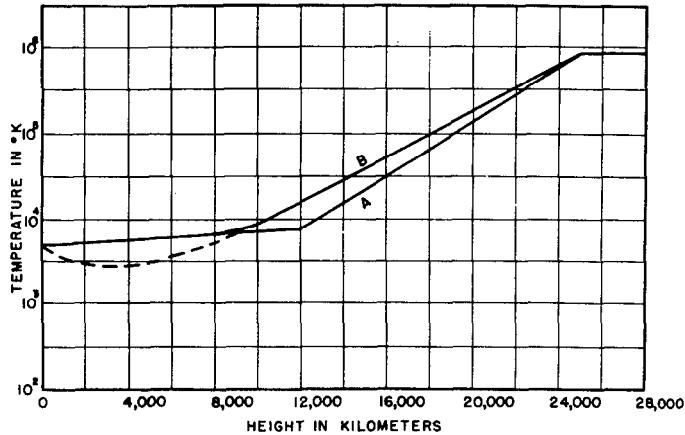
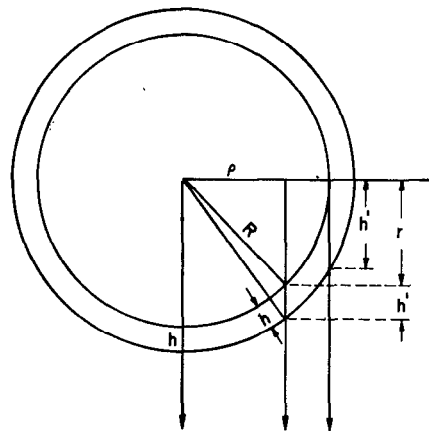


Figure 23 - Temperature at various heights above the photosphere

The height in the sun's atmosphere at which the optical depth becomes unity and the equivalent temperature at the center and the limb for 8.5 millimeters, 3.14 centimeters, 10.6 centimeters, and 50 centimeters has been computed. Since this report is particularly concerned with the 8.5 millimeter measurement, principal emphasis has been put there, but the other wavelengths have been included to provide a better understanding of the variation of temperature with height, as will shortly be pointed out. The computation is performed in Tables 10 through 17 (pp. 66 through 74) where the summation is continued to the point where  $e^{-\Sigma K \Delta h}$  becomes  $\ll 1$  and the contribution to the equivalent temperature negligible.

Figure 24 is the construction used to aid in the calculation of the optical depth at the limb. Since this construction will be used later for regions that are neither at the center nor at the limb, the general derivation will be given. Using the notation of Figure 24,



$$(r+h')^2 + \rho^2 = (R+h)^2, \quad (72)$$

$$R^2 = r^2 + \rho^2. \quad (73)$$

Figure 24 - Construction for computing the ray path length in the sun's atmosphere

TABLE 8  
The Absorption Coefficients for 8.5 mm, 3.14 cm, 10.6 cm,  
and 50 cm at Various Heights above the Photosphere

h km	T °K	K 8.5mm per cm	K 3.14 cm per cm	K 10.6 cm per cm	K 50 cm per cm
5,000					
5,500	$5.92 \times 10^3$	$6.55 \times 10^{-8}$			
6,000	$6.01 \times 10^3$	$4.24 \times 10^{-8}$			
6,500	$6.14 \times 10^3$	$2.75 \times 10^{-8}$			
7,000	$6.24 \times 10^3$	$1.88 \times 10^{-8}$			
7,500	$6.38 \times 10^3$	$1.13 \times 10^{-8}$			
8,000	$6.51 \times 10^3$	$6.37 \times 10^{-9}$	$8.69 \times 10^{-8}$		
8,500	$6.64 \times 10^3$	$4.36 \times 10^{-9}$	$5.95 \times 10^{-8}$		
9,000	$6.92 \times 10^3$	$2.63 \times 10^{-9}$	$3.59 \times 10^{-8}$		
9,500	$7.60 \times 10^3$	$1.52 \times 10^{-9}$	$2.07 \times 10^{-8}$		
10,000	$8.10 \times 10^3$	$8.66 \times 10^{-10}$	$1.18 \times 10^{-8}$		
10,500	$9.20 \times 10^3$	$4.49 \times 10^{-10}$	$6.13 \times 10^{-9}$		
11,000	$1.07 \times 10^4$	$2.27 \times 10^{-10}$	$3.10 \times 10^{-9}$	$5.27 \times 10^{-8}$	
11,500	$1.29 \times 10^4$	$1.09 \times 10^{-10}$	$1.49 \times 10^{-9}$		
12,000	$1.45 \times 10^4$	$5.49 \times 10^{-11}$	$7.49 \times 10^{-10}$	$1.28 \times 10^{-8}$	
12,500	$1.70 \times 10^4$	$3.09 \times 10^{-11}$	$4.22 \times 10^{-10}$		
13,000	$1.95 \times 10^4$	$1.83 \times 10^{-11}$	$2.50 \times 10^{-10}$	$3.81 \times 10^{-9}$	$1.00 \times 10^{-7}$
13,500	$2.29 \times 10^4$	$1.09 \times 10^{-11}$	$1.49 \times 10^{-10}$		
14,000	$2.73 \times 10^4$	$6.62 \times 10^{-12}$	$9.03 \times 10^{-11}$	$1.36 \times 10^{-9}$	$3.16 \times 10^{-8}$
14,500	$3.16 \times 10^4$	$4.28 \times 10^{-12}$	$5.84 \times 10^{-11}$		
15,000	$3.71 \times 10^4$	$2.93 \times 10^{-12}$	$4.00 \times 10^{-11}$	$5.60 \times 10^{-10}$	$1.41 \times 10^{-8}$
16,000	$4.68 \times 10^4$	$1.89 \times 10^{-12}$	$2.58 \times 10^{-11}$	$2.94 \times 10^{-10}$	$7.03 \times 10^{-9}$
17,000	$6.46 \times 10^4$	$9.62 \times 10^{-13}$	$1.31 \times 10^{-11}$	$1.50 \times 10^{-10}$	$3.55 \times 10^{-9}$
18,000	$8.50 \times 10^4$	$5.85 \times 10^{-13}$	$7.98 \times 10^{-12}$	$9.10 \times 10^{-11}$	$2.14 \times 10^{-9}$
19,000	$1.20 \times 10^5$	$3.59 \times 10^{-13}$	$4.90 \times 10^{-12}$	$5.58 \times 10^{-11}$	$1.31 \times 10^{-9}$

TABLE 8 (Cont.)

h km	T °K	K 8.5mm per cm	K 3.14 cm per cm	K 10.6 cm per cm	K 50 cm per cm
19,000					
20,000	$1.55 \times 10^5$	$2.22 \times 10^{-13}$	$3.03 \times 10^{-12}$	$3.45 \times 10^{-11}$	$8.04 \times 10^{-10}$
22,000	$2.51 \times 10^5$	$1.10 \times 10^{-13}$	$1.50 \times 10^{-12}$	$1.71 \times 10^{-11}$	$3.96 \times 10^{-10}$
24,000	$4.60 \times 10^5$	$4.73 \times 10^{-14}$	$6.45 \times 10^{-13}$	$7.36 \times 10^{-12}$	$1.70 \times 10^{-10}$
26,000	$7.82 \times 10^5$	$2.26 \times 10^{-14}$		$3.51 \times 10^{-12}$	$8.07 \times 10^{-11}$
28,000	$8.4 \times 10^5$	$1.36 \times 10^{-14}$		$2.11 \times 10^{-12}$	$4.84 \times 10^{-11}$
30,000	$8.4 \times 10^5$	$9.60 \times 10^{-15}$		$1.49 \times 10^{-12}$	$3.41 \times 10^{-11}$
32,000	$8.4 \times 10^5$	$8.77 \times 10^{-15}$		$1.36 \times 10^{-12}$	
34,000	$8.4 \times 10^5$	$8.17 \times 10^{-15}$		$1.27 \times 10^{-12}$	$2.96 \times 10^{-11}$
36,000	$8.4 \times 10^5$	$7.70 \times 10^{-15}$		$1.20 \times 10^{-12}$	
38,000	$8.4 \times 10^5$	$7.31 \times 10^{-15}$		$1.14 \times 10^{-12}$	
40,000	$8.4 \times 10^5$	$6.98 \times 10^{-15}$		$1.08 \times 10^{-12}$	
35,000	$8.4 \times 10^5$				
40,000	$8.4 \times 10^5$	$7.20 \times 10^{-15}$			$2.55 \times 10^{-11}$
45,000	$8.4 \times 10^5$	$6.50 \times 10^{-15}$		$1.01 \times 10^{-12}$	$2.29 \times 10^{-11}$
50,000	$8.4 \times 10^5$	$5.93 \times 10^{-15}$		$9.22 \times 10^{-13}$	$2.09 \times 10^{-11}$
55,000	$8.4 \times 10^5$	$5.38 \times 10^{-15}$		$8.37 \times 10^{-13}$	$1.89 \times 10^{-11}$
60,000	$8.4 \times 10^5$	$4.77 \times 10^{-15}$		$7.42 \times 10^{-13}$	$1.70 \times 10^{-11}$
65,000	$8.4 \times 10^5$	$4.18 \times 10^{-15}$		$6.50 \times 10^{-13}$	$1.47 \times 10^{-11}$
70,000	$8.4 \times 10^5$	$3.58 \times 10^{-15}$		$5.57 \times 10^{-13}$	$1.26 \times 10^{-11}$
139,000	$8.4 \times 10^5$	$1.95 \times 10^{-15}$			$6.82 \times 10^{-12}$
278,000	$8.4 \times 10^5$	$3.53 \times 10^{-16}$			$1.22 \times 10^{-12}$
417,000	$8.1 \times 10^5$	$3.98 \times 10^{-17}$			$1.38 \times 10^{-13}$
695,000	$7.3 \times 10^5$	$7.55 \times 10^{-18}$			$2.61 \times 10^{-15}$
1,390,000	$6.7 \times 10^5$	$5.58 \times 10^{-19}$			$1.93 \times 10^{-16}$

Substituting (73) in (72),

$$2rh' + h'^2 = 2Rh + h^2 \quad . \quad (74)$$

Solving for  $h'$ ,

$$h' = -r + (r^2 + 2rh + h^2)^{\frac{1}{2}} \quad . \quad (75)$$

Thus at the limb where  $r = 0$  ,

$$h' = (2Rh + h^2)^{\frac{1}{2}} \quad . \quad (76)$$

In Tables 10 through 17 the value of  $h'$  for various values of  $h$  is calculated and the average absorption coefficient for the region between two successive values of  $h$  is written in, (for the central ray,  $h' = h$ ); then the product  $K\Delta h'$  is taken. The following columns carry out the calculation indicated by equation (51) where finally the sum of the column headed  $C \cdot B_{r+1}$  yields the equivalent temperature. An inspection of the column  $\sum K\Delta h$  shows the depth where  $\tau = 1$ . Note that it is necessary to carry the calculation deeper than this point for there are still appreciable contributions to the total emission as can be seen from the  $C \cdot B_{r+1}$  column. To present a graphical picture of the contributions of the various layers to the total emission for the central ray at the several wavelengths, the contribution to the total emission by a layer 1,000 kilometers thick at each value of  $h$  used in the tables was computed. The numerical value for this contribution is given in the column next to the column headed  $C \cdot B_{r+1}$  from which it is computed. The results are shown in Figures 25 and 26.

In Figure 25 the results for all four wavelengths are plotted to the same scale; in Figure 26 the result for 8.5 millimeters is plotted to a larger scale. It is clear that at the shorter wavelengths the emission comes from a relatively thin shell deep in the atmosphere, whereas at the longer wavelengths the emission arises in thick layers of the atmosphere with the outer layers making a measurable contribution. This indicates that the sun would appear to have a sharp boundary at the shorter wavelengths but a very hazy one at the longer wavelengths. In addition Table 9 shows that there is little limb brightening at the shorter wavelengths but severe brightening at the

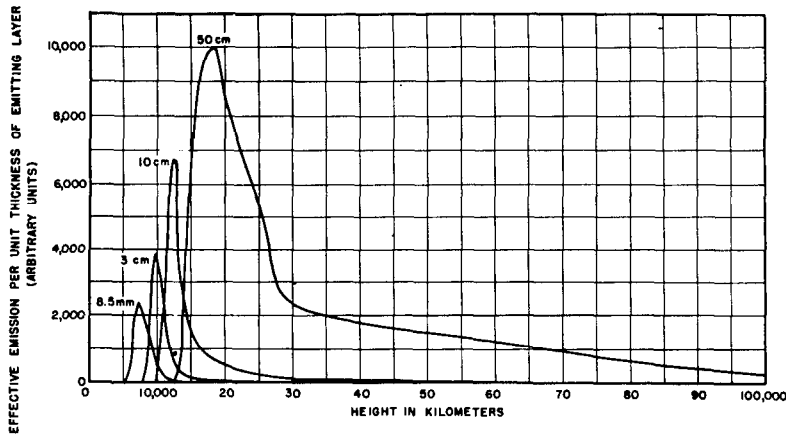


Figure 25 - The contribution of the various layers of the sun's atmosphere, at indicated heights above the photosphere, to the total equivalent temperature for the four wavelengths 8.5 millimeters, 3.14 centimeter, 10.6 centimeters, and 50 centimeters

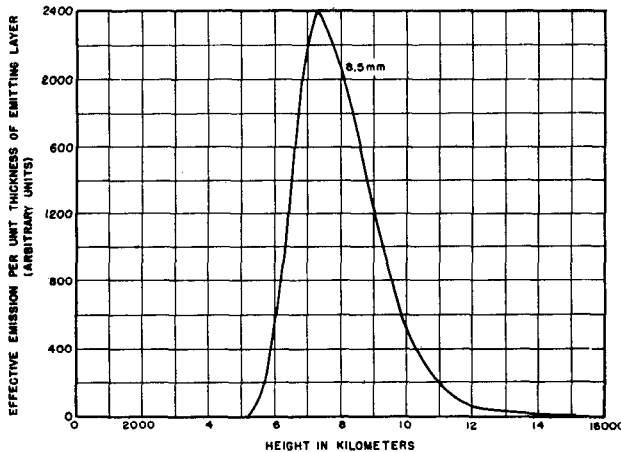


Figure 26 - The contribution of the various layers of the sun's atmosphere, at indicated heights above the photosphere, to the total equivalent temperature for the wavelength 8.5 millimeters

longer. If the computations had been carried out for even longer wavelengths where the optical depth of unity falls well out in the corona, then there would be limb darkening—the sun would appear as a large hazy ball with an ill-defined edge.

TABLE 9  
The Theoretical Equivalent Temperature and Height Above the  
Photosphere for which  $\tau = 1$  for Various Wavelengths

Wavelength	Equivalent Temperature ° K		Height for $\tau = 1$ km	
	Center	Limb	Center	Limb
8.5 mm	6804	8250	7600	9250
3.14 cm	9980	15560	9900	11200
10.6 cm	25950	53500	12400	13900
50 cm	212000	437000	16600	20800

In the first section of this report, the measured equivalent temperature of the sun at the various wavelengths is given. If we consider the equivalent temperature as measured at the radio wavelengths 8.5 millimeters, 3.14 centimeters, 10.6 centimeters, and 50 centimeters, it clearly must lie between the computed values for the center and limb. The first few columns of Tables 10 through 17 determine where in the atmosphere the main body of the emission originates. The temperature distribution must be so assigned that the computed values of the equivalent temperature agree with the observed values. In addition the fact that little limb brightening is observed to exist at 8.5 millimeters must also be considered. Applying this criterion, it is seen why the severe modification of the temperature distribution assumed earlier was made. It is obvious that the temperature remains sensibly constant and near the photospheric temperature through most of the chromosphere, then rises rapidly as the transition from chromosphere to corona is made.

TABLE 10

Calculation of the Equivalent Temperature for the Central Ray at 8.5 Millimeters Wavelength

r	h km	T ° K	K cm	Δh cm	KΔh	A 1-e <sup>-KΔh</sup>	ΣKΔh	B e <sup>-ΣKΔh</sup>	C T·A °K	C·B <sub>r+1</sub> % K	C·B <sub>r+1</sub> Δh <sub>km</sub> ° K	1000
1	5000	5.92x10 <sup>3</sup>	6.55x10 <sup>-8</sup>	5x10 <sup>7</sup>	3.275	0.9622	9.1082	1.108x10 <sup>-4</sup>	5.696x10 <sup>3</sup>	1.668x10 <sup>0</sup>	3.34x10 <sup>0</sup>	
2	5500	6.01	4.24	5x10 <sup>7</sup>	2.120	0.87997	5.8332	2.929x10 <sup>-4</sup>	5.290x10 <sup>3</sup>	1.291x10 <sup>2</sup>	2.58x10 <sup>2</sup>	
3	6000	6.14	2.75	5x10 <sup>7</sup>	1.375	0.7472	3.7132	2.440x10 <sup>-2</sup>	4.588x10 <sup>3</sup>	4.427x10 <sup>2</sup>	8.85	
4	6500	6.24	1.88	5x10 <sup>7</sup>	0.9400	0.6094	2.3382	9.650x10 <sup>-2</sup>	3.803x10 <sup>3</sup>	9.395x10 <sup>2</sup>	1.88x10 <sup>3</sup>	
5	7000	6.38	1.13	5x10 <sup>7</sup>	0.5650	0.4316	1.3982	2.4705x10 <sup>-1</sup>	2.754x10 <sup>3</sup>	1.197x10 <sup>3</sup>	2.39	
6	7500	6.51	6.37x10 <sup>-9</sup>	5x10 <sup>7</sup>	0.3185	0.2728	0.8332	0.4347	1.776x10 <sup>3</sup>	1.062x10 <sup>3</sup>	2.12	
7	8000	6.64	4.36	5x10 <sup>7</sup>	0.2180	0.1959	0.5147	0.5977	1.3008x10 <sup>3</sup>	9.669x10 <sup>2</sup>	1.93	
8	8500	6.92	2.63	5x10 <sup>7</sup>	0.1315	0.1232	0.2967	0.7433	8.525x10 <sup>2</sup>	7.227x10 <sup>2</sup>	1.45	
9	9000	7.60	1.52	5x10 <sup>7</sup>	0.0760	0.0732	0.1652	0.8477	5.563x10 <sup>2</sup>	5.088x10 <sup>2</sup>	1.02	
10	9500	8.10	8.66x10 <sup>-10</sup>	5x10 <sup>7</sup>	0.0433	0.0424	0.08918	0.9147	3.434x10 <sup>2</sup>	3.280x10 <sup>2</sup>	6.56x10 <sup>2</sup>	
11	10000	9.20	4.49	5x10 <sup>7</sup>	0.02245	.0222	0.04588	0.9551	2.042x10 <sup>2</sup>	1.995x10 <sup>2</sup>	3.99	
12	10500	1.07x10 <sup>4</sup>	2.27	5x10 <sup>7</sup>	0.01135	.0113	0.02343	0.9769	1.209x10 <sup>2</sup>	1.194x10 <sup>2</sup>	2.39	
13	11000	1.29	1.09	5x10 <sup>7</sup>	0.005450		0.01208	0.9880	7.031x10 <sup>1</sup>	6.984x10 <sup>1</sup>	1.40	
14	11500	1.45	5.49x10 <sup>-11</sup>	5x10 <sup>7</sup>	0.002745		.006630	0.9934	3.980x10 <sup>1</sup>	3.964x10 <sup>1</sup>	7.93x10 <sup>1</sup>	
15	12000	1.70	3.09	5x10 <sup>7</sup>	0.001545		.003885	0.9961	2.626x10 <sup>1</sup>	2.620x10 <sup>1</sup>	5.24	
16	12500	1.95	1.83	5x10 <sup>7</sup>	0.000915		.002340	0.9977	1.784x10 <sup>1</sup>	1.782x10 <sup>1</sup>	3.56	
17	13000	2.29	1.09	5x10 <sup>7</sup>	0.000545		.001425	0.9986	1.248x10 <sup>1</sup>	1.247x10 <sup>1</sup>	2.49	
18	13500	2.73	6.62x10 <sup>-12</sup>	5x10 <sup>7</sup>	0.000331		.000880	0.9991	9.036x10 <sup>0</sup>	9.031x10 <sup>0</sup>	1.81	
19	14000	3.16	4.28	5x10 <sup>7</sup>	0.000214		.000549	0.9995	6.762x10 <sup>0</sup>	6.760x10 <sup>0</sup>	1.35	
20	14500	3.71	2.93	5x10 <sup>7</sup>	0.000146		.000335	0.9997	5.417x10 <sup>0</sup>	5.416x10 <sup>0</sup>	1.08	
21	15000	4.68	1.89	1x10 <sup>8</sup>	0.000189		.000189	0.9998	8.845x10 <sup>0</sup>			
	16000											

ΣC·B<sub>r+1</sub> = 6800° K

TABLE 11  
Calculation of the Equivalent Temperature at the Limb  
at 8.5 Millimeters Wavelength

r	h km	T °K	K cm	2Rh 10 <sup>16</sup> cm <sup>2</sup>	h <sup>2</sup> 10 <sup>16</sup> cm <sup>2</sup>	(h') <sup>2</sup> 10 <sup>16</sup> cm <sup>2</sup>	h' cm	Δh' cm	KΔh'	A 1-e <sup>-KΔh'</sup>	ΣK·Δh'	B e <sup>-ΣK·Δh'</sup>	C T <sup>A</sup> °K	C <sup>B</sup> ·T <sup>A+1</sup> °K
1	5000	5.92x10 <sup>3</sup>	6.55x10 <sup>-8</sup>	6950	25.00	6975.00	8.3517x10 <sup>9</sup>	4.09x10 <sup>8</sup>	26.780	1.000	69.809	4.812x10 <sup>-31</sup>	5.92x10 <sup>3</sup>	1.217x10 <sup>-15</sup>
2	5500	6.01	4.24	7645	30.25	7675.25	8.7609	3.91	16.578	1.000	43.029	2.055x10 <sup>-19</sup>	6.01x10 <sup>3</sup>	1.956x10 <sup>-8</sup>
3	6000	6.14	2.75	8340	36.00	8376.00	9.1521	3.75	10.312	1.000	26.451	3.254x10 <sup>-12</sup>	6.14x10 <sup>3</sup>	6.013x10 <sup>-4</sup>
4	6500	6.24	1.88	9035	42.25	9077.25	9.5275	3.61	6.787	0.9989	16.139	9.793x10 <sup>-8</sup>	6.23x10 <sup>3</sup>	5.407x10 <sup>-1</sup>
5	7000	6.38	1.13	9730	49.00	9779.00	9.8889	3.49	3.944	0.9806	9.352	8.679x10 <sup>-5</sup>	6.26x10 <sup>3</sup>	2.805x10 <sup>1</sup>
6	7500	6.51	6.37x10 <sup>-9</sup>	10425	56.25	10481.25	1.0238x10 <sup>10</sup>	3.37	2.147	0.8832	5.408	4.481x10 <sup>-3</sup>	5.750x10 <sup>3</sup>	2.205x10 <sup>2</sup>
7	8000	6.64	4.36	11120	64.00	11184.00	1.0575	3.28	1.430	0.7607	3.261	3.835x10 <sup>-2</sup>	5.051x10 <sup>3</sup>	8.097x10 <sup>2</sup>
8	8500	6.92	2.63	11815	72.25	11887.25	1.0903	3.18	0.8363	0.5667	1.8310	1.603x10 <sup>-1</sup>	3.922x10 <sup>3</sup>	1.450x10 <sup>3</sup>
9	9000	7.60	1.52	12510	81.00	12591.00	1.1221	3.09	0.4697	0.3748	0.9947	0.36983	2.848x10 <sup>3</sup>	1.685x10 <sup>3</sup>
10	9500	8.10	8.66x10 <sup>-10</sup>	13205	90.25	13295.25	1.1530	3.02	0.2615	0.2301	0.5250	0.59156	1.864x10 <sup>3</sup>	1.432x10 <sup>3</sup>
11	10000	9.20	4.49	13900	100.00	14000.00	1.1832	2.94	0.1320	0.1237	0.2635	0.7684	1.138x10 <sup>3</sup>	9.978x10 <sup>2</sup>
12	10500	1.07x10 <sup>4</sup>	2.27	14595	110.25	14705.25	1.2126	2.88	0.06538	0.0633	0.1315	0.8768	6.773x10 <sup>2</sup>	6.339x10 <sup>2</sup>
13	11000	1.29	1.09	15290	121.00	15411.00	1.2414	2.81	0.03063	0.03010	0.06617	0.9359	3.883x10 <sup>2</sup>	3.747x10 <sup>2</sup>
14	11500	1.45	5.49x10 <sup>-11</sup>	15985	132.25	16117.25	1.2695	2.76	0.01515	0.01515	0.03554	0.9651	2.197x10 <sup>2</sup>	2.153x10 <sup>2</sup>
15	12000	1.70	3.09	16680	144.00	16824.00	1.2971	2.69	0.008312	0.008312	0.02039	0.9798	1.413x10 <sup>2</sup>	1.396x10 <sup>2</sup>
16	12500	1.95	1.83	17375	156.25	17531.25	1.3240	2.65	0.004850	0.004850	0.01208	0.9880	9.458x10 <sup>1</sup>	9.390x10 <sup>1</sup>
17	13000	2.29	1.09	18070	169.00	18239.00	1.3505	2.60	0.002834		0.007228	0.9928	6.490x10 <sup>1</sup>	6.461x10 <sup>1</sup>
18	13500	2.73	6.62x10 <sup>-12</sup>	18765	182.25	18947.25	1.3765	2.55	0.001688		0.004394	0.9956	4.608x10 <sup>1</sup>	4.596x10 <sup>1</sup>
19	14000	3.16	4.28	19460	196.00	19656.00	1.4020	2.51	0.001074		0.002706	0.9973	3.394x10 <sup>1</sup>	3.389x10 <sup>1</sup>
20	14500	3.71	2.93	20155	210.25	20365.25	1.4271	2.46	0.0007208		0.001632	0.9984	2.674x10 <sup>1</sup>	2.672x10 <sup>1</sup>
21	15000	4.68	1.89	20850	225.00	21075.00	1.4517	4.32	0.0009110		0.000911	0.9991	4.263x10 <sup>1</sup>	
21	16000			22240	256.00	22496.00	1.4999x10 <sup>10</sup>							

$$\Sigma = 8250^\circ \text{K}$$

TABLE 12

Calculation of the Equivalent Temperature for the Central Ray at 3.14 Centimeters Wavelength

r	h km	$\sigma^T$ °K	K cm	$\Delta h$ cm	K $\Delta h$	$1 - e^{-K\Delta h}$	$\sum K \cdot \Delta h$	$e^{-\sum K \cdot \Delta h}$	$\frac{C}{T \cdot A}$ °K	$\frac{C \cdot Br + 1}{K}$	$\frac{C \cdot Br + 1}{h \text{ km}}$ 1000
1	7500	6.51x10 <sup>3</sup>	8.69x10 <sup>-8</sup>	5.00x10 <sup>7</sup>	4.345	0.9870	11.3698	1.154x10 <sup>-5</sup>	6.425x10 <sup>3</sup>	5.715x10 <sup>0</sup>	1.14x10 <sup>1</sup>
2	8000	6.64	5.95	5.00x10 <sup>7</sup>	2.975	0.9490	7.0248	8.895x10 <sup>-4</sup>	6.301	1.098x10 <sup>2</sup>	2.20x10 <sup>2</sup>
3	8500	6.92	3.59	5.00x10 <sup>7</sup>	1.795	0.8339	4.0498	1.743x10 <sup>-2</sup>	5.771	6.054x10 <sup>2</sup>	1.21x10 <sup>3</sup>
4	9000	7.60	2.07	5.00x10 <sup>7</sup>	1.035	0.6448	2.2548	1.049x10 <sup>-1</sup>	4.900	1.447x10 <sup>3</sup>	2.89
5	9500	8.10	1.18	5.00x10 <sup>7</sup>	.5900	0.4457	1.2198	0.2953	3.610	1.923x10 <sup>3</sup>	3.85
6	10000	9.20	6.13x10 <sup>-9</sup>	5.00x10 <sup>7</sup>	.3065	0.2640	0.6298	0.5327	2.429	1.758x10 <sup>3</sup>	3.52
7	10500	1.07x10 <sup>4</sup>	3.10	5.00x10 <sup>7</sup>	.1550	0.1436	0.3233	0.7238	1.537	1.299x10 <sup>3</sup>	2.60
8	11000	1.29	1.49	5.00x10 <sup>7</sup>	.0745	0.0718	0.1683	0.8451	9.262x10 <sup>2</sup>	8.433x10 <sup>2</sup>	1.65
9	11500	1.45	7.49x10 <sup>-10</sup>	5.00x10 <sup>7</sup>	.03745	0.0368	0.09384	0.9105	5.336	5.044x10 <sup>2</sup>	1.09
10	12000	1.70	4.22	5.00x10 <sup>7</sup>	.02110	0.0209	0.05640	0.9452	3.553	3.430x10 <sup>2</sup>	6.86x10 <sup>2</sup>
11	12500	1.95	2.50	5.00x10 <sup>7</sup>	.01250	0.0124	0.03530	0.9653	2.418	2.364x10 <sup>2</sup>	4.73
12	13000	2.29	1.49	5.00x10 <sup>7</sup>	.007450		0.02280	0.9775	1.706	1.680x10 <sup>2</sup>	3.36
13	13500	2.73	9.03x10 <sup>-11</sup>	5.00x10 <sup>7</sup>	.004515		0.01534	0.9848	1.233	1.220x10 <sup>2</sup>	2.44
14	14000	3.16	5.84	5.00x10 <sup>7</sup>	.002920		0.01083	0.9893	9.227x10 <sup>1</sup>	9.154x10 <sup>1</sup>	1.83
15	14500	3.71	4.00	5.00x10 <sup>7</sup>	.002000		0.007910	.9921	7.420	7.376x10 <sup>1</sup>	1.47
16	15000	4.68	2.58	1.00x10 <sup>8</sup>	.00258		0.005910	.9941	1.207x10 <sup>2</sup>	1.203x10 <sup>2</sup>	1.20
17	16000	6.46	1.31	1.00x10 <sup>8</sup>	.00131		0.003330	.9967	8.463x10 <sup>1</sup>	8.446x10 <sup>1</sup>	8.45x10 <sup>1</sup>
18	17000	8.50	7.98x10 <sup>-12</sup>	1.00x10 <sup>8</sup>	.000798		0.002020	.9980	6.783	6.775x10 <sup>1</sup>	6.78
19	18000	1.20x10 <sup>5</sup>	4.90	1.00x10 <sup>8</sup>	.000490		0.001222	.9988	5.880	5.876x10 <sup>1</sup>	5.88
20	19000	1.55	3.03	1.00x10 <sup>8</sup>	.000303		0.000732	.9993	4.696	4.694x10 <sup>1</sup>	4.69
21	20000	2.51	1.50	2.00x10 <sup>8</sup>	.000300		0.000429	.9996	7.530	7.529x10 <sup>1</sup>	3.76
22	22000	4.60	6.45x10 <sup>-13</sup>	2.00x10 <sup>8</sup>	.000129		0.000129	.9999	5.934		
	24000										

$\sum = 9980^\circ \text{K}$

071170071200

TABLE 13

Calculation of the Equivalent Temperature at the Limb at 3.14 Centimeters Wavelength

r	h km	T °K	K cm	$\frac{2}{10^{16}} \text{Rh}$ cm <sup>2</sup>	$\frac{h^2}{10^{16}}$ cm <sup>2</sup>	$\frac{(h')^2}{10^{16}}$ cm <sup>2</sup>	h' cm	$\Delta h'$ cm	$K \Delta h'$	A $1 - e^{-K \Delta h'}$	$\sum K \cdot \Delta h'$	B $e^{-\sum K \Delta h'}$	C $\frac{T \cdot A}{K}$	$\frac{C_r^B}{K} r + 1$
1	7500	6.51x10 <sup>3</sup>	8.69x10 <sup>-8</sup>	10425	56.25	10481.25	1.0238x10 <sup>10</sup>	3.37x10 <sup>8</sup>	29.2853	1.000	73.7912	8.972x10 <sup>-33</sup>	6.51x10 <sup>3</sup>	3.054x10 <sup>-16</sup>
2	8000	6.64	5.95	11120	64.00	11184.00	1.0575	3.28	19.5160	1.000	44.5059	4.692x10 <sup>-20</sup>	6.64x10 <sup>3</sup>	9.316x10 <sup>-8</sup>
3	8500	6.92	3.59	11815	72.25	11887.25	1.0903	3.18	11.4162	1.000	24.9899	1.403x10 <sup>-11</sup>	6.92x10 <sup>3</sup>	8.813x10 <sup>-3</sup>
4	9000	7.60	2.07	12510	81.00	12591.00	1.1221	3.09	6.3963	.9983	13.5737	1.2736x10 <sup>-6</sup>	7.59x10 <sup>3</sup>	5.796x10 <sup>0</sup>
5	9500	8.10	1.18	13205	90.25	13295.25	1.1530	3.02	3.5636	.9717	7.1774	7.637x10 <sup>-4</sup>	7.87x10 <sup>3</sup>	2.121x10 <sup>2</sup>
6	10000	9.20	6.13x10 <sup>-9</sup>	13900	100.00	14000.00	1.1832	2.94	1.8022	.8351	3.6138	2.6949x10 <sup>-2</sup>	7.68x10 <sup>3</sup>	1.255x10 <sup>3</sup>
7	10500	1.07x10 <sup>4</sup>	3.10	14595	110.25	14705.25	1.2126	2.88	0.8928	.5995	1.8116	0.1634	6.32x10 <sup>3</sup>	2.522x10 <sup>3</sup>
8	11000	1.29	1.49	15290	121.00	15411.00	1.2414	2.81	0.4187	.3421	.9188	0.3990	4.41x10 <sup>3</sup>	2.675x10 <sup>3</sup>
9	11500	1.45	7.49x10 <sup>-10</sup>	15985	132.25	16117.25	1.2695	2.76	0.2067	.1867	.5001	0.6065	2.71x10 <sup>3</sup>	2.021x10 <sup>3</sup>
10	12000	1.70	4.22	16680	144.00	16824.00	1.2971	2.69	0.1135	.1073	.29342	0.7457	1.82x10 <sup>3</sup>	1.520x10 <sup>3</sup>
11	12500	1.95	2.50	17375	156.25	17531.25	1.3240	2.65	0.06625	.0641	.17992	0.8354	1.25x10 <sup>3</sup>	1.116x10 <sup>3</sup>
12	13000	2.29	1.49	18070	169.00	18239.00	1.3505	2.60	0.03874	.0380	.11368	0.8925	8.70x10 <sup>2</sup>	8.072x10 <sup>2</sup>
13	13500	2.73	9.03x10 <sup>-11</sup>	18765	182.25	18947.25	1.3765	2.55	0.02303	.0227	.07494	0.9278	6.20x10 <sup>2</sup>	5.886x10 <sup>2</sup>
14	14000	3.16	5.84	19460	196.00	19656.00	1.4020	2.51	0.01466	.0146	.05190	0.9494	4.61x10 <sup>2</sup>	4.442x10 <sup>2</sup>
15	14500	3.71	4.00	20155	210.25	20365.25	1.4271	2.46	0.00984	.00984	.03724	0.9635	3.65x10 <sup>2</sup>	3.551x10 <sup>2</sup>
16	15000	4.68	2.58	20850	225.00	21075.00	1.4517	4.82	0.01243	.0123	.02740	0.9730	5.76x10 <sup>2</sup>	5.674x10 <sup>2</sup>
17	16000	6.46	1.31	22240	256.00	22496.00	1.4999	4.67	0.006118	.00612	.01498	0.9851	3.95x10 <sup>2</sup>	3.915x10 <sup>2</sup>
18	17000	8.50	7.98x10 <sup>-12</sup>	23630	289.00	23919.00	1.5466	4.54	0.003623	.00362	.008857	0.9911	3.08x10 <sup>2</sup>	3.064x10 <sup>2</sup>
19	18000	1.20x10 <sup>5</sup>	4.90	25020	324.00	25344.00	1.5920	4.42	0.002166	.00217	.005234	0.9948	2.60x10 <sup>2</sup>	2.592x10 <sup>2</sup>
20	19000	1.55	3.03	26410	361.00	26771.00	1.6362	4.31	0.001306	.00131	.003068	0.9969	2.03x10 <sup>2</sup>	2.026x10 <sup>2</sup>
21	20000	2.51	1.50	27800	400.00	28200.00	1.6793	8.32	0.001248	.00125	.001762	0.9982	3.14x10 <sup>2</sup>	3.138x10 <sup>2</sup>
22	22000	4.60	6.45x10 <sup>-13</sup>	30580	484.00	31064.00	1.7625	7.97	0.000514	.000514	.000514	0.9995	2.36x10 <sup>2</sup>	
23	24000			33360	576.00	33936.00	1.8422							

$\Sigma = 15,560^\circ \text{K}$

TABLE 14  
Calculation of the Equivalent Temperature for the Central  
Ray at 10.6 Centimeters Wavelength

r	h km	T °K	K cm <sup>-1</sup>	Δh cm	K·Δh	A		B		C		C <sub>0</sub> B <sub>r</sub> K <sup>-1</sup> +1	C <sub>0</sub> B <sub>r</sub> +1 h <sub>cm</sub> °K	1000
						1-e <sup>-KΔh</sup>	ΣK·Δh	e <sup>-ΣK·Δh</sup>	T·A °K					
1	9500	8.10x10 <sup>3</sup>	1.18x10 <sup>-7</sup>	5x10 <sup>7</sup>	6.85	0.999	14.331		8.08x10 <sup>3</sup>	4.56x10 <sup>0</sup>	9.12x10 <sup>0</sup>			
2	10000	9.95	5.27x10 <sup>-8</sup>	1x10 <sup>8</sup>	5.27	0.9948	7.481	5.637x10 <sup>-4</sup>	9.898	1.085x10 <sup>3</sup>	1.08x10 <sup>3</sup>			
3	11000	1.37x10 <sup>4</sup>	1.28	1x10 <sup>8</sup>	1.28	.7220	2.211	0.1096	9.891	3.897x10 <sup>3</sup>	3.90			
4	12000	1.82	6.67x10 <sup>-9</sup>	1x10 <sup>8</sup>	.6670	.4868	.9314	.3940	8.860	6.802x10 <sup>3</sup>	6.80			
5	13000	2.51	1.36	1x10 <sup>8</sup>	.1360	.1272	.2644	.7677	3.193	2.808x10 <sup>3</sup>	2.81			
6	14000	3.43	5.60x10 <sup>-10</sup>	1x10 <sup>8</sup>	.0560	.0545	.1284	.8795	1.869	1.738x10 <sup>3</sup>	1.74			
7	15000	4.68	2.94	1x10 <sup>8</sup>	.0294	.0290	.07241	.9302	1.357	1.300x10 <sup>3</sup>	1.30			
8	16000	6.46	1.50	1x10 <sup>8</sup>	.0150	.0149	.04301	.9579	9.625x10 <sup>2</sup>	9.359x10 <sup>2</sup>	9.36x10 <sup>2</sup>			
9	17000	8.50	9.10x10 <sup>-11</sup>	1x10 <sup>8</sup>	.00910	.00910	.02801	.9724	7.735	7.590x10 <sup>2</sup>	7.59			
10	18000	1.20x10 <sup>5</sup>	5.58	1x10 <sup>8</sup>	.00558	.00558	.01891	.9813	6.696	6.608x10 <sup>2</sup>	6.61			
11	19000	1.55	3.45	1x10 <sup>8</sup>	.00345		.01333	.9868	5.348	5.295x10 <sup>2</sup>	5.30			
12	20000	2.51	1.71	2x10 <sup>8</sup>	.00342		.009882	.9901	8.584	8.528x10 <sup>2</sup>	4.26			
13	22000	4.60	7.36x10 <sup>-12</sup>	2x10 <sup>8</sup>	.001472		.006462	.9935	6.771	6.737x10 <sup>2</sup>	3.37			
14	24000	7.82	3.51	2x10 <sup>8</sup>	.000702		.004990	.9950	5.490	5.466x10 <sup>2</sup>	2.73			
15	26000	8.4x10 <sup>5</sup>	2.11	2x10 <sup>8</sup>	.000422		.004288	.9957	3.545	3.531x10 <sup>2</sup>	1.77			
16	28000	8.4	1.49	2x10 <sup>8</sup>	.000298		.003866	.9961	2.503	2.494x10 <sup>2</sup>	1.25			
17	30000	8.4	1.36	2x10 <sup>8</sup>	.000272		.003568	.9964	2.285	2.277x10 <sup>2</sup>	1.14			
18	32000	8.4	1.27	2x10 <sup>8</sup>	.000254		.003296	.9967	2.134	2.128x10 <sup>2</sup>	1.06			
19	34000	8.4	1.20	2x10 <sup>8</sup>	.000240		.003042	.9970	2.016	2.010x10 <sup>2</sup>	1.00			
20	36000	8.4	1.14	2x10 <sup>8</sup>	.000228		.002802	.9972	1.915	1.910x10 <sup>2</sup>	9.55x10 <sup>1</sup>			
21	38000	8.4	1.08	2x10 <sup>8</sup>	.000216		.002574	.9974	1.814	1.810x10 <sup>2</sup>	9.05			
22	40000	8.4	1.01	5x10 <sup>8</sup>	.000505		.002358	.9976	4.242	4.234x10 <sup>2</sup>	8.47			
23	45000	8.4	9.22x10 <sup>-13</sup>	5x10 <sup>8</sup>	.000461		.001853	.9981	3.872	3.867x10 <sup>2</sup>	7.73			
24	50000	8.4	8.37	5x10 <sup>8</sup>	.000418		.001392	.9986	3.511	3.507x10 <sup>2</sup>	7.01			
25	55000	8.4	7.42	5x10 <sup>8</sup>	.000371		.000974	.9990	3.116	3.114x10 <sup>2</sup>	6.23			
26	60000	8.4	6.50	5x10 <sup>8</sup>	.000325		.000603	.9994	2.730	2.729x10 <sup>2</sup>	5.46			
27	65000	8.4	5.57	5x10 <sup>8</sup>	.000278		.000278	.9997	2.335					
	70000													

Σ = 25,950° K

TABLE 15

Calculation for the Equivalent Temperature at the Limb at 10.6 Centimeters Wavelength

r	h km	T ° K	K cm	$\frac{2.8h}{10^{16} \text{cm}^2}$	$\frac{h^2}{10^{16} \text{cm}^2}$	$\frac{(h')^2}{10^{16} \text{cm}^2}$	h' cm	$\frac{\Delta h'}{\text{cm}}$	K $\Delta h'$	$1 - e^{-K\Delta h'}$	$\frac{K\Delta h'}{1 - e^{-K\Delta h'}}$	A	B	C	$\frac{C_2 B_T}{6 K} + 1$
1	10000	$9.95 \times 10^3$	$5.27 \times 10^{-8}$	13900	100	14000	$1.1832 \times 10^8$	$5.82 \times 10^8$	30.6714	1.000	42.6699	$2.943 \times 10^{-18}$	$9.95 \times 10^3$	$6.123 \times 10^{-2}$	
2	11000	$1.37 \times 10^4$	1.28	15290	121	15411	$1.2414$	$5.57 \times 10^8$	7.1296	0.9992	11.9985	$6.153 \times 10^{-6}$	$1.369 \times 10^4$	$1.052 \times 10^2$	
3	12000	1.82	$6.67 \times 10^{-9}$	16680	144	16824	1.2971	$5.34 \times 10^8$	3.5618	0.9716	4.869	$7.682 \times 10^{-3}$	$1.768 \times 10^4$	$4.785 \times 10^3$	
4	13000	2.51	1.36	18070	169	18239	1.3505	$5.15 \times 10^8$	.7004	.5036	1.307	0.27063	$1.264 \times 10^4$	$6.890 \times 10^3$	
5	14000	3.43	$5.60 \times 10^{-10}$	19460	196	19656	1.4020	$4.97 \times 10^8$	.2783	.2429	.6067	.5451	$8.331 \times 10^3$	$5.999 \times 10^3$	
6	15000	4.68	2.94	20850	225	21075	1.4517	$4.82 \times 10^8$	.1417	.1321	.3284	.7201	$6.182 \times 10^3$	$5.129 \times 10^3$	
7	16000	6.46	1.50	22240	256	22496	1.4999	$4.67 \times 10^8$	.07005	.0677	.1867	.8297	$4.373 \times 10^3$	$3.892 \times 10^3$	
8	17000	8.50	$9.10 \times 10^{-11}$	23630	289	23919	1.5466	$4.54 \times 10^8$	.04131	.0405	.1166	.8899	$3.442 \times 10^3$	$3.192 \times 10^3$	
9	18000	$1.20 \times 10^5$	5.58	25020	324	25344	1.5920	$4.42 \times 10^8$	.02466	.0244	.07533	.9275	$2.928 \times 10^3$	$2.783 \times 10^3$	
10	19000	1.55	3.45	26410	361	26771	1.6362	$4.31 \times 10^8$	.01487	.0148	.05067	.9506	$2.294 \times 10^3$	$2.213 \times 10^3$	
11	20000	2.51	1.71	27800	400	28200	1.6793	$4.22 \times 10^8$	.01423	.0141	.03580	.9648	$3.539 \times 10^3$	$3.463 \times 10^3$	
12	22000	4.60	$7.36 \times 10^{-12}$	30580	484	31064	1.7625	$7.97 \times 10^8$	.005866	.005866	.02157	.9786	$2.698 \times 10^3$	$2.656 \times 10^3$	
13	24000	7.82	3.51	33360	576	33936	1.8422	$7.66 \times 10^8$	.002689	.002689	.01571	.9844	$2.103 \times 10^3$	$2.076 \times 10^3$	
14	26000	8.4	2.11	36140	676	36816	1.9188	$7.38 \times 10^8$	.001557		.01302	.9871	$1.308 \times 10^3$	$1.293 \times 10^3$	
15	28000	8.4	1.49	38920	784	39704	1.9926	$7.14 \times 10^8$	.001064		.01146	.9886	$8.938 \times 10^2$	$8.846 \times 10^2$	
16	30000	8.4	1.36	41700	900	42600	2.0640	$6.92 \times 10^8$	.0009411		.01040	.9897	$7.905 \times 10^2$	$7.830 \times 10^2$	
17	32000	8.4	1.27	44480	1024	45504	2.1332	$6.72 \times 10^8$	.0008534		.009456	.9905	$7.169 \times 10^2$	$7.107 \times 10^2$	
18	34000	8.4	1.20	47260	1156	48416	2.2004	$6.54 \times 10^8$	.0007848		.008602	.9914	$6.592 \times 10^2$	$6.541 \times 10^2$	
19	36000	8.4	1.14	50040	1296	51336	2.2658	$6.37 \times 10^8$	.0007262		.007818	.9922	$6.100 \times 10^2$	$6.057 \times 10^2$	
20	38000	8.4	1.08	52820	1444	54264	2.3295	$6.22 \times 10^8$	.0006718		.007092	.9929	$5.643 \times 10^2$	$5.607 \times 10^2$	
21	40000	8.4	1.01	55600	1600	57200	2.3917	$1.495 \times 10^9$	.0006150		.006420	.9936	$1.268 \times 10^3$	$1.262 \times 10^3$	
22	45000	8.4	$9.22 \times 10^{-13}$	62550	2025	64575	2.5412	$1.421 \times 10^9$	.001310		.004910	.9951	$1.100 \times 10^3$	$1.096 \times 10^3$	
23	50000	8.4	8.37	69500	2500	72000	2.6833	$1.358 \times 10^9$	.001137		.003600	.9964	$9.551 \times 10^2$	$9.527 \times 10^2$	
24	55000	8.4	7.42	76450	3025	79475	2.8191	$1.305 \times 10^9$	.0009683		.002463	.9975	$8.134 \times 10^2$	$8.122 \times 10^2$	
25	60000	8.4	6.50	83400	3600	87000	2.9496	$1.257 \times 10^9$	.0008171		.001494	.9985	$6.864 \times 10^2$	$6.859 \times 10^2$	
26	65000	8.4	5.57	90350	4225	94575	3.0753	$1.216 \times 10^9$	.0006773		.0006773	.9993	$5.689 \times 10^2$		
27	70000			97300	4900	102200	3.1969								

TABLE 16  
Calculation of the Equivalent Temperature for the  
Central Ray at 50 Centimeters Wavelength

r	h km	T ° K	K cm	h cm	K · Δh	A		B		C		C <sub>0</sub> B <sub>r</sub> +1 ° K	C <sub>0</sub> B <sub>r</sub> +1 h/cm ° K	1000
						1-e <sup>-KΔh</sup>	Σ KΔh	·Σ KΔh	T·A ° K					
1	12000	1.82x10 <sup>4</sup>	1.00x10 <sup>-7</sup>	1x10 <sup>8</sup>	10.0	1.0	16.346	0.000	1.82x10 <sup>4</sup>	3.1x10 <sup>0</sup>	3.1x10 <sup>0</sup>	3.1x10 <sup>0</sup>		
2	13000	2.51	3.16x10 <sup>-8</sup>	1x10 <sup>8</sup>	3.16	0.958	6.346	.0017	2.40x10 <sup>4</sup>	9.9x10 <sup>2</sup>	9.9x10 <sup>2</sup>	9.9x10 <sup>2</sup>		
3	14000	3.44	1.41	1x10 <sup>8</sup>	1.41	.756	3.186	.0413	2.60x10 <sup>4</sup>	4.40x10 <sup>3</sup>	4.4x10 <sup>3</sup>	4.4x10 <sup>3</sup>		
4	15000	4.68	7.03x10 <sup>-9</sup>	1x10 <sup>8</sup>	0.7030	.5049	1.7763	.1693	2.363x10 <sup>4</sup>	8.079x10 <sup>3</sup>	8.08x10 <sup>3</sup>	8.08x10 <sup>3</sup>		
5	16000	6.46	3.55	1x10 <sup>8</sup>	.3550	.2988	1.0733	.3419	1.930x10 <sup>4</sup>	9.411x10 <sup>3</sup>	9.41x10 <sup>3</sup>	9.41x10 <sup>3</sup>		
6	17000	8.50	2.14	1x10 <sup>8</sup>	.2140	.1927	.7183	.4876	1.638x10 <sup>4</sup>	9.894x10 <sup>3</sup>	9.89x10 <sup>3</sup>	9.89x10 <sup>3</sup>		
7	18000	1.20x10 <sup>5</sup>	1.31	1x10 <sup>8</sup>	.1310	.1228	.5043	.6040	1.474x10 <sup>4</sup>	1.015x10 <sup>4</sup>	1.02x10 <sup>4</sup>	1.02x10 <sup>4</sup>		
8	19000	1.55	8.04x10 <sup>-10</sup>	1x10 <sup>8</sup>	.08040	.0773	.3733	.6885	1.198x10 <sup>4</sup>	8.938x10 <sup>3</sup>	8.94x10 <sup>3</sup>	8.94x10 <sup>3</sup>		
9	20000	2.51	3.96	2x10 <sup>8</sup>	.07920	.0761	.2929	.7461	1.910x10 <sup>4</sup>	1.542x10 <sup>4</sup>	7.71x10 <sup>3</sup>	7.71x10 <sup>3</sup>		
10	22000	4.60	1.70	2x10 <sup>8</sup>	.03400	.0334	.2137	.8076	1.536x10 <sup>4</sup>	1.283x10 <sup>4</sup>	6.42x10 <sup>3</sup>	6.42x10 <sup>3</sup>		
11	24000	7.82	8.07x10 <sup>-11</sup>	2x10 <sup>8</sup>	.01614	.0160	.1797	.8355	1.251x10 <sup>4</sup>	1.062x10 <sup>4</sup>	5.31x10 <sup>3</sup>	5.31x10 <sup>3</sup>		
12	26000	8.4	4.84	2x10 <sup>8</sup>	.009680	.00968	.1636	.8491	8.131x10 <sup>3</sup>	6.972x10 <sup>3</sup>	3.49x10 <sup>3</sup>	3.49x10 <sup>3</sup>		
13	28000	8.4	3.41	2x10 <sup>8</sup>	.006820	.00682	.1539	.8574	5.729x10 <sup>3</sup>	4.945x10 <sup>3</sup>	2.47x10 <sup>3</sup>	2.47x10 <sup>3</sup>		
14	30000	8.4	2.96	5x10 <sup>8</sup>	.01480	.0147	.1471	.8632	1.235x10 <sup>4</sup>	1.082x10 <sup>4</sup>	2.16x10 <sup>3</sup>	2.16x10 <sup>3</sup>		
15	35000	8.4	2.55	5x10 <sup>8</sup>	.01275	.0127	.1323	.8761	1.067x10 <sup>4</sup>	9.469x10 <sup>3</sup>	1.89x10 <sup>3</sup>	1.89x10 <sup>3</sup>		
16	40000	8.4	2.29	5x10 <sup>8</sup>	.01145	.0113	.1195	.8874	9.492x10 <sup>3</sup>	8.519x10 <sup>3</sup>	1.70x10 <sup>3</sup>	1.70x10 <sup>3</sup>		
17	45000	8.4	2.09	5x10 <sup>8</sup>	.01045	.0103	.1081	.8975	8.652x10 <sup>3</sup>	7.847x10 <sup>3</sup>	1.57x10 <sup>3</sup>	1.57x10 <sup>3</sup>		
18	50000	8.4	1.89	5x10 <sup>8</sup>	.009450	.00945	.09762	.9070	7.938x10 <sup>3</sup>	7.268x10 <sup>3</sup>	1.45x10 <sup>3</sup>	1.45x10 <sup>3</sup>		
19	55000	8.4	1.70	5x10 <sup>8</sup>	.008500	.00850	.08817	.9156	7.140x10 <sup>3</sup>	6.593x10 <sup>3</sup>	1.32x10 <sup>3</sup>	1.32x10 <sup>3</sup>		
20	60000	8.4	1.47	5x10 <sup>8</sup>	.007350	.00735	.07967	.9234	6.174x10 <sup>3</sup>	5.744x10 <sup>3</sup>	1.15x10 <sup>3</sup>	1.15x10 <sup>3</sup>		
21	65000	8.4	1.26	5x10 <sup>8</sup>	.006300	.00630	.07232	.9303	5.292x10 <sup>3</sup>	4.954x10 <sup>3</sup>	9.91x10 <sup>2</sup>	9.91x10 <sup>2</sup>		
22	70000	8.4	6.82x10 <sup>-12</sup>	6.9x10 <sup>9</sup>	.04706	.04600	.06602	.9361	3.864x10 <sup>4</sup>	3.791x10 <sup>4</sup>	2.73x10 <sup>2</sup>	2.73x10 <sup>2</sup>		
23	139000	8.4	1.22	1.39x10 <sup>10</sup>	.01696	.0168	.01896	.9812	1.411x10 <sup>4</sup>	1.408x10 <sup>4</sup>	1.02x10 <sup>2</sup>	1.02x10 <sup>2</sup>		
24	278000	8.1	1.38x10 <sup>-13</sup>	1.39x10 <sup>10</sup>	.001918	.001918	.002004	.9980	1.554x10 <sup>3</sup>	1.554x10 <sup>3</sup>	1.12x10 <sup>1</sup>	1.12x10 <sup>1</sup>		
25	417000	7.3	2.61x10 <sup>-15</sup>	2.78x10 <sup>10</sup>	.00007256	.00007256	.00008570	.9999	5.297x10 <sup>1</sup>	5.297x10 <sup>1</sup>	1.9x10 <sup>-1</sup>	1.9x10 <sup>-1</sup>		
26	695000	6.7	1.93x10 <sup>-16</sup>	6.95x10 <sup>10</sup>	.00001341	.00001341	.00001341	1.000	8.985x10 <sup>0</sup>					
27	1390000	5.6												Σ = 217,460° K

UNCLASSIFIED

TABLE 17

Calculation of the Equivalent Temperature at the  
Limb at 50 Centimeters Wavelength

r	h km	T °K	K cm	$10^{16} \frac{R_h}{cm^2}$	$10^{16} \frac{h^2}{cm^2}$	$(\frac{h'}{10^{16}})^2$	$h'$ cm $10^{-8}$	$\Delta h'$ cm	$K \Delta h'$	A $1 - e^{-K \Delta h'}$	$\sum K \Delta h'$	B $e^{-\sum K \Delta h'}$	C $\frac{T \cdot A}{O \cdot K}$	$C \cdot B_r + 1$
1	15000	$4.68 \times 10^4$	$7.03 \times 10^{-9}$	20850	225	21075	$145.17 \times 10^{10}$	$4.82 \times 10^8$	3.3885	0.9662	7.8922	0.0003737	$4.522 \times 10^4$	$5.006 \times 10^2$
2	16000	6.46	3.55	22240	256	22496	149.99	4.67	1.6579	.8095	4.5037	.01107	$5.229 \times 10^4$	$3.038 \times 10^3$
3	17000	8.50	2.14	23630	289	23919	154.66	4.54	0.9716	.6215	2.8458	.05809	$5.283 \times 10^4$	$8.109 \times 10^3$
4	18000	$1.20 \times 10^5$	1.31	25020	324	25344	159.20	4.42	.5790	.4395	1.8742	.1535	$5.274 \times 10^4$	$2.444 \times 10^4$
5	19000	1.55	$8.04 \times 10^{-10}$	26410	361	26771	163.62	4.31	.3465	.2928	1.2952	.2738	$4.538 \times 10^4$	$1.757 \times 10^4$
6	20000	2.51	3.96	27800	400	28200	167.93	8.32	.3295	.2807	.9487	.3872	$7.046 \times 10^4$	$3.794 \times 10^4$
7	22000	4.60	1.70	30580	484	31064	176.25	7.97	.1355	.1267	.6192	.5384	$5.828 \times 10^4$	$3.593 \times 10^4$
8	24000	7.82	$8.07 \times 10^{-11}$	33360	576	33936	184.22	7.66	.06182	.0599	.4837	.6165	$4.684 \times 10^4$	$3.072 \times 10^4$
9	26000	8.4	4.84	36140	676	36816	191.88	7.38	.03572	.0351	.4219	.6558	$2.948 \times 10^4$	$2.004 \times 10^4$
10	28000	8.4	3.41	38920	784	39704	199.26	7.14	.02435	.0240	.3861	.6797	$2.016 \times 10^4$	$1.404 \times 10^4$
11	30000	8.4	2.96	41700	900	42600	206.40	$1.69 \times 10^9$	.05002	.0488	.3618	.6964	$4.099 \times 10^4$	$3.001 \times 10^4$
12	35000	8.4	2.55	48650	1225	49875	223.33	1.58	.04029	.0395	.3118	.7321	$3.318 \times 10^4$	$2.529 \times 10^4$
13	40000	8.4	2.29	55600	1600	57200	239.17	1.495	.03424	.0336	.2715	.7622	$2.822 \times 10^4$	$2.226 \times 10^4$
14	45000	8.4	2.09	62550	2025	64575	254.12	1.421	.02970	.0293	.2372	.7888	$2.461 \times 10^4$	$2.000 \times 10^4$
15	50000	8.4	1.89	69500	2500	72000	268.33	1.358	.02567	.0254	.2075	.8126	$2.134 \times 10^4$	$1.779 \times 10^4$
16	55000	8.4	1.70	76450	3025	79475	281.91	1.305	.02218	.0220	.1819	.8337	$1.848 \times 10^4$	$1.575 \times 10^4$
17	60000	8.4	1.47	83400	3600	87000	294.96	1.257	.01848	.0183	.1597	.8524	$1.537 \times 10^4$	$1.335 \times 10^4$
18	65000	8.4	1.26	90350	4225	94575	307.53	1.216	.01532	.0152	.1412	.8683	$1.277 \times 10^4$	$1.126 \times 10^4$
19	70000	8.4	$6.82 \times 10^{-12}$	97300	4900	102200	319.69	1.173	.0124	.0124	.1242	.8817	$1.037 \times 10^4$	$9.795 \times 10^3$
20	139000	8.4	1.22	193210	19321	212531	461.01	1.132	.009638	.00919	.1259	.8817	$7.720 \times 10^4$	$7.495 \times 10^4$
21	278000	8.4	1.22	386420	77284	463704	680.96	2.1995	.02683	.0264	.02951	.9709	$2.218 \times 10^4$	$2.212 \times 10^4$
22	417000	8.1	$1.38 \times 10^{-13}$	579630	173889	753519	868.05	1.8709	.002582	.002582	.002684	.9973	$2.091 \times 10^3$	$2.091 \times 10^3$
23	695000	7.3	$2.61 \times 10^{-15}$	966050	483025	1449075	$120.38 \times 10^{11}$	3.3575	.00008763	.00008763	.0001023	.9999	$6.397 \times 10^1$	$6.397 \times 10^1$
24	1390000	6.7	$1.93 \times 10^{-16}$	1932100	1932100	3864200	$196.58 \times 10^{11}$	7.620	.00001471	.00001471	.00001471	1.0000	$9.856 \times 10^0$	
24	5.6													

 $\sum = 4.37,000^\circ K$

## THE OBSERVED DATA AT 8.5 MILLIMETERS WAVELENGTH

The equivalent temperature of the sun as a radiator at several radio wavelengths was computed assuming a distribution of free electrons in the sun's atmosphere according to the analysis of Baumbach and Wildt and using a temperature distribution in the outer atmosphere following Alfven. The temperature distribution in the lower atmosphere was selected in such a way that the computed equivalent temperatures of the sun would agree reasonably well with the radio data presently available. The error in assigning the equivalent temperature of the sun at the various radio wavelengths is rather high. This is due to several causes. Equation (20) shows that when the radio beam is larger in diameter than the sun, the assigned temperature of the sun is determined among other things by the gain of the antenna. In all cases except the one dealt with in this report this condition holds. At the longer wavelengths it is a difficult process to measure the antenna gain with precision. None of the reports of the measurements on the sun is sufficiently detailed to provide an indication of the experimental error in measuring the gain of the antenna, but from the experience of others in making measurements at these wavelengths it is not unreasonable to say that the few good measurements are probably in error by at least  $\pm 10\%$  and the others are undoubtedly in error by more than this amount. It is also dubious if the sensitivity of the receivers was known with any precision. The second factor making it difficult to assign the proper equivalent temperature is that the radiation from the sun is extremely variable at the longer wavelengths, and it is not always clear that the temperatures published are those for the sun in its most quiet state. One further uncertainty in interpreting the published results is that the effective diameter of the sun is greater for the longer wavelengths and also the illumination across the surface of the sun varies; in fact there is considerable limb brightening in the middle wavelength range. In assigning an equivalent temperature, it should be made clear whether the effective diameter used is the optical diameter or the radio diameter and whether limb brightening was taken into account. This is not always done. It is important to repeat these experiments or to recompute the data if the parameters of the system are sufficiently well known.

At 8.5 millimeter wavelength with a ten-foot diameter antenna the beamwidth is  $0.2^\circ$ , so that the entire beam of the antenna may be made to fall upon the sun. When this is done, equation (22) applies. The equivalent temperature of the sun at 8.5 millimeters then will be the waveguide temperature  $t_s$  corrected for the loss in the waveguide

between the feed horn and the converter and corrected for the attenuation of the signal from the sun in our atmosphere. The loss in the waveguide has been measured to be 2.05 decibels  $\pm 0.15$  decibels, which corresponds to a power ratio of  $1.60 \pm 0.055$  or  $1.60 \pm 3.5\%$ . Using the data of Van Vleck<sup>5,3,5,4</sup> on the attenuation due to oxygen and water vapor, the loss in the atmosphere may be taken as 0.5 decibels, which corresponds to a power ratio of 1.12. Hence the total correction to be applied to the waveguide temperature to arrive at the equivalent temperature of the sun is the sum of these two, i.e., 2.55 decibels or a power ratio of 1.80. As was seen earlier, the error in calibration was  $\pm 5\%$ , so that the uncertainty in the equivalent temperature of the sun may be taken as  $\pm 10\%$ . The data on the temperature of the sun covering a period of several months is shown in Table 18. There is

TABLE 18  
Equivalent Temperature of the Sun at 8.5 Millimeters Wavelength

Date	Spot Area	$T_e$ ° K	Average Temperature ° K
September 17	2363	7950	Calibration not made during this period
18	2762	9430	
20	3002	8560	
22	3087	9470	
October 15	2743	12600	
17		10800	
21	2182	13800	
30	968	8650	
November 1	1200	8800	
3	1141	8370	
7	925	9580	
8	1077	9650	
11	895	7180	
14		10500	
15	1248	8200	
16	1192	12000	
18	1996	8270	
19	2386	8400	
February 4	3563	6500	
5	4230	7180	
5		6500	
6		6900	
8	3282	6720	
24	3029	6300	
24		5800	
March 14		8030	

considerable variation in the equivalent temperature over this period. The maximum value is  $13,800^{\circ}$  and the minimum  $5800^{\circ}$  Kelvin. The average of all the data yields a temperature of  $8700^{\circ}$ ; whereas the average of the recent data yields  $6740^{\circ}$ . The data taken through November 19 should not be included in computing the average temperature of the sun, since during that period the calibration process for the receiver had not been perfected, and this data has little meaning in absolute terms. During this period contours of the sun were taken and the data are usable for that purpose since the receiver parameters do not vary during the period of one day's observations. Using the recent data, the temperature of the sun at 8.5 millimeters is  $6740^{\circ}$  Kelvin  $\pm 10\%$ . The minimum measured temperature in this period was  $5800^{\circ}$  and the maximum  $8030^{\circ}$ . Table 8, previously presented, shows that the computed central temperature at 8.5 millimeters is  $6800^{\circ}$  Kelvin and the computed temperature at the limb is  $8250^{\circ}$  Kelvin. The observed temperature falls between these at a value much closer to the central temperature as it should, since the computed temperature is based on the temperature distribution in the chromosphere chosen to yield a computed result which would be consistent with the observed result. The theory reveals that there will be a very narrow, bright rim on the sun and that the brightening in the ring amounts to 20%. The total contribution due to this brightening in the very narrow rim is so small that it is not observed experimentally.

If the temperature in the sun's atmosphere is considered to fall uniformly from its high value at the base of the corona to  $4830^{\circ}$  Kelvin at the limb, then the computed equivalent temperature at 8.5 millimeters would have a value in excess of  $10,000^{\circ}$  Kelvin. Since this is not so, it was necessary to assume the temperature distribution shown earlier which yields an equivalent temperature of  $6800^{\circ}$ , and is more in agreement with the measured value. This new distribution also gives reasonable values for the equivalent temperature at 3 centimeters. The computed equivalent temperatures at 10 and 50 centimeters are not affected so much by the assumed temperature distribution low in the chromosphere since large contributions are made to the emission at these two longer wavelengths by regions higher in the atmosphere.

### Variation in Emission Across the Surface of the Sun

In addition to measuring the equivalent temperature of the sun, countour diagrams of the distribution of intensity across the disc of the sun were obtained. Previously, it has been pointed out that the

guiding telescope is provided with a reticule which permits the antenna to be moved in nine equal steps in either right ascension or declination across the surface of the sun. Figure 27 illustrates how the reticule is used. For example, to scan the sun in right ascension where the antenna beam is pointed directly at the sun, the first position would be that represented by  $a$ , where the left-handed ruling is tangent to the western limb of the sun. The antenna is then moved to the east and measurements made as each successive ruling of the reticule becomes tangent to the western limb until

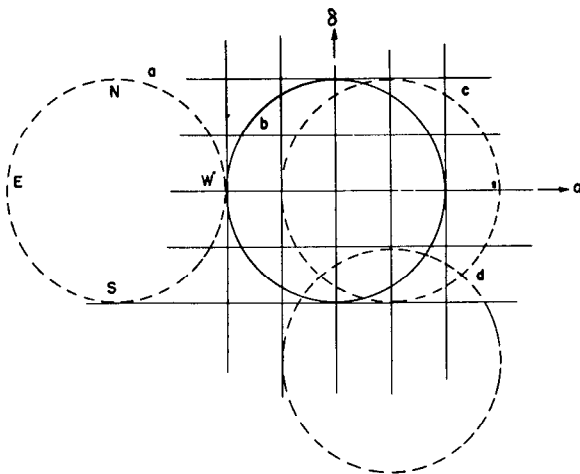
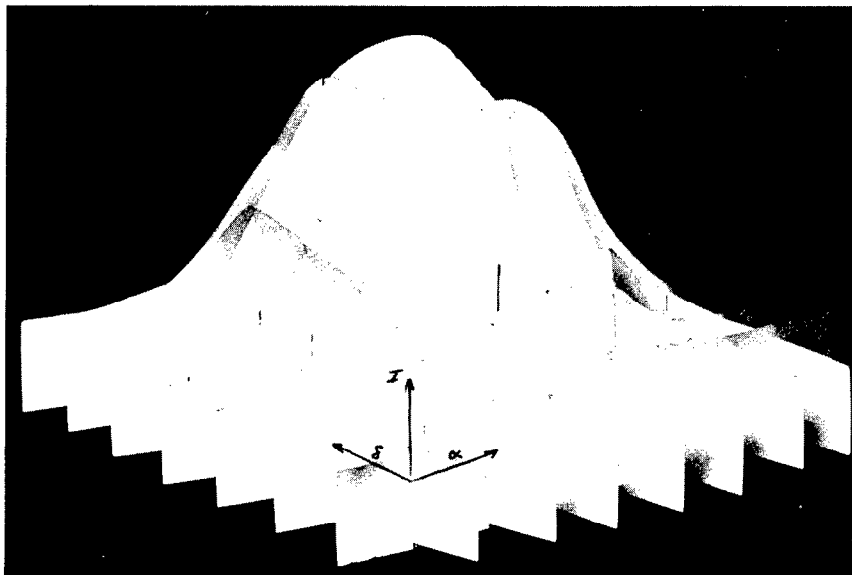


Figure 27 - Construction illustrating the use of the reticule

position  $b$  is reached; then the motion is continued and readings taken as successive rulings become tangent to the eastern limb. In this way nine nearly equal steps are taken, and the total movement in right ascension is two diameters of the sun. The same process is carried out in declination. The amount of movement required in scanning the sun is dictated by the diameter of the sun and by the total diameter of the antenna beam. When the beam is pointed  $0.5^\circ$  away from the center of the sun, the intensity of the received signal has fallen sensibly to zero. This can be seen by referring to Figure 14 which gives a curve of the antenna beam pattern.

The sun is scanned in order to determine variations in the intensity of the illumination across the surface of the sun. A lack of uniformity might appear in either of two ways. In the first place, there may be sensible limb brightening, and secondly there may be "hot spots" associated perhaps with the sunspots or with some other solar activity. It is of considerable theoretical interest to determine whether either of these conditions prevails. To do this, a series of contour maps of the intensity of the radiation from the sun was constructed. Data were taken on the intensity of each of the eighty-one points of intersection on the reticule grid. These data may be presented either as a series of curves representing the variation of intensity with right ascension for each of the nine positions in declination, or a three-dimensional graph may be constructed, where the coordinates are right ascension, declination, and intensity. The

three-dimensional graph shows at a glance any major deviation from normalcy, and has proved quite helpful in interpreting results. Figure 28 is a photograph of such a three-dimensional presentation.



*Figure 28 - Photograph of a three-dimensional graph of the variation in intensity across the surface of the sun at 8.5 millimeter wavelength*

The interpretation of the response curves for the sun is difficult since the source and the beam pattern are commensurate in size. If the beam were very much smaller than the source or, conversely, if the beamwidth were large and the source small, the matter of interpretation would be quite simple.

The method used to analyze the data is to construct an idealized pattern assuming that the sun is a uniformly illuminated disc and that the antenna pattern has its measured characteristics. It is extremely difficult to obtain an antenna beam pattern which is a true figure of revolution about the axis of the beam. To do this, it would be necessary to have the illumination of the parabola independent of angular position about the center of the parabola, and this would require a very special design of the waveguide feed horn. Since this symmetry is not a requirement in the operation of the apparatus, a conventional feed horn was used where the illumination was more sharply tapered in

the plane of the electric vector. The illumination resulted in a beam pattern which was slightly elliptical in cross section. This pattern can be seen in Figure 14, where the measured patterns in both E vector and H vector planes are given. If there were true symmetry in the pattern, a moderately simple analytical expression could be written down for the antenna pattern, and then integrations could be performed to obtain the resulting response as an extended source, whose illumination could also be written as an analytical function, is scanned by the antenna pattern.

### An Example of the Relation of Radio Measurement to Solar Activity

For the case in hand, it is much simpler and sufficiently accurate to perform a numerical integration. To do this, the antenna pattern was represented graphically by sixteen concentric circles, the smallest of which had a radius of one minute of arc, the next, two minutes of arc, and so on out to sixteen minutes of arc. The relative intensity in each of these rings can then be assigned for three rings can then be assigned for three planes of intersection with the antenna beam. The measured intensity pattern for two of these planes is shown in Figure 14, and the computed pattern for the plane half-way between the two measured planes is given in Figure 29. It should be noticed that the principal variations between these patterns occur near the edges. A disc thirty-two minutes in diameter was moved in one-minute steps toward the center of this system of circles. See Figure 30. The fractional area of each ring of the antenna pattern covered at each successive step in the motion of the circle representing the sun was computed with the help of a mechanical construction and the results tabulated in Table 19. The weight to be assigned to the successive rings is determined by the antenna pattern and can be taken from values on the curves shown in Figures 14 and 29. The values are also given in Table 19 for the three planes considered. The product of the fractional area covered and the weight for each successive ring was taken and summed for each of the steps in the separation of the centers of the two discs. This calculation is shown in Tables 20, 21, and 22 (see pages 82-85). In Table 20 the weights are assigned for the average antenna pattern, which was assumed to apply in the  $45^\circ$  positions. Table 21 is for the plane of the electric vector, which coincides with motion in right ascension. Table 22 is for the plane of the magnetic vector, which coincides with motion in declination. The last column in Tables 20, 21, and 22 are the normalized functions obtained as the beam moves uniformly across the surface of the sun along a diagonal so that the axis of the beam crosses the center of the sun. The functions are for motion across the sun in

declination, in right ascension, and at the 45° position. These functions are shown in Figures 31, 32 and 33. The position with respect to the center of the sun of each of the eighty-one intersections of the grid lines of Figure 27 can be computed. From Tables 20, 21, and 22 or Figures 31, 32 and 33, values can be obtained of the normalized intensity at each of the eighty-one positions of the antenna beam as it scans the sun. The intensity distribution is shown in Table 23. When the distribution of Table 23 is subtracted from the data as observed after normalizing, the residual should show the regions on the sun which are radiating in excess of that expected from a uniformly illuminated disc the size of the sun.

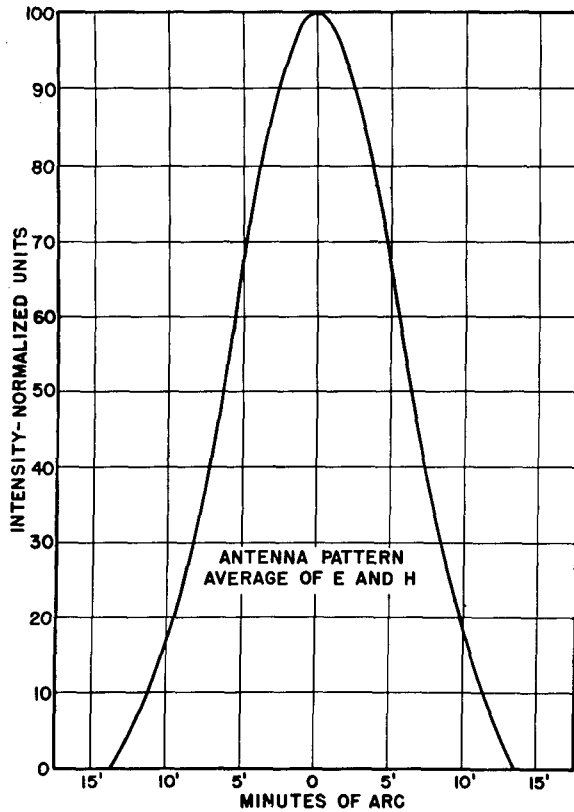


Figure 29 - Antenna pattern, average of E and H planes

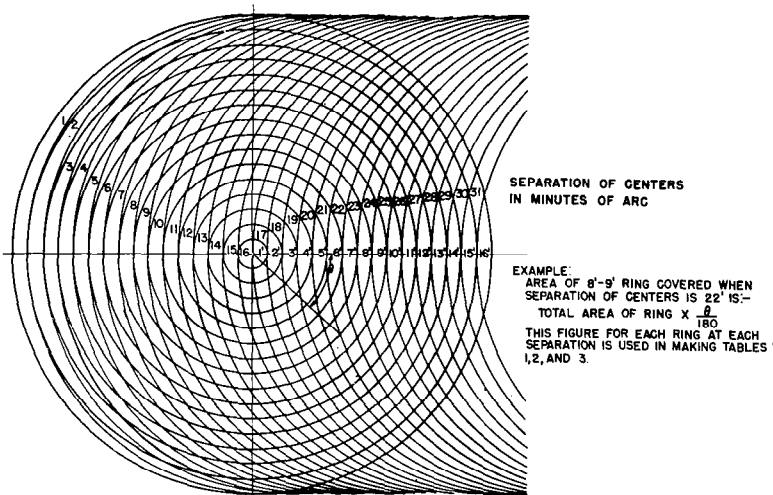


Figure 30 - Construction for obtaining normalized function



**TABLE 20**  
**Calculation of Normalized Function for Plane at 45°**  
**to the Electric and Magnetic Vectors**

Separation of Centers Minutes of arc	Zone														Sum	Normalized Sum
	0-1	1-2	2-3	3-4	4-5	5-6	6-7	7-8	8-9	9-10	10-11	11-12	12-13	13-13.6		
	Area X Weight															
0	198.7	575	898	1148	1287	1320	1261	1140	986	808	630	473	225	26	10940	1.000
1	198.7	575	898	1148	1287	1320	1261	1140	986	808	630	473	225	26	10940	1.000
2	198.7	575	898	1148	1287	1320	1261	1140	986	808	630	473	225	26	10940	1.000
3	198.7	575	898	1148	1287	1320	1261	1140	986	808	630	473	225	22	10936	1.000
4	198.7	575	898	1148	1287	1320	1261	1140	986	808	630	473	185	18	10892	.993
5	198.7	575	898	1148	1287	1320	1261	1140	986	808	630	361	160	16	10789	.985
6	198.7	575	898	1148	1287	1320	1261	1140	986	808	528	312	146	15	10623	.971
7	198.7	575	898	1148	1287	1320	1261	1140	986	680	459	258	134	14	10386	.949
8	198.7	575	898	1148	1287	1320	1261	1140	827	588	414	262	125	13	10057	.919
9	198.7	575	898	1148	1287	1320	1261	967	722	538	387	247	119	13	9681	.883
10	198.7	575	898	1148	1287	1320	1067	831	658	471	360	234	113	12	9173	.837
11	198.7	575	898	1148	1287	1112	913	746	598	458	336	220	108	12	8610	.786
12	198.7	575	898	1148	1072	949	823	684	545	431	317	209	102	11	7963	.726
13	198.7	575	898	935	902	836	740	627	516	402	298	198	98	11	7235	.660
14	198.7	575	715	752	781	748	674	579	477	376	281	188	94	10	6447	.588
15	198.7	417	547	650	678	659	604	526	442	349	264	177	88	10	5620	.513
16	99.4	286	432	533	587	592	549	485	409	326	248	167	85	9	4807	.439
17		157	317	438	508	517	494	439	377	304	234	158	80	9	4032	.368
18			178	326	408	439	437	394	344	281	216	148	76	8	3235	.295
19				177	301	364	372	347	308	255	200	139	71	8	2542	.232
20					177	276	315	302	277	232	184	129	67	8	1967	.180
21						159	241	252	240	208	167	120	62	7	1456	.133
22							136	190	201	181	150	106	58	7	1029	.094
23								106	155	151	131	97	53	6	699	.064
24									92	115	110	86	47	5	455	.042
25										65	84	72	40	5	266	.024
26											48	55	34	4	141	.013
27												31	26	4	61	.006
28													14	3	17	.002
29														1	1	.000

TABLE 21  
Calculation of Normalized Function for Plane of the Electric Vector ( $\alpha$ )

Separation of Centers Minutes of Arc	Zone														Normalized	
	0-1	1-2	2-3	3-4	4-5	5-6	6-7	7-8	8-9	9-10	10-11	11-12	12-13	13-13.6	Sum	Sum
	Area X Weight															
0	199	575	899	1148	1296	1302	1216	1050	881	674	452	244	100	8	10044	1.000
1	199	575	899	1148	1296	1302	1216	1050	881	674	452	244	100	8	10044	1.000
2	199	575	899	1148	1296	1302	1216	1050	881	674	452	244	100	8	10044	1.000
3	199	575	899	1148	1296	1302	1216	1050	881	674	452	244	100	7	10043	1.000
4	199	575	899	1148	1296	1302	1216	1050	881	674	452	244	100	6	10024	.998
5	199	575	899	1148	1296	1302	1216	1050	881	674	452	201	71	5	9969	.992
6	199	575	899	1148	1296	1302	1216	1050	881	674	378	174	64	5	9861	.982
7	199	575	899	1148	1296	1302	1216	1050	881	568	329	159	60	4	9686	.964
8	199	575	899	1148	1296	1302	1216	1050	738	491	297	146	56	4	9417	.938
9	199	575	899	1148	1296	1302	1216	890	643	450	277	138	53	4	9090	.905
10	199	575	899	1148	1296	1302	1028	766	586	393	258	130	50	4	8634	.860
11	199	575	899	1148	1296	1098	880	687	533	381	240	123	48	4	8111	.808
12	199	575	899	1148	1080	937	793	630	486	360	227	115	45	4	7498	.746
13	199	575	899	935	907	825	713	578	460	337	214	110	44	3	6799	.677
14	199	575	713	761	786	738	650	533	425	315	201	105	42	3	6046	.602
15	199	408	546	649	682	650	583	485	394	292	189	99	39	3	5218	.520
16	99	286	431	533	590	584	529	447	365	272	178	93	38	3	4448	.443
17		157	316	438	511	510	476	404	336	254	168	88	36	3	3697	.368
18			178	326	410	433	421	363	307	234	155	83	34	3	2947	.293
19				177	302	359	359	320	275	213	143	77	32	2	2259	.203
20					178	272	304	278	247	193	132	72	30	2	1708	.170
21						157	232	232	214	174	120	67	28	2	1226	.122
22								131	175	179	151	108	59	2	831	.083
23									98	126	94	54	23	2	535	.053
24										82	96	78	48	2	327	.032
25											55	60	40	2	175	.017
26												34	30	1	80	.008
27													17	1	30	.003
28														1	7	.001
29														0	0	.000

**TABLE 22**  
**Calculation of Normalized Function for Plane of the Magnetic Vector ( $\delta$ )**

Separation of Center Minutes of Arc	Zone															Sum	Normalized Sum	
	0-1	1-2	2-3	3-4	4-5	5-6	6-7	7-8	8-9	9-10	10-11	11-12	12-13	13-14	14-15			15-16
	Area X Weight																	
0	198.7	574	899	114.8	1305	1375	1360	1275	1131	921	756	575	420	286	174	68	124.66	1.000
1	198.7	574	899	114.8	1305	1375	1360	1275	1131	921	756	575	420	286	174	46	124.44	.998
2	198.7	574	899	114.8	1305	1375	1360	1275	1131	921	756	575	420	286	134	37	12395	.994
3	198.7	574	899	114.8	1305	1375	1360	1275	1131	921	756	575	420	224	110	35	12307	.987
4	198.7	574	899	114.8	1305	1375	1360	1275	1131	921	756	575	346	194	101	33	12192	.978
5	198.7	574	899	114.8	1305	1375	1360	1275	1131	921	756	475	299	174	93	33	12017	.964
6	198.7	574	899	114.8	1305	1375	1360	1275	1131	921	633	410	270	163	89	31	11783	.945
7	198.7	574	899	114.8	1305	1375	1360	1275	1131	776	551	375	250	154	85	31	11488	.922
8	198.7	574	899	114.8	1305	1375	1360	1275	948	671	497	345	234	146	82	31	11089	.890
9	198.7	574	899	114.8	1305	1375	1360	1081	828	614	464	325	222	140	79	29	10642	.854
10	198.7	574	899	114.8	1305	1375	1150	930	754	537	432	308	212	134	76	29	10062	.807
11	198.7	574	899	114.8	1305	1158	985	835	686	523	403	290	202	127	73	26	9433	.757
12	198.7	574	899	114.8	1087	990	887	765	625	492	380	274	192	124	71	26	8733	.700
13	198.7	574	899	935	914	871	798	702	592	460	358	260	183	118	68	26	7957	.638
14	198.7	574	713	761	791	779	727	647	547	430	338	247	175	112	66	24	7130	.572
15	198.7	408	546	649	687	686	652	589	517	399	317	232	165	108	63	24	6241	.501
16	99.4	286	431	533	594	616	592	543	470	372	298	220	158	103	61	24	5400	.433
17		157	316	438	515	539	532	491	432	347	281	208	150	98	58	22	4584	.368
18			178	326	413	458	471	441	394	320	260	195	141	93	56	21	3767	.302
19				177	304	379	402	388	354	291	240	182	133	88	53	20	3011	.242
20					179	288	340	338	317	264	221	170	124	83	50	20	2394	.192
21						166	259	282	275	238	201	158	116	78	47	18	1838	.147
22							146	212	231	206	180	140	108	73	44	18	1358	.109
23								119	177	173	161	128	97	68	42	17	982	.079
24									105	132	131	112	87	62	38	16	683	.055
25										75	101	95	74	55	35	14	449	.036
26											58	72	64	49	32	13	288	.023
27												40	49	41	28	12	170	.014
28														27	31	11	93	.007
29															18	19	46	.004
30																7	17	.001
31																5	5	.0004

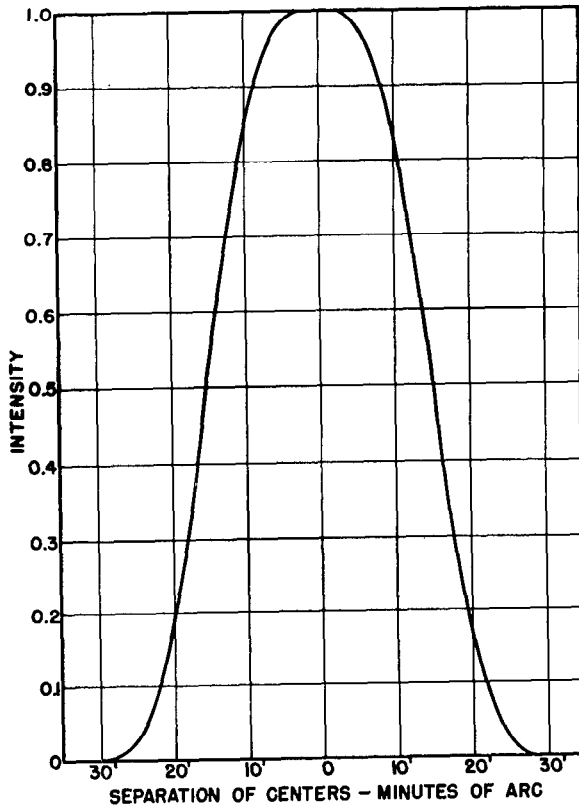


Figure 31 - Normalized function variation in signal using average pattern

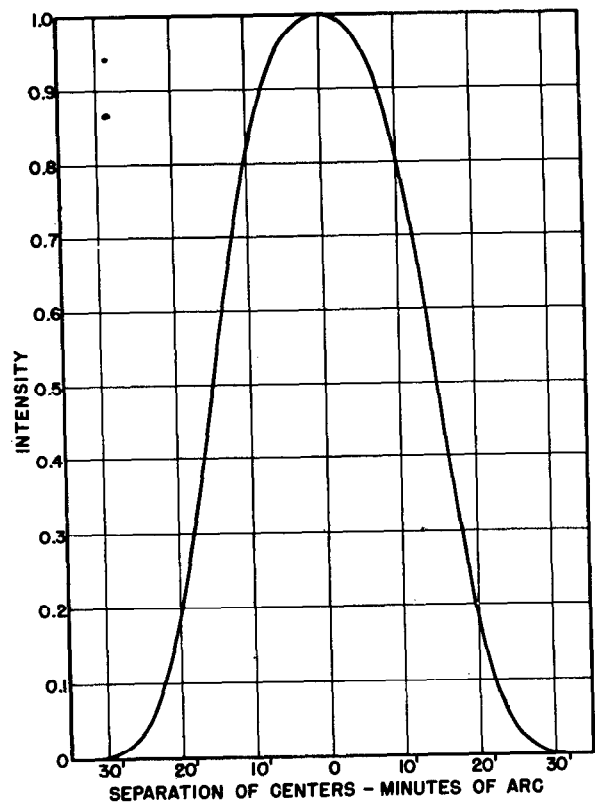


Figure 32 - Normalized function variation in signal with declination

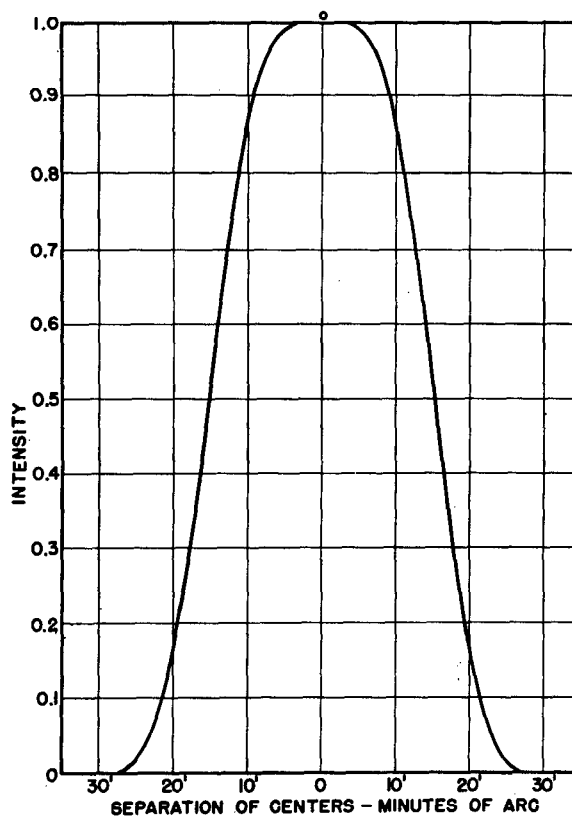


Figure 33 - Normalized function - variation in signal with right ascension

Figure 28 is a photograph of a three-dimensional curve of the intensity distribution as measured with this apparatus. Table 24 shows the data for November 18, 1948 treated in this fashion. It is seen that on this day there was an area on the western limb of the sun where the intensities were higher than normal.

An analysis of this sort was carried out for the week of September 17, when a large and isolated spot group passed across the disc of the sun. The presence of the activity associated with the spot caused a bulge to appear on the contours. This bulge moved across the sun with the spot group. Figure 34 shows the relative position of the spot group and of the measured perturbation in the pattern for the five days during the transit of the spot when measurements were made. The increase in intensity due to the spot was seven parts in a hundred. If the radio emission is assumed to come from an area equal to the visual area of the spot, then the equivalent temperature of the excited area is approximately equal to  $100,000^{\circ}$  Kelvin. This increase in temperature near the spot could be due to an increase in the electron densities in and about the spot by a factor of 10 to 20.

NAVAL RESEARCH LABORATORY

TABLE 23  
Computed Intensities for Uniform Sun

32'	0	0	0	0	0	0	0	0	0
24'	0	0	0.25	2.6	5.5	2.6	0.25	0	0
16'	0	0	7.6	30.5	43.3	30.5	7.6	0	0
8'	0	1.65	29.9	76.2	89.0	76.2	29.9	1.65	0
0	0	3.2	44.3	93.8	100	93.8	44.3	3.2	0
8'	0	1.65	29.9	76.2	89.0	76.2	29.9	1.65	0
16'	0	0	7.6	30.5	43.3	30.5	7.6	0	0
24'	0	0	0.25	2.6	5.5	2.6	0.25	0	0
32'	0	0	0	0	0	0	0	0	0
Right Ascension $\alpha$									
32'	24'	16'	8'	0	8'	16'	24'	32'	

TABLE 24  
Difference between Computed and Measured Intensities for 18 November 1948

			0	1.2	2.4	1.2	1.0	0	
		0	0	3.4	6.5	5.2	4.0	1.2	0
	1.2	2	4.9	13.7	16.9	12.8	3.6	0	
0	0	2	0	4.2	10.6	16.0	23.1	9.1	0
0	0	1.6	2.3	2.8	8.6	11.2	33.7	13.4	0
0	0	2.6	0	5.4	16.6	24	24.9	13.4	0
	1	3.2	9.1	19.7	27.1	24.2	9.6	0	
	0	2.2	7	11.3	14.2	8.2	0		
	1	1.8	2.4	2.4	1				
Right Ascension $\alpha$									

REF ID: A61100

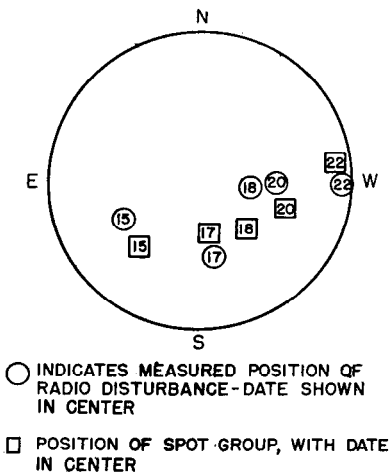


Figure 34 - Relative position on the sun of radio disturbance and spot group 15 September to 22 September 1948

As can be seen from Figure 19, an increase in electron density of this amount would so increase the opacity that the maximum depth of penetration would change from 7,000 or 8,000 kilometers to 16,000 or 18,000 kilometers, and thus cause the emission to come from the effectively hotter regions nearer the base of the corona. A second possibility for the high equivalent temperature around the spot is that electrons of high velocities react with the strong magnetic field associated with the spot, and produce increased radio emission by the magnetron effect. To determine which of these two effects predominates or whether perhaps there is some other mechanism for the effect will require a detailed study of the "disturbed" sun.

In addition to the motion of a bulge across the contour coinciding with the motion of a spot across the sun, one other peculiarity in the measurements was noted and as yet is unexplained. On October 17 the contour map of the sun had a pronounced bulge at the southern limb. Attempts to correlate this observation with observed irregularities in the sun by other workers have not been successful. The Naval Observatory, in spectrohelioscope observations, showed high prominences in this region on the 16th and on the 18th. They did not take data on the 17th. The High Altitude Observatory at the University of Colorado took data on the 17th of October and observed a prominence which was an "eruption of extreme violence and very short duration" on this day, but unfortunately the location of the prominence they observed was at  $310^{\circ}$ , which is on the other side of the sun from the region containing the effect observed here. They point out that the life of the prominence observed with respect to activity and observable material was certainly less than one and one-half hours and was probably less than an hour. They give data for no other prominence on that day.

**Possibility of Detecting other Extra-Terrestrial Objects**

The equivalent temperature of the moon has been measured on several days. The average equivalent temperature is  $150^{\circ}$  Kelvin  $\pm 40\%$ .

No variation in intensity across the surface of the moon was observable nor were the measurements sufficiently inclusive to reveal any variation in the intensity of the radiation with phase of the moon. A more careful study of the radiation from the moon should be made to determine the equivalent temperature of the surface when fully illuminated by the sun and when dark.

Radiation from Venus was looked for but not found, and this is of course to be expected when a reasonable surface temperature is assumed. If at its closest approach to the earth Venus has a 30 seconds of arc semi-diameter, then its area will be one-quarter the area of the central circle in Figure 30. Referring to Table 20 and assuming that the antenna is pointed directly at Venus, then the ratio of the product of the area of Venus times the weight of the central zone to the summation of the area and weights for the whole pattern will be 0.0046. Even if the surface temperature of Venus were the surface temperature of the sun the intensity of the signal observed at 8.5 millimeters would be 0.46% of that for the sun. If the surface temperature of Venus is 300° Centigrade then the signal would be 0.05% of that of the sun. This is smaller than the experimental error. If the fifty-foot antenna has a surface usable at 8.5 millimeters, then Venus will probably be measurable. For then at closest approach, Venus will cover the first two and one-half zones. It is assumed here that a table similar to Table 19 is made for the fifty-foot antenna with the dimensions scaled so that the first circle will be 0.2 minutes in radius, the second 0.4, and so on. In this case the signal from Venus would be about one percent of that from the sun.

#### THE OBSERVATIONS ON THE 20 MAY 1947 TOTAL ECLIPSE OF THE SUN

A total eclipse of the sun offers a unique opportunity to measure the variation of the intensity of the radiation across the surface of the sun and thereby offers a solution to the problem of obtaining higher resolution in those cases where the antenna beam-widths cannot be made sufficiently small because of size and wavelength limitations. Some measurements on partial eclipses have been made by Sander,<sup>55</sup> Dicke and Beringer,<sup>56</sup> and Covington<sup>57</sup> at wavelengths of 1.25, 3.5, and 10 centimeters.

On May 20, 1947, there was a total eclipse of the sun of long duration, whose path of totality extended from Brazil to Africa.

Measurements were made of the intensity of the sun's radiation during this eclipse by a group from the Naval Research Laboratory. At this time the only equipment for measuring solar radiation at the Laboratory functioned at a wavelength of 3.2 centimeters. The equipment was bulky, required a very well stabilized source of sixty-cycle power, and in addition the antenna reflector was a large aluminum paraboloid which would not stand rough handling. Considering these factors and the time element involved, it was decided that the eclipse could best be observed from shipboard, where the antenna and the rest of the apparatus could be installed at the Laboratory and could be adjusted during the trip to the eclipse location. The location chosen for the measurements was longitude west  $20^{\circ}$ ; latitude north  $1^{\circ}$ , which was in the center of the path of totality, and at this location the duration of totality was 5 minutes, 5.5 seconds. Figure 35 is a chart of the path of totality taken from the *Supplement To The American Ephemeris 1947*, and on it is shown a chart of the course of the ship for the period during which observations were made of the eclipse.

The location chosen for the observations was one giving nearly maximum duration of totality. Records of previous years indicated that the chances of having favorable weather for observations were better at this location than at any other available. The principal difficulty due to operation on shipboard was that of stabilizing the antenna during the observation of the eclipse, but this problem was more easily solved than any alternative plan which would necessarily require extensive modification of equipment.

The width of the path of totality at the point chosen for observations was about 100 miles. The course the ship took and the speed it ran during the observation of the eclipse were determined by the nature of the surface of the sea and the roll characteristics of the ship. In order to make the problem of stabilizing the antenna as simple as possible, the ship was maneuvered to minimize motion. The navigation of the ship was the responsibility of the ship's officers, and their records show that the maximum distance of the ship from the true center of the eclipse during the full course of the eclipse was five miles, and that during totality the ship was not more than one-half mile off the predicted center line. To arrive at this answer the ship's navigator took extreme care in taking his bearings on the day before the eclipse, the eclipse day, and the following day.

The times and positions of the contacts computed for the position of the ship at mid-totality are taken from a series of

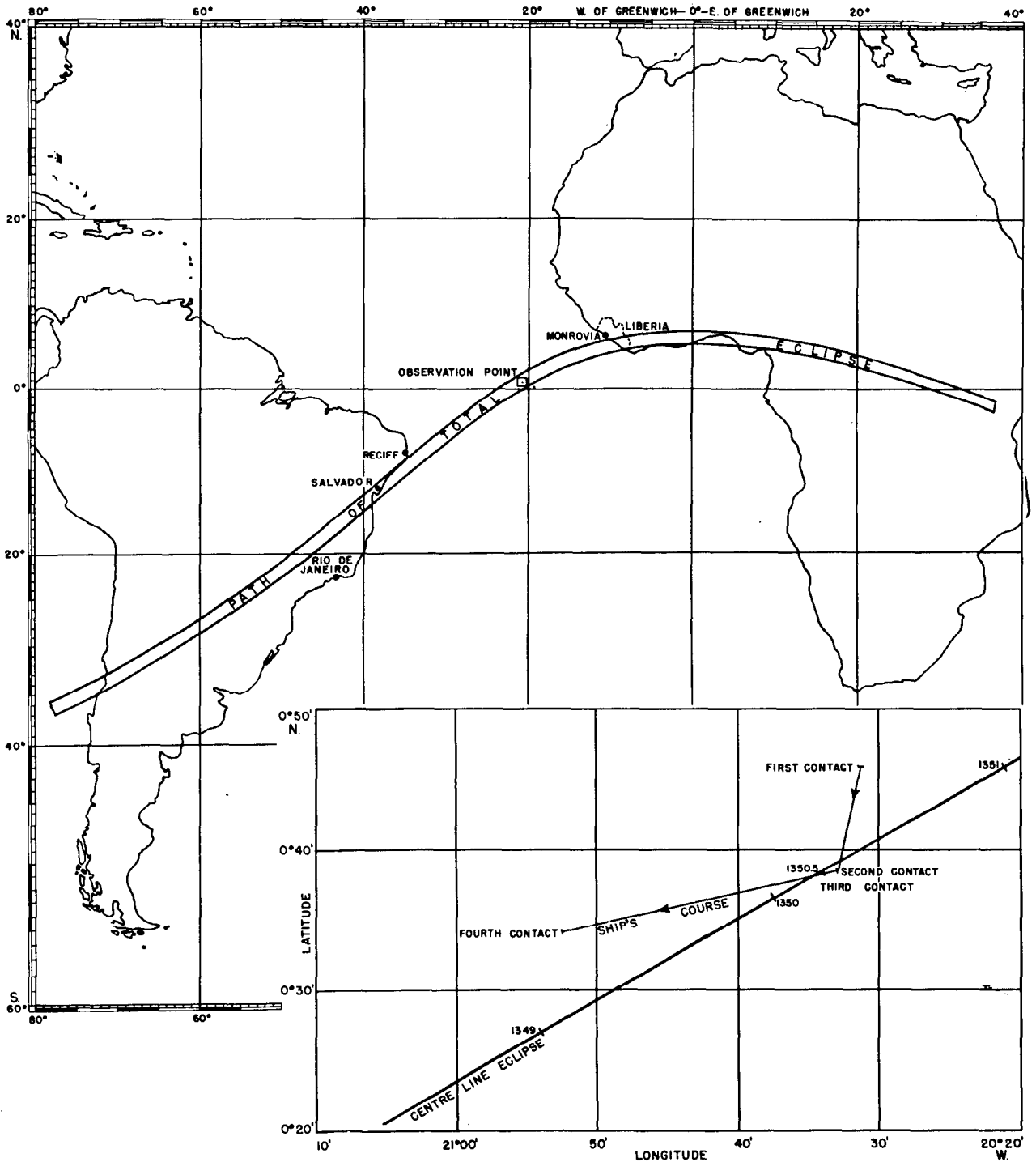


Figure 35 - Chart of the path of the total eclipse of May 20, 1947, with an insert showing the course of the ship during the progress of the eclipse

calculations by the Naval Observatory staff extending the *Supplement To The Ephemeris* for this location and are given in Table 25. The magnitude of the eclipse for this position was 1.039. Corrections were then made on the times and positions of the contacts due to the changing position of the ship. This resulted in the corrected values

TABLE 25

Times of Mid-Totality and Semi-Duration of Total Eclipse for Points on the Central Line in the South Atlantic Ocean

G.C.T. of Mid-Totality		Semi-Duration of Total Eclipse		Latitude		Longitude	
13 <sup>h</sup>	0 <sup>m</sup>	2 <sup>m</sup>	16 <sup>s</sup> .1	-9°	52.6	+34°	42.6
	1	2	16.8	9	36.5	34	23.4
	2	2	17.5	9	20.6	34	4.4
	3	2	18.2	9	4.3	33	45.5
	4	2	19.0	8	49.2	33	26.8
13	5	2	19.7	-8	33.7	+33	8.3
	6	2	20.3	8	18.5	32	50.0
	7	2	20.9	8	3.4	32	31.8
	8	2	21.6	7	48.5	32	13.8
	9	2	22.2	7	33.7	31	55.9
13	10	2	22.8	-7	19.0	+31	38.1
	11	2	23.4	7	4.5	31	20.5
	12	2	24.0	6	50.2	31	3.0
	13	2	24.7	6	36.0	30	45.6
	14	2	25.3	6	22.0	30	28.3
13	15	2	25.8	-6	8.1	+30	11.1
	16	2	26.3	5	54.4	29	54.0
	17	2	26.8	5	40.8	29	37.0
	18	2	27.4	5	27.4	29	20.1
	19	2	27.9	5	14.1	29	3.3
13	20	2	28.4	-5	0.9	+28	46.6
	21	2	28.9	4	47.9	28	29.9
	22	2	29.4	4	35.0	28	13.3
	23	2	29.8	4	22.2	27	56.7
	24	2	30.3	3	9.6	27	40.2
13	25	2	30.7	-3	57.0	+27	23.8
	26	2	31.1	3	44.6	27	7.4
	27	2	31.5	3	32.3	26	51.0
	28	2	31.9	3	20.2	26	34.7
	29	2	32.3	3	8.2	26	18.4
13 <sup>h</sup>	30 <sup>m</sup>	2 <sup>m</sup>	32 <sup>s</sup> .6	-2°	56.3	+26°	2.1
	31	2	33.0	2	44.5	25	45.9
	32	2	33.3	2	32.8	25	29.7
	33	2	33.6	2	21.3	25	13.5
	34	2	33.9	2	9.9	24	57.3

TABLE 25 (cont.)

G.C.T. of Mid-Totality		Semi-Duration of Total Eclipse		Latitude		Longitude	
13	35	2	34.2	-1	58.6	+24	41.1
	36	2	34.5	1	47.4	24	24.9
	37	2	34.8	1	36.4	24	8.7
	38	2	35.0	1	25.5	23	52.5
	39	2	35.3	1	14.7	23	36.3
13	40	2	35.5	-1	4.0	+23	20.3
	41	2	35.7	0	53.4	23	4.1
	42	2	35.9	0	43.0	22	47.9
	43	2	36.1	0	32.7	22	31.7
	44	2	36.2	0	22.5	22	15.5
13	45	2	36.4	-0	12.3	+21	59.3
	46	2	36.6	-0	2.3	21	43.0
	47	2	36.7	+0	7.6	21	26.7
	48	2	36.8	0	17.4	21	10.3
	49	2	36.8	0	27.1	20	53.9
13	50	2	36.9	+0	36.6	+20	37.5
	51	2	37.0	0	46.0	20	21.0
	52	2	37.0	0	55.3	20	4.5
	53	2	37.0	1	4.5	19	47.9
	54	2	37.1	1	13.6	19	31.3
13	55	2	37.1	+1	22.5	+19	14.6
	56	2	37.0	1	31.3	18	57.9
	57	2	37.0	1	40.0	18	41.1
	58	2	36.9	1	48.6	18	24.2
	59	2	36.8	1	57.1	18	7.2
14	0	2	36.8	+2	5.6	+17	50.2
	1	2	36.7	2	13.9	17	33.1
	2	2	36.6	2	22.0	17	15.9
	3	2	36.4	2	30.0	16	58.6
	4	2	36.2	2	37.9	16	41.2
14 <sup>n</sup>	5 <sup>m</sup>	2 <sup>m</sup>	36 <sup>s</sup> 0	+2 <sup>o</sup>	45 <sup>i</sup> 8	+16 <sup>o</sup>	23 <sup>i</sup> 8
	6	2	35.8	2	53.5	16	6.2
	7	2	35.6	3	1.1	15	48.5
	8	2	35.4	3	8.5	15	30.7
	9	2	35.2	3	15.8	15	12.8
14	10	2	35.0	+3	23.0	+14	55.0
	11	2	34.7	3	30.1	14	36.9
	12	2	34.4	3	37.0	14	18.7
	13	2	34.1	3	43.8	14	0.4
	14	2	33.8	3	50.5	13	41.9
14	15	2	33.4	+3	57.0	+13	23.3
	16	2	33.0	4	3.4	13	4.6
	17	2	32.6	4	9.7	12	45.7
	18	2	32.2	4	15.9	12	26.7
	19	2	31.8	4	21.9	12	7.5

TABLE 25 (cont.)

G.C.T. of Mid-Totality		Semi-Duration of Total Eclipse		Latitude		Longitude	
14	20	2	31.4	+4	27.8	+11	48.1
	21	2	31.0	4	33.6	11	28.5
	22	2	30.5	4	39.2	11	8.8
	23	2	30.0	4	44.7	10	48.9
	24	2	29.5	4	50.0	10	28.9
14	25	2	29.0	+4	55.2	+10	8.8

for the times and positions given in Table 26. From the data on the four contact points it was then possible to determine the position of the center of the moon with respect to the center of the sun for three positions: that of first and last contact and that of mid-totality. Through these three points a circle was drawn which is

TABLE 26  
Times of Contact for Positions of Ship

Contact	Times of Contact for position: Long. 20° 33.4 W Lat. 38.4 N	Ship's Position		Times of Contact corrected for ship's position
		Long.	Lat.	
I	12 <sup>h</sup> 16 <sup>m</sup> 23 <sup>s</sup>	20° 31.3 N	45.8 N	12 <sup>h</sup> 16 <sup>m</sup> 37 <sup>s</sup>
II	13 47 37	20 33.0	38.4	13 47 39
III	13 52 51	20 33.9	38.3	13 52 49
IV	15 25 34	20 52.5	34.3	15 24 38

used for the path of the moon's center across the solar disc as shown in Figure 36. The deviation of this path from the true path is small enough to be neglected in this experiment. When this path divided into even subdivisions of time, it was a simple matter to determine the time of occultation of the sunspots by using a transparent template representing the moon.

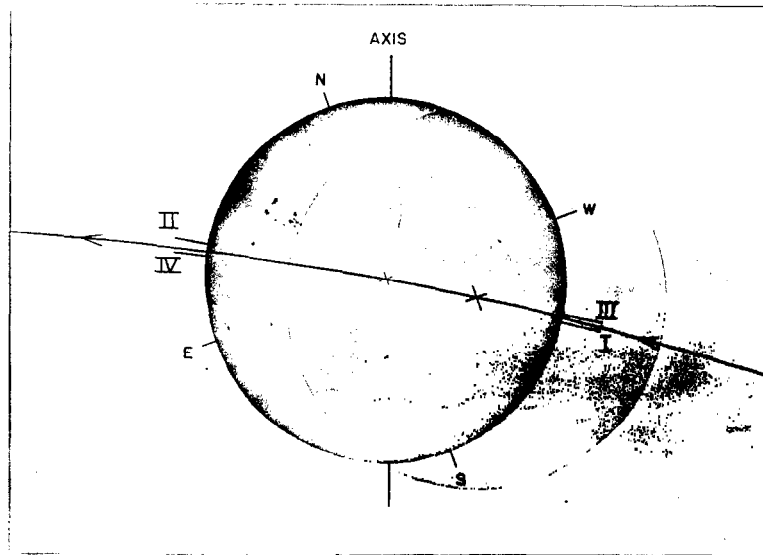


Figure 36 - Path of moon's center across solar disk

### Observed Eclipse Function

The weather on the day of the eclipse started out overcast with high clouds; there had been an extremely heavy rain on the previous day. The weather cleared progressively as the day went on, so that it was possible to see the sun during breaks in the clouds during the entire period of the eclipse. At the time of first contact the sun was in the clear so that the time of contact could be determined optically. During the first half of the eclipse the sun was covered intermittently with light clouds at least half the time. The sun was in the clear during the entire period of totality and remained pretty much uncovered during the latter half of the eclipse. The clouds did not interfere seriously with the radio measurements, but they did make it difficult to keep the sharp radio beam on the sun by optical means, and, of course, interfered with the monitoring photographs taken to check pointing accuracy.

The receiving arrangement used in the 3.2 centimeter apparatus differs from that described earlier for 8.5 millimeters. Figure 37 is a block diagram of the receiver. The arrangement was originally

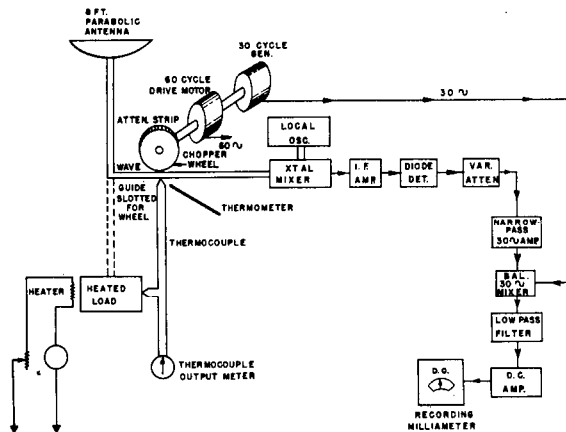


Figure 37 - Block diagram of 3.14 centimeter radiometer

designed by Dicke.<sup>41</sup> It is essentially a superheterodyne receiver which looks alternately at the signal through the antenna and at a matched load at ambient temperature. The switching is done at a rate of thirty times a second. The signal applied to the receiver is then one with a thirty-cycle variation in amplitude. The maximum amplitude is that of the incoming signal and the minimum amplitude is that due to the Johnson noise in the waveguide termination. The maximum and minimum positions are reversed, of course, if the antenna is pointed at something having lower than ambient temperature; the thirty-cycle output will be zero when the antenna is pointed at something which is at the same temperature as the waveguide termination. The thirty-cycle output from the receiver is amplified and later detected and measured in a recording milliammeter.

The antenna used for the experiment was a parabolic reflector eight feet in diameter mounted on a pedestal which allowed the stabilized antenna to be trained in azimuth and elevation by hand control through an electromechanical linkage. The beamwidth of the antenna was  $0.8^\circ$  between half-power points. The degree of stabilization was such that the total motion of the ship was not taken out of the antenna, and it was necessary for the operator to make corrections in the pointing using the hand controls with the aid of a telescope. In so far as possible the records were checked against photographs of the sun taken at five-second intervals through a telescope bolted to the antenna mount.

The signal received from the sun caused a deflection in the output meter of the receiver of about 1.5 milliamperes. This deflection was shown earlier in the report to be proportional to the antenna temperature. The output of the receiver was connected to an Esterline-Angus recording milliammeter to record the variations in intensity during the progress of the eclipse. To calibrate the deflection of the recording milliammeter in terms of intensity of the incident radiation, the receiver was connected to a matched termination whose temperature could be varied in a known fashion. The deflection of the output instrument could be accurately calibrated with a thermocouple in terms of antenna temperature.

To convert from antenna temperature to the true temperature of the sun, a knowledge of the pattern and gain of the antenna is required. See equation (20). At periodic intervals during the series of measurements the antenna was pointed at the sky some distance from the sun and the equivalent temperature of the sky recorded. The constancy of the sky reading gives a measure of the stability of the receiving arrangement, for since the sky temperature is less than the temperature of the termination against which it is compared, then any variation in gain of the receiver will be revealed by a lack of constancy of the sky reading.

The antenna arrangement was mounted on an existing tripod mast in such a way that the center of the antenna was seventy-five feet above water level. The antenna had an unobstructed view in all directions except for dead ahead at zero elevation, where the foremast and rigging of the ship interfered.

### An Interpretation of the Observed Function

During the observation of the eclipse, the sun was in such a position relative to the ship that the antenna had an unobstructed view of the sun. The results of the observation during the eclipse are given in Figure 38. Here the rectified current at the output of the receiver, which is proportional to the intensity of the received radiation, is plotted as a function of time. Each point shown is the mean of many observed points except for the expanded region for the time of totality, where all points are shown. The times of the four eclipse contacts are indicated on the curve. It can be seen that the

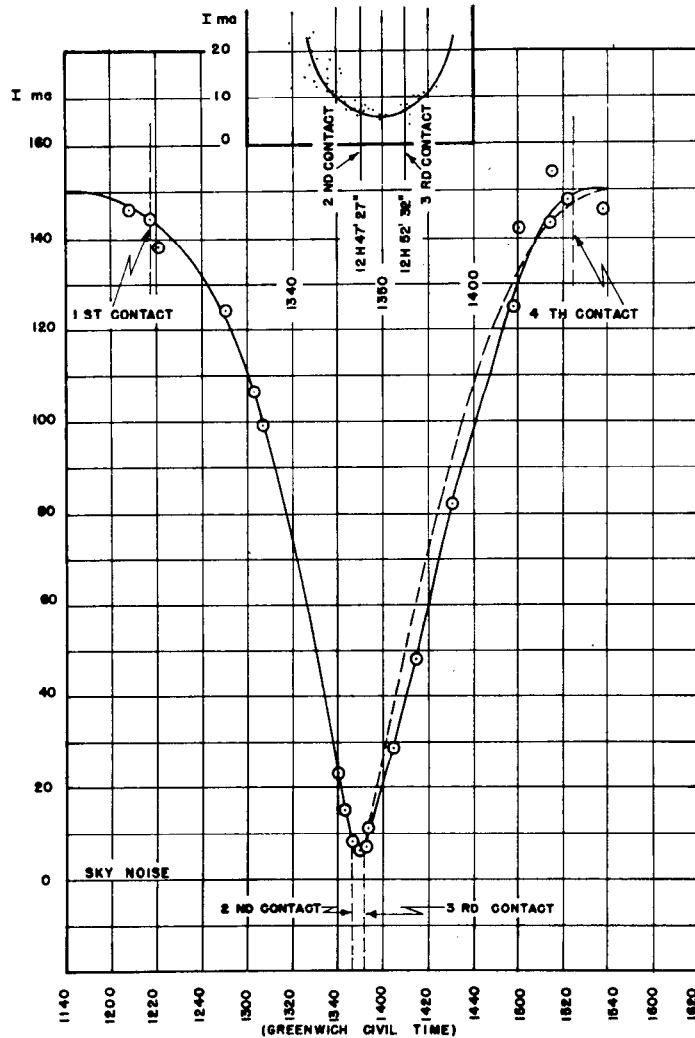


Figure 38 - Variation of received signal at 3.2 centimeters during the May 20, 1947 eclipse. The full line passes through the average of the observed points; the dotted line represents a symmetrical curve. The individual points are shown to an expanded scale near totality

radio-frequency radiation from the sun at 3.2 centimeters wavelength was not totally eclipsed. The intensity fell to only 4% of the total radiation. An inspection of the figure will show that the eclipse curve is not symmetrical about the time of midtotality. The data was analyzed to evaluate the relative effect of the variation in brightness across the surface of the sun, the excess radiation associated with sunspot activity, and, finally, the radiation due to the corona. For purposes of analysis the observed points are plotted in Figure 39 with relative intensity as ordinate and apparent separation of the the centers of the sun and moon as abscissa.

Consider first the residual radiation at the time of totality. This signal can be accounted for in three possible ways: (1) radiation

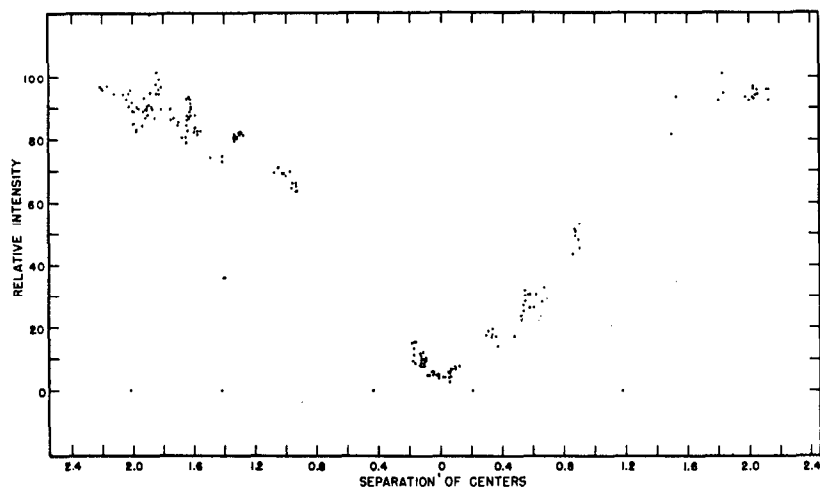


Figure 39 - The observed relative intensity during the eclipse of May 20, 1947 plotted against apparent separation of the centers of the sun and the moon in units of solar radii

from that part of the corona which is unobscured; (2) radiation from the near side of the moon; (3) diffraction around the edge of the moon. Calculations show that the radiation diffracted around the moon from an extended source such as the sun at this frequency can be neglected. The radiation from the back or cold side of the moon has been independently measured as somewhat less than 1% of the radiation from the sun at this wavelength. The conclusion that must be drawn then is that the part of the corona which is visible during totality radiates an amount of energy at this wavelength which is 3% to 4% of that of the uneclipsed sun.

A calculation has been made of the expected radiation from the corona during the period of totality using the data and methods presented in this report. This analysis indicates that the residual radiation should be 4% of that of the uneclipsed sun. Table 27 gives the calculation for the effective temperature of the corona at distances  $\rho = 1.04, 1.05, 1.06, 1.07,$  and  $1.10$  from the center of the sun. The construction used is similar to that previously used for the analysis of the equivalent temperature at the limb, where in this instance the limb is replaced by the sphere of radius  $R$ . The absorption for each layer is now  $2K\Delta h$ , since the ray penetrates the entire corona. Table 28 provides a series of values for the summation of  $2K\Delta h$ . From these data the value at 1.055, 1.065, etc., were obtained by interpolation, and the curve was extrapolated

TABLE 27  
Calculation of the Absorption for  $\rho = 1.04$

$h_s$ $10^8 \text{ cm}$	$x$ $10^8 \text{ cm}$	$x^2$ $10^{16} \text{ cm}^2$	$2Rx$ $10^{16} \text{ cm}^2$	$h'^2$ $10^{16} \text{ cm}^2$	$h'$ $10^8 \text{ cm}$	$\Delta h'$ $10^8 \text{ cm}$	$K$ per cm	$2K \cdot \Delta h'$
28	0	0	0	0	0	38.171	$1.39 \times 10^{-13}$	$1.061 \times 10^{-3}$
29	1	1	1456	1457	38.171	15.829	1.33	$4.211 \times 10^{-4}$
30	2	4	2912	2916	54.000	12.159	1.28	3.113
31	3	9	4368	4377	66.159	10.261	1.23	2.524
32	4	16	5824	5840	76.420	9.049	1.18	2.136
33	5	25	7280	7305	85.469	8.190	1.13	1.851
34	6	36	8736	8772	93.659	7.54	1.09	1.644
35	7	49	10192	10241	101.20	7.02	1.06	1.488
36	8	64	11648	11712	108.22	6.61	1.02	1.348
37	9	81	13104	13185	114.83	6.25	$9.8 \times 10^{-14}$	1.225
38	10	100	14560	14660	121.08	5.95	9.55	1.136
39	11	121	16016	16137	127.03	5.70	9.21	1.049
40	12	144	17472	17616	132.73	5.46	8.98	$9.828 \times 10^{-5}$
41	13	169	18928	19097	138.19	5.27	8.70	9.170
42	14	196	20384	20580	143.46	5.08	8.42	8.534
43	15	225	21840	22065	148.54	4.93	8.10	7.987
44	16	256	23296	23552	153.47	4.77	8.00	7.632
45	17	289	24752	25041	158.24	4.65	7.80	7.254
46	18	324	26208	26532	162.89	4.52	7.60	6.870
47	19	361	27664	28025	167.41	4.40	7.40	6.512
48	20	400	29120	29520	171.81	4.31	7.22	6.206
49	21	441	30576	31017	176.12	4.20	7.03	5.922
50	22	484	32032	32516	180.32	19.78	6.60	$2.611 \times 10^{-4}$
55	27	729	39312	40041	200.10	18.11	5.90	2.137
60	32	1024	46592	47616	218.21	16.82	5.30	1.783
65	37	1369	53872	55241	235.03	15.80	4.80	1.517
70	42	1764	61152	62916	250.83	166.23	2.70	8.976
139	111	12321	161616	173937	417.06	236.01	$4.90 \times 10^{-15}$	2.312
278	250	62500	364000	426500	653.07	194.11	$5.50 \times 10^{-16}$	$2.136 \times 10^{-5}$
417	389	151321	566384	717705	847.18			
								$\Sigma = 5.947 \times 10^{-3}$

TABLE 27  
Calculation of the Absorption for  $\rho = 1.05$

$h_g$ $10^8 \text{ cm}$	$x$ $10^8 \text{ cm}$	$x^2$ $10^{16} \text{ cm}^2$	$27x$ $10^{16} \text{ cm}^2$	$h^2$ $10^{16} \text{ cm}^2$	$h'$ $10^8 \text{ cm}$	$\Delta h'$ $10^8 \text{ cm}$	K per cm	$2K \cdot \Delta h'$
35	0	0	0	0	0	38.354	$1.06 \times 10^{-13}$	$8.131 \times 10^{-4}$
36	1	1	1470	1471	38.354	15.905	1.02	3.245
37	2	4	2940	2944	54.259	12.217	$9.8 \times 10^{-14}$	2.395
38	3	9	4410	4419	66.476	10.310	9.55	1.969
39	4	16	5880	5896	76.786	9.092	9.21	1.673
40	5	25	7350	7375	85.878	8.229	8.98	1.481
41	6	36	8820	8856	94.107	7.57	8.70	1.317
42	7	49	10290	10339	101.68	7.06	8.42	1.186
43	8	64	11760	11824	108.74	6.63	8.10	1.074
44	9	81	13230	13311	115.37	6.29	8.00	1.006
45	10	100	14700	14800	121.66	5.98	7.80	$9.329 \times 10^{-5}$
46	11	121	16170	16291	127.64	5.72	7.60	8.694
47	12	144	17640	17784	133.36	5.49	7.40	8.125
48	13	169	19110	19279	138.85	5.29	7.22	7.618
49	14	196	20580	20776	144.14	5.11	7.03	7.205
50	15	225	22050	22275	149.25	23.38	6.60	$3.086 \times 10^{-4}$
55	20	400	29400	29800	172.63	20.07	5.90	2.368
60	25	625	36750	37375	193.33	18.80	5.30	1.993
65	30	900	44100	45000	212.13	17.38	4.80	1.668
70	35	1225	51450	52675	229.51	175.08	2.70	9.454
139	104	10816	152880	163696	404.59	240.59	$4.9 \times 10^{-15}$	2.358
278	243	59049	357210	416259	645.18	195.93	$5.5 \times 10^{-16}$	$2.156 \times 10^{-5}$
417	382	145924	561540	707464	841.11			$\Sigma = 4.872 \times 10^{-3}$

TABLE 27  
Calculation of the Absorption for  $\rho = 1.06$

$h_s$ $10^8 \text{cm}$	$x$ $10^8 \text{cm}$	$x^2$ $10^{16} \text{cm}^2$	$2Rx$ $10^{16} \text{cm}^2$	$h'^2$ $10^{16} \text{cm}^2$	$h'$ $10^8 \text{cm}$	$\Delta h'$ $10^8 \text{cm}$	K per cm	$2K \cdot \Delta h'$
42	0	0	0	0	0			
43	1	1	1484	1485	38.536	38.536	$8.42 \times 10^{-14}$	$6.474 \times 10^{-4}$
44	2	4	2968	2972	54.516	15.980	8.10	2.589
45	3	9	4452	4461	66.791	12.275	8.00	1.964
46	4	16	5936	5952	77.149	10.358	7.80	1.616
47	5	25	7420	7445	86.284	9.135	7.60	1.389
48	6	36	8904	8940	94.552	8.268	7.40	1.224
49	7	49	10388	10437	102.16	7.61	7.22	1.096
50	8	64	11872	11936	109.25	7.09	7.03	$9.997 \times 10^{-5}$
55	13	169	19292	19461	139.50	30.25	6.60	$3.993 \times 10^{-4}$
60	18	324	26712	27036	164.43	24.93	5.90	2.942
65	23	529	34132	34661	186.18	21.75	5.30	2.306
70	28	784	41552	42336	205.76	19.58	4.80	1.880
139	97	9409	143948	153357	391.61	185.85	2.70	$1.004 \times 10^{-2}$
278	236	55696	350224	405920	637.12	245.51	$4.9 \times 10^{-15}$	$2.406 \times 10^{-4}$
417	389	151321	577276	728597	853.58	216.46	$5.5 \times 10^{-16}$	$2.382 \times 10^{-5}$
								$\Sigma = 4.115 \times 10^{-3}$

TABLE 27  
Calculation of the Absorption for  $\rho = 1.07$

$h_s$ $10^8 \text{cm}$	$x$ $10^8 \text{cm}$	$x^2$ $10^{16} \text{cm}^2$	$2Rx$ $10^{16} \text{cm}^2$	$h'^2$ $10^{16} \text{cm}^2$	$h'$ $10^8 \text{cm}$	$\Delta h'$ $10^8 \text{cm}$	$K$ per cm	$2K \cdot \Delta h'$
49	0	0	0	0	0			
50	1	1	1498	1499	$38.717 \times 10^9$	38.717	$7.03 \times 10^{-14}$	$5.444 \times 10^{-4}$
55	6	36	8988	9024	$94.995 \times 10^9$	56.278	6.60	$7.429 \times 10^{-4}$
60	11	121	16478	16599	$128.84 \times 10^{10}$	33.845	5.90	$3.994 \times 10^{-4}$
65	16	256	23968	24224	$155.64 \times 10^{10}$	26.80	5.30	$2.841 \times 10^{-4}$
70	21	441	31458	31899	$178.60 \times 10^{10}$	22.96	4.80	$2.204 \times 10^{-4}$
139	90	8100	134820	142920	$378.05 \times 10^{10}$	199.5	2.7	$1.077 \times 10^{-3}$
278	229	52441	343042	395483	$628.88 \times 10^{10}$	250.8	$4.9 \times 10^{-15}$	$2.458 \times 10^{-4}$
417	368	135424	551264	686688	$828.67 \times 10^{10}$	199.8	$5.5 \times 10^{-16}$	$2.198 \times 10^{-5}$
								$\Sigma = 3.536 \times 10^{-3}$

TABLE 27  
Calculation of the Absorption for  $\rho = 1.10$

$h_s$ $10^8 \text{cm}$	$x$ $10^8 \text{cm}$	$x^2$ $10^{16} \text{cm}^2$	$2Rx$ $10^{16} \text{cm}^2$	$h'^2$ $10^{16} \text{cm}^2$	$h'$ $10^8 \text{cm}$	$\Delta h'$ $10^8 \text{cm}$	$K$ per cm	$2K \cdot \Delta h'$
70	0	0	0	0	0			
139	69	4761	106260	111021	333.20	$3.332 \times 10^{10}$	$2.7 \times 10^{-14}$	$1.799 \times 10^{-3}$
278	208	43264	320320	363584	602.98	$2.698 \times 10^{10}$	$4.9 \times 10^{-15}$	$2.644 \times 10^{-4}$
417	347	120409	534380	654789	809.19	$2.062 \times 10^{10}$	$5.5 \times 10^{-16}$	$2.268 \times 10^{-5}$
								$\Sigma = 2.086 \times 10^{-3}$

$x$  = height of the top of the layer above the reference circle

$h_s$  = height of the top of the layer above the sun's surface,

$$h_s = (R - R_0) + x$$

$$h'^2 = 2Rx + x^2$$

$$R = 7.28 \times 10^{10} \text{ cm}$$

$$R_0 = 7 \times 10^{10} \text{ cm}$$

$$\rho = \frac{R}{R_0}$$

TABLE 28  
 Calculation of Residual Radiation at Time of  
 Totality and the Equivalent Temperature of  
 the Corona at 3.14 Centimeters Wavelength

	A	B	C	$\frac{I_c}{I_s}$	Equivalent Temperature of Ring ° K
	$\sum 2K\Delta h$	$\frac{A_{ring}}{A_{sun}}$	$\frac{T_r}{T_s}$ 3.14	A·B·C	
1.04	$5.35 \times 10^{-3}$	0.0209	70	0.00784	$4.5 \times 10^3$
1.05	4.48	.0211	70	.00662	3.76
1.06	3.81	.0213	70	.00568	3.19
1.07	3.28	.0215	70	.00516	2.75
1.08	2.78	.0217	70	.00422	2.33
1.09	2.30	.0219	70	.00352	1.92
1.10	1.85	.0221	70	.00285	1.55
1.11	1.38	.0223	70	.00216	1.16
1.12	0.92	.0225	70	.00145	0.77
1.13	0.45	.0227	70	.00071	0.377
1.14				$\sum = 0.04021$	

to obtain the probable values beyond 1.1. Since the absorption had fallen to a quite low value at 1.1, any error in the extrapolation will make only a small error in the final result. Successive rings from 1.04 to 1.05, 1.05 to 1.06, etc., out to 1.13 are computed for area and shown as a ratio to the area of the sun (see column 3). The temperature of the corona over this region is taken to be uniform at  $8.4 \times 10^5$  degrees Kelvin. The contribution due to the exposed corona may be calculated in the following manner:

$$\frac{I_c}{I_s} = \sum \frac{A_r \cdot T_r \cdot \sum 2K\Delta h}{A_s T_e} \quad (77)$$

where  $A_r$  = the area of the individual ring  
 $T_r$  =  $8.4 \times 10^5$  degrees Kelvin, the equivalent temperature of the material in the ring  
 $\sum 2K\Delta h$  = the absorption of a ray passing through the ring  
 $A_s$  = area of the sun

## NAVAL RESEARCH LABORATORY

$T_e$  = equivalent temperature of the sun  
 $I_c$  = emission from the exposed corona  
 $I_s$  = emission from the entire sun.

The contribution from each ring is tabulated in column 5 of Table 28, and the sum is the ratio of the total emission from the unclipped corona to the emission of the entire sun. It is seen that there is excellent agreement between the computed and observed values.

The earlier analysis also yields the temperature distribution across the solar disc. The distribution computed on this basis is shown in Figure 40. The computation yielding the data for Figure 42

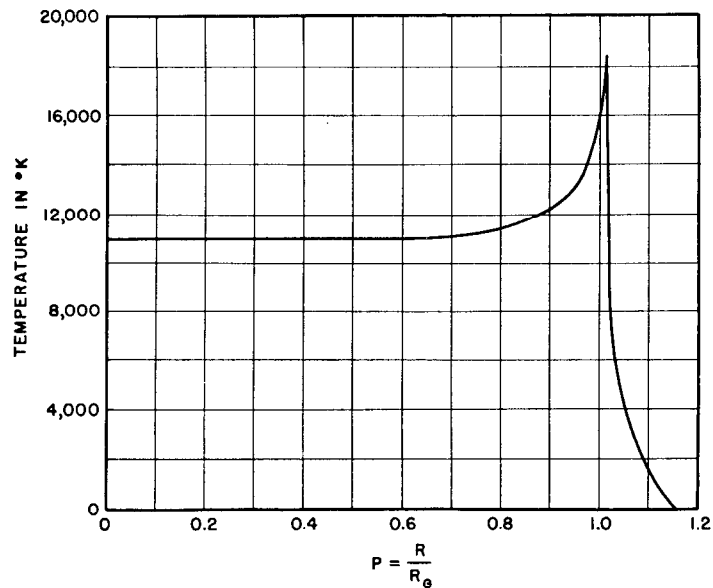


Figure 40 - Calculated temperature distribution across the surface of the sun at a wavelength of 3.14 centimeters

is given in Tables 12, 13, 27, 29, 30 and 31. These tables give the equivalent temperature for rays emerging at the center and at  $\rho = 0.791$ , 0.935, 1.0, 1.015, 1.04, and out to  $\rho = 1.10$ . It is seen that limb brightening becomes appreciable at 3.14 centimeters and that the effective diameter of the sun is some 15,000 to 20,000 kilometers greater than the optical diameter.

TABLE 29

Calculation of the Equivalent Temperature at  $\rho = 0.791$  at 3.14 Centimeters Wavelength

r	h KM	T °K	K CM <sup>-1</sup>	R + h 10 <sup>6</sup> cm	(R+h) <sup>2</sup> 10 <sup>20</sup> cm <sup>2</sup>	(R+h) <sup>2</sup> -x <sup>2</sup> 10 <sup>20</sup> cm <sup>2</sup>	$\sqrt{(R+h)^2-x^2}$ 10 <sup>10</sup> cm	h <sub>0</sub> 10 <sup>6</sup> cm	$\Delta h_0^2$ 10 <sup>12</sup> cm <sup>2</sup>	K $\Delta h_0^2$	A 1-e <sup>-K<math>\Delta h_0^2</math></sup>	$\sum K\Delta h_0^2$	B e <sup>-<math>\sum K\Delta h_0^2</math></sup>	C $\frac{T \cdot A}{K}$	C <sub>0</sub> B <sub>T</sub> +1 $\frac{C_0}{K}$
1	7500	6.51x10 <sup>3</sup>	8.69x10 <sup>-8</sup>	702.5	49.351	19.101	437.05	12.17	0.80	6.952	0.9990	18.1898	1.2597x10 <sup>-8</sup>	6.503x10 <sup>3</sup>	8.563x10 <sup>-2</sup>
2	8000	6.64	5.95	703.0	49.421	19.171	437.85	12.97	0.80	4.760	.9914	11.2378	1.3168x10 <sup>-5</sup>	6.583x10 <sup>3</sup>	1.012x10 <sup>1</sup>
3	8500	6.92	3.59	703.5	49.491	19.241	438.65	13.77	0.80	2.872	.9434	6.4778	1.5371x10 <sup>-3</sup>	6.528x10 <sup>3</sup>	1.773x10 <sup>2</sup>
4	9000	7.60	2.07	704.0	49.562	19.312	439.45	14.57	0.80	1.656	.8091	3.6058	2.7164x10 <sup>-2</sup>	6.119x10 <sup>3</sup>	8.750x10 <sup>2</sup>
5	9500	8.10	1.18	704.5	49.632	19.382	440.25	15.37	0.80	0.9440	.6109	1.9498	0.1423	4.948x10 <sup>3</sup>	1.810x10 <sup>3</sup>
6	10000	9.20	6.13x10 <sup>-9</sup>	705.0	49.702	19.452	441.05	16.17	0.80	.4904	.3876	1.0058	0.3658	3.566x10 <sup>3</sup>	2.130x10 <sup>3</sup>
7	10500	1.07x10 <sup>4</sup>	3.10	705.5	49.773	19.523	441.85	16.97	0.80	.2480	.2196	.5154	.5973	2.350x10 <sup>3</sup>	1.799x10 <sup>3</sup>
8	11000	1.29	1.49	706.0	49.844	19.594	442.65	17.77	0.80	.1177	.1110	.2674	.7654	1.432x10 <sup>3</sup>	1.233x10 <sup>3</sup>
9	11500	1.45	7.49x10 <sup>-10</sup>	706.5	49.914	19.664	443.44	18.56	0.80	.05992	.0581	.1497	.8610	8.424x10 <sup>2</sup>	7.700x10 <sup>2</sup>
10	12000	1.70	4.22	707.0	49.985	19.735	444.24	19.36	0.80	.03376	.0332	.08978	.9111	5.644x10 <sup>2</sup>	5.336x10 <sup>2</sup>
11	12500	1.95	2.50	707.5	50.056	19.806	445.04	20.16	0.79	.01975	.0196	.05602	.9455	3.822x10 <sup>2</sup>	3.686x10 <sup>2</sup>
12	13000	2.29	1.49	708.0	50.126	19.876	445.83	20.95	0.79	.01177	.0117	.03627	.9644	2.679x10 <sup>2</sup>	2.614x10 <sup>2</sup>
13	13500	2.73	9.03x10 <sup>-11</sup>	708.5	50.197	19.947	446.62	21.74	0.80	.007224	.007224	.02450	.9758	1.972x10 <sup>2</sup>	1.938x10 <sup>2</sup>
14	14000	3.16	5.84	709.0	50.268	20.018	447.42	22.54	0.79	.004614		.01727	.9828	1.458x10 <sup>2</sup>	1.440x10 <sup>2</sup>
15	14500	3.71	4.00	709.5	50.339	20.089	448.21	23.33	0.79	.003160		.01266	.9874	1.172x10 <sup>2</sup>	1.161x10 <sup>2</sup>
16	15000	4.68	2.58	710.0	50.410	20.160	449.00	24.12	1.58	.002076		.009499	.9905	1.908x10 <sup>2</sup>	1.898x10 <sup>2</sup>
17	16000	6.46	1.31	711.0	50.552	20.302	450.58	25.70	1.57	.002057		.005423	.9916	1.329x10 <sup>2</sup>	1.324x10 <sup>2</sup>
18	17000	8.50	7.98x10 <sup>-12</sup>	712.0	50.694	20.444	452.15	27.27	1.58	.001261		.003366	.9966	1.072x10 <sup>2</sup>	1.070x10 <sup>2</sup>
19	18000	1.20x10 <sup>5</sup>	4.90	713.0	50.837	20.587	453.73	28.85	1.57	.0007693		.002105	.9979	9.232x10 <sup>1</sup>	9.220x10 <sup>1</sup>
20	19000	1.55	3.03	714.0	50.980	20.730	455.30	30.42	1.56	.0004727		.001336	.9987	7.327x10 <sup>1</sup>	7.320x10 <sup>1</sup>
21	20000	2.51	1.50	715.0	51.122	20.872	456.86	31.98	3.13	.0004695		.0008631	.9991	1.178x10 <sup>2</sup>	1.178x10 <sup>2</sup>
22	22000	4.60	6.45x10 <sup>-13</sup>	717.0	51.409	21.159	459.99	35.11	3.11	.0002006		.0003936	.9996	9.228x10 <sup>1</sup>	9.226x10 <sup>1</sup>
23	24000	7.82	3.08	719.0	51.696	21.446	463.10	38.22	3.10	.00009548		.0001930	.9998	7.467x10 <sup>1</sup>	7.466x10 <sup>1</sup>
24	26000	8.40	1.86	721.0	51.984	21.734	466.20	41.32	3.09	.00005747		.00009753	.9999	4.827x10 <sup>1</sup>	4.827x10 <sup>1</sup>
25	28000	8.40	1.305	723.0	52.273	22.023	469.29	44.41	3.07	.00004006		.00004006	1.0000	3.365x10 <sup>1</sup>	
25	30000			725.0	52.562	22.312	472.36	47.48							

$\Sigma = 11,350^\circ K$

$$k' = -r + \sqrt{r^2 + 2rk + k^2}$$

but  $r^2 = R^2 - x^2$

therefore  $k' = -\sqrt{R^2 - x^2} + \sqrt{(R+k)^2 - x^2}$

$$= \sqrt{(R+k)^2 - x^2} - 4.2488 \times 10^{10} \text{ cm}$$

TABLE 30

Calculation of the Equivalent Temperature at  $\rho = 0.935$  at 3.14 Centimeters Wavelength

r	h MM	$\frac{T}{\circ K}$	K CM <sup>-1</sup>	$\frac{R+h}{10^3 \text{ cm}}$	$\frac{(R+h)^2}{10^{20} \text{ cm}^2}$	$\frac{(R+h)^2-x^2}{10^{20} \text{ cm}^2}$	$\sqrt{\frac{(R+h)^2-x^2}{10^{20} \text{ cm}^2}}$	$\frac{h}{10^3 \text{ cm}}$	$\frac{\Delta h'}{10^3 \text{ cm}}$	K $\cdot\Delta h'$	A $1-e^{-K\cdot\Delta h'}$	$\sum K\cdot\Delta h'$	B $e^{-\sum K\Delta h'}$	C $\frac{T\cdot A}{\circ K}$	$C^B K + 1$
1	7500	6.51x10 <sup>3</sup>	8.69x10 <sup>-8</sup>	702.5	49.351	7.101	266.48	20.46	1.31	11.3839	1.000	29.6623	1.312x10 <sup>-13</sup>	6.51x10 <sup>3</sup>	7.506x10 <sup>-5</sup>
2	8000	6.64	5.95	703.0	49.421	7.171	267.79	21.77	1.30	7.7350	0.9996	18.2784	1.153x10 <sup>-8</sup>	6.637	1.750x10 <sup>-1</sup>
3	8500	6.92	3.59	703.5	49.491	7.241	269.09	23.07	1.32	4.7388	.9912	10.5434	2.637x10 <sup>-5</sup>	6.859	2.067x10 <sup>1</sup>
4	9000	7.60	2.07	704.0	49.562	7.312	270.41	24.39	1.29	2.6703	.9308	5.8046	3.0139x10 <sup>-3</sup>	7.074	1.324x10 <sup>2</sup>
5	9500	8.10	1.18	704.5	49.632	7.382	271.70	25.68	1.28	1.5104	.7792	3.1343	1.8710x10 <sup>-2</sup>	6.312	1.244x10 <sup>3</sup>
6	10000	9.20	6.13x10 <sup>-9</sup>	705.0	49.702	7.452	272.98	26.96	1.30	0.7969	.5493	1.6239	1.971x10 <sup>-1</sup>	5.054	2.211x10 <sup>3</sup>
7	10500	1.07x10 <sup>4</sup>	3.10	705.5	49.773	7.523	274.28	28.26	1.29	.3999	.3296	.8270	0.4374	3.527	2.301x10 <sup>3</sup>
8	11000	1.29	1.49	706.0	49.844	7.594	275.57	29.55	1.27	.1892	.1721	.4271	.6524	2.224	1.753x10 <sup>3</sup>
9	11500	1.45	7.49x10 <sup>-10</sup>	706.5	49.914	7.664	276.84	30.82	1.28	.09587	.09140	.2379	.7883	1.325	1.149x10 <sup>3</sup>
10	12000	1.70	4.22	707.0	49.985	7.735	278.12	32.10	1.27	.05359	.05220	.1421	.8675	8.874x10 <sup>2</sup>	8.122x10 <sup>2</sup>
11	12500	1.95	2.50	707.5	50.056	7.806	279.39	33.37	1.25	.03125	.03080	.08847	.9153	6.006	5.672x10 <sup>2</sup>
12	13000	2.25	1.49	708.0	50.126	7.876	280.64	34.62	1.26	.01877	.01860	.05722	.9444	4.259	4.098x10 <sup>2</sup>
13	13500	2.73	9.03x10 <sup>-11</sup>	708.5	50.197	7.947	281.90	35.88	1.26	.01138	.0113	.03845	.9622	3.085	3.003x10 <sup>2</sup>
14	14000	3.16	5.84	709.0	50.268	8.018	283.16	37.14	1.25	.007300	.007270	.02707	.9733	2.297	2.252x10 <sup>2</sup>
15	14500	3.71	4.00	709.5	50.339	8.089	284.41	38.39	1.25	.005000	.005000	.01977	.9804	1.855	1.828x10 <sup>2</sup>
16	15000	4.68	2.58	710.0	50.410	8.160	285.66	39.64	1.24	.00373	.00373	.01477	.9853	2.983	2.958x10 <sup>2</sup>
17	16000	6.46	1.31	711.0	50.552	8.302	288.13	42.11	1.24	.003223	.003223	.008401	.9916	2.082	2.071x10 <sup>2</sup>
18	17000	8.50	7.98x10 <sup>-12</sup>	712.0	50.694	8.444	290.59	44.57	1.24	.001955	.001955	.005178	.9948	1.662	1.657x10 <sup>2</sup>
19	18000	1.20x10 <sup>5</sup>	4.90	713.0	50.837	8.587	293.04	47.02	1.23	.001191	.001191	.003223	.9968	1.129	1.426x10 <sup>2</sup>
20	19000	1.55	3.03	714.0	50.980	8.730	295.47	49.45	1.23	.0007242	.0007242	.002032	.9980	1.122	1.121x10 <sup>2</sup>
21	20000	2.51	1.50	715.0	51.122	8.872	297.86	51.84	1.23	.0007170	.0007170	.001308	.9987	1.800	1.799x10 <sup>2</sup>
22	22000	4.60	6.45x10 <sup>-13</sup>	717.0	51.409	9.159	302.64	56.62	1.20	.0003032	.0003032	.0005912	.9994	1.395	1.395x10 <sup>2</sup>
23	24000	7.82	3.08	719.0	51.696	9.446	307.34	61.32	1.18	.0001132	.0001132	.0002880	.9997	1.120	1.120x10 <sup>2</sup>
24	26000	8.40	1.86	721.0	51.984	9.734	311.99	65.97	1.17	.00008556	.00008556	.0001448	.9999	7.187x10 <sup>1</sup>	7.187x10 <sup>1</sup>
25	28000	8.40	1.395	723.0	52.273	10.023	316.59	70.57	1.16	.00005925	.00005925	.00005925	1.000	4.977	
26	30000	8.40	1.195	725.0	52.562	10.312	321.13	75.11							

$\sum = 12,740^\circ K$

TABLE 31

Calculation of the Equivalent Temperature at  $\rho = 1.012$  at 3.14 Centimeters Wavelength

r	h km	T °K	K cm <sup>-1</sup>	h <sub>1</sub> 10 <sup>8</sup> cm	2R <sub>1</sub> h <sub>1</sub> 10 <sup>16</sup> cm <sup>2</sup>	h <sub>1</sub> <sup>2</sup> 10 <sup>16</sup> cm <sup>2</sup>	(h') <sup>2</sup> 10 <sup>16</sup> cm <sup>2</sup>	h' 10 <sup>8</sup> cm	Δ h' 10 <sup>8</sup> cm	K'Δ h'	1-e <sup>-KΔ h'</sup>	Σ K'Δ h'	∫ KΔ h'	T <sub>e</sub> °K	C <sub>∞</sub> <sup>3</sup> ρ <sub>∞</sub> <sup>-1</sup>
1	8000	6.64x10 <sup>3</sup>	5.95x10 <sup>-8</sup>	0	0	0	0	0	26.519	157.79	1.000	230.7007	6.426x10 <sup>-101</sup>	6.64x10 <sup>3</sup>	1.437x10 <sup>-28</sup>
2	8500	6.92	3.59	0.5	703	.25	703.25	26.519	11.232	40.323	1.000	72.9107	2.164x10 <sup>-32</sup>	6.92x10 <sup>3</sup>	4.869x10 <sup>-11</sup>
3	9000	7.60	2.07	1.0	1406	1.0	1407	37.751	8.197	16.968	1.000	32.5877	7.036x10 <sup>-15</sup>	7.60x10 <sup>3</sup>	1.250x10 <sup>-3</sup>
4	9500	8.10	1.18	1.5	2109	2.25	2111.25	45.948	7.118	8.9992	0.9998	15.620	1.645x10 <sup>-7</sup>	8.09x10 <sup>3</sup>	5.917x10 <sup>0</sup>
5	10000	9.20	6.13x10 <sup>-9</sup>	2.0	2812	4.00	2816.00	53.066	6.274	3.8460	0.9786	7.2205	7.314x10 <sup>-4</sup>	9.003x10 <sup>3</sup>	3.082x10 <sup>2</sup>
6	10500	1.07x10 <sup>4</sup>	3.10	2.5	3515	6.25	3521.25	59.340	5.675	1.7592	.8278	3.3745	3.423x10 <sup>-2</sup>	8.857x10 <sup>3</sup>	1.761x10 <sup>3</sup>
7	11000	1.29	1.49	3.0	4218	9.00	4227.00	65.015	5.222	0.7781	.5407	1.6153	1.988x10 <sup>-1</sup>	6.975x10 <sup>3</sup>	3.019x10 <sup>3</sup>
8	11500	1.45	7.49x10 <sup>-10</sup>	3.5	4921	12.25	4933.25	70.237	4.863	.3442	.3052	.8372	0.4329	4.425x10 <sup>3</sup>	2.757x10 <sup>3</sup>
9	12000	1.70	4.22	4.0	5624	16.00	5640.00	75.100	4.570	.1929	.1754	.4730	.6231	2.982x10 <sup>3</sup>	2.253x10 <sup>3</sup>
10	12500	1.95	2.50	4.5	6327	20.25	6347.25	79.670	4.324	.1081	.1025	.2801	.7557	1.999x10 <sup>3</sup>	1.683x10 <sup>3</sup>
11	13000	2.29	1.49	5.0	7030	25.00	7055.00	83.994	4.116	.06133	.0595	.1720	.8420	1.363x10 <sup>3</sup>	1.220x10 <sup>3</sup>
12	13500	2.73	9.03x10 <sup>-11</sup>	5.5	7733	30.25	7763.25	88.110	3.934	.03552	.0349	.1107	.8952	9.528x10 <sup>2</sup>	8.838x10 <sup>2</sup>
13	14000	3.16	5.84	6.0	8436	36.00	8472.00	92.044	3.775	.02205	.0218	.07516	.9276	6.889x10 <sup>2</sup>	6.533x10 <sup>2</sup>
14	14500	3.71	4.00	6.5	9139	42.25	9181.25	95.819	3.634	.01454	.0144	.05311	.9483	5.342x10 <sup>2</sup>	5.140x10 <sup>2</sup>
15	15000	4.68	2.58	7.0	9842	49.00	9891.00	99.453	3.507	.008502	.008502	.03857	.9621	4.237x10 <sup>2</sup>	4.067x10 <sup>2</sup>
16	16000	6.46	1.31	8.0	11248	64.00	11312	106.36	3.419	.005908	.005908	.02075	.9794	3.492x10 <sup>2</sup>	3.426x10 <sup>2</sup>
17	17000	8.50	7.98x10 <sup>-12</sup>	9.0	12654	81.00	12735	112.85	3.345	.004267	.004267	.01225	.9879	2.817x10 <sup>2</sup>	2.812x10 <sup>2</sup>
18	18000	1.20x10 <sup>5</sup>	4.90	10.0	14060	100.00	14160	119.00	3.280	.003167	.003167	.007338	.9927	2.440x10 <sup>2</sup>	2.425x10 <sup>2</sup>
19	19000	1.55	3.03	11.0	15466	121	15587	124.85	3.221	.002352	.002352	.004471	.9955	2.130x10 <sup>2</sup>	2.123x10 <sup>2</sup>
20	20000	2.51	1.50	12.0	16872	144	17016	130.45	3.166	.001767	.001767	.002774	.9972	1.871x10 <sup>2</sup>	1.866x10 <sup>2</sup>
21	22000	4.60	6.45x10 <sup>-13</sup>	14.0	19684	196	19880	141.00	3.114	.001352	.001352	.001922	.9988	1.652x10 <sup>2</sup>	1.648x10 <sup>2</sup>
22	24000	7.82	3.08	16.0	22496	256	22752	150.84	3.064	.001027	.001027	.001477	.9994	1.483x10 <sup>2</sup>	1.480x10 <sup>2</sup>
23	26000	8.40	1.86	18.0	25308	324	25632	160.10	3.019	.000782	.000782	.001122	.9997	1.352x10 <sup>2</sup>	1.349x10 <sup>2</sup>
24	28000	8.40	1.305	20.0	28120	400	28520	168.88	2.977	.000597	.000597	.000867	.9999	1.253x10 <sup>2</sup>	1.250x10 <sup>2</sup>
25	30000	8.40	1.195	22.0	30932	484	31416	177.25	2.937	.000462	.000462	.000672	.9999	1.173x10 <sup>2</sup>	1.170x10 <sup>2</sup>

Σ = 18,480° K

This calculation is similar to that of Tables 9 through 16 and is for the ray at the limb tangent to the boundary of the layer where maximum penetration occurs.

$R = 6.95 \times 10^{10}$  cm

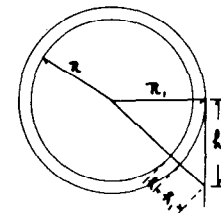
$R_1 = 7.03 \times 10^{10}$  cm

$h' = \sqrt{2R_1h_1 + h_1^2}$

where h = 8000 + h<sub>1</sub> kilometers

h = height above sun's limb

h<sub>1</sub> = height above R<sub>1</sub>



In the analysis of the observed eclipse curve, three temperature distribution curves were chosen to give an idea as to the effect of the different temperature distributions upon the resulting eclipse curves. The purpose here was to use a curve-fitting technique to establish the fact that only a sun with a bright limb could produce the variation observed during the eclipse. The temperature distribution curves chosen for trial are: a uniform distribution across the disc; a distribution similar to that of Figure 40; and a distribution half of which is due to a uniform center and the other half to a bright periphery. These distributions are shown in Figure 41. The distribution assumed for the corona is exponential and drops to a vanishingly small number at  $\rho = 1.16$ . It is only near totality that the distribution in the corona has a measurable effect on the shape of the eclipse curve. From these temperature distribution curves it was possible to calculate the resulting eclipse functions by using a numerical integration technique based upon previously reported values.<sup>58</sup>

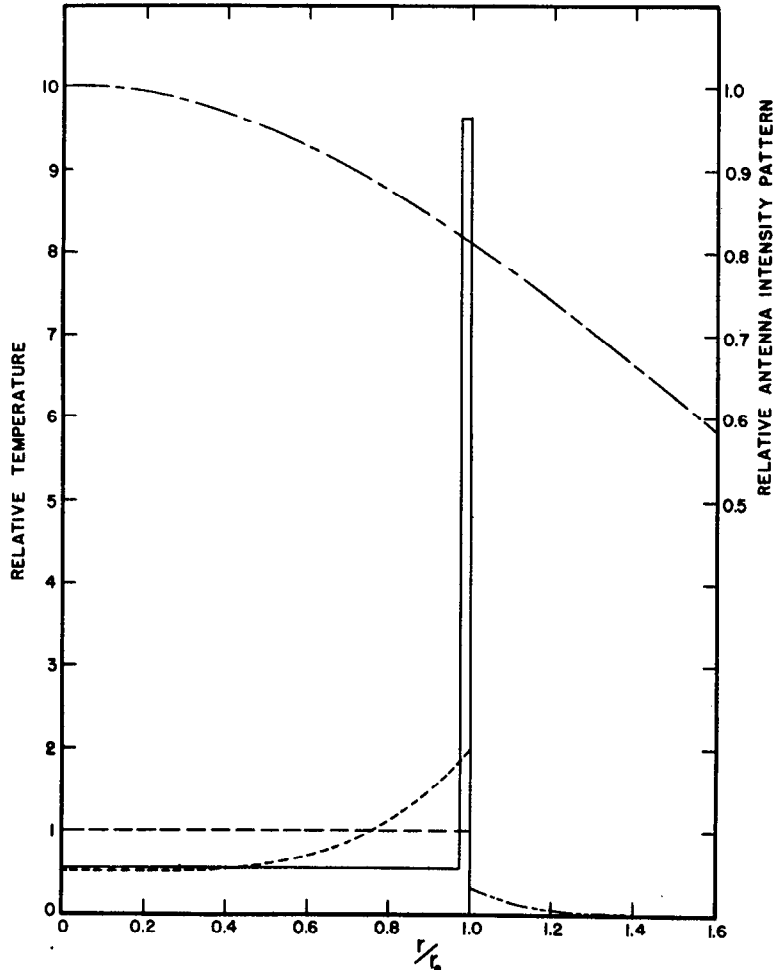


Figure 41 - Distributions used in computing the data for Figure 43

The reduction of the times of occultation of each independent sunspot was determined graphically by placing the center of a circular transparent template on the path of the moon's center across the solar disc as shown in Figure 36 in such a manner that the edge of the template just covered the sunspot in question. Then the distance between the center of the photograph of the sun and the center of the template was measured in units of the solar radius. The sunspot areas and magnetic fields for that day were obtained from other sources.<sup>59</sup> A curve showing the percentage of total sunspot area and square root of sunspot area times magnetic field of the spots uncovered as a function of the separation of the centers was drawn. This is shown in Figure 42. Combining the distribution

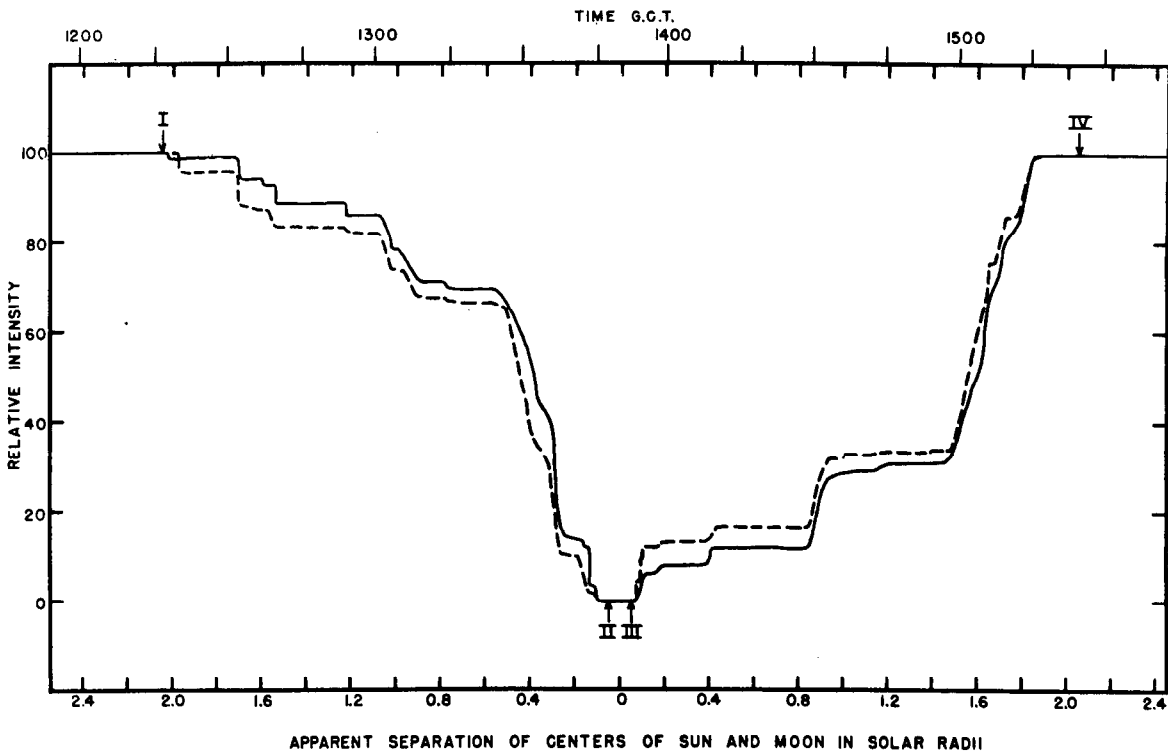
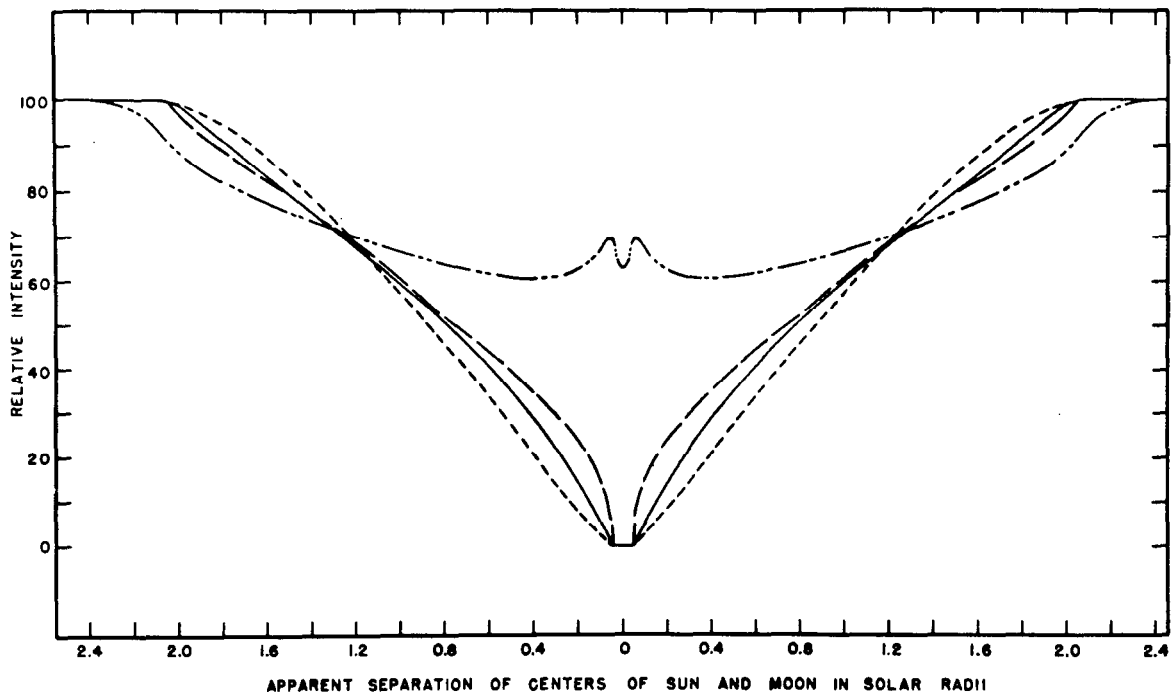


Figure 42 - Percentage of spots uncovered as a function of the apparent separation of the centers of the sun and the moon in units of solar radii

----- Area of spots      ——— Square root of area times the magnetic field

function, the sunspot function, and the corona function in different proportions, several eclipse curves were obtained which were combined into two sets. The first set emphasizes the effect of giving varying emphasis to the sunspot contribution. The second set assumes a constant sunspot contribution but illustrates the effect of different

temperature distributions. The contribution from the corona and the moon were assumed the same throughout, since these effects were determined by the residual radiation at totality. Comparing the curves where the various parameters are emphasized in Figures 43 and 44 with



*Figure 43 - Trial eclipse functions using the distributions of Figure 41 with no sunspot contribution*

----- uniform distribution      - - - - uniform plus narrow bright  
 ——— distribution of Figure 40      ring at limb  
 - · - · - corona and upper chromosphere alone

the observed data given in Figure 39 and plotted on Figure 44, it is seen from the shapes of the curves in Figure 43 that the distribution of Figure 40 yields the kind of eclipse curve necessary to fit the observed points. In Figure 44 varying emphasis on spot contribution is shown, and from this it is clear that the full line corresponding to a 30% spot contribution gives the best fit. The various contributions to the total emission now are: sunspot, 30%; quiet sun background, 67%; corona, 3%. It can be seen that although this does not constitute a precise determination of the true distributions, it does show, as anticipated from the theoretical work, that there is asymmetry in the eclipse curve due to enhanced radiation from sunspots, and it shows also that it is necessary to postulate limb brightening to fit the curve and that the definite but small amount of radiation from the corona may be associated with this limb brightening.

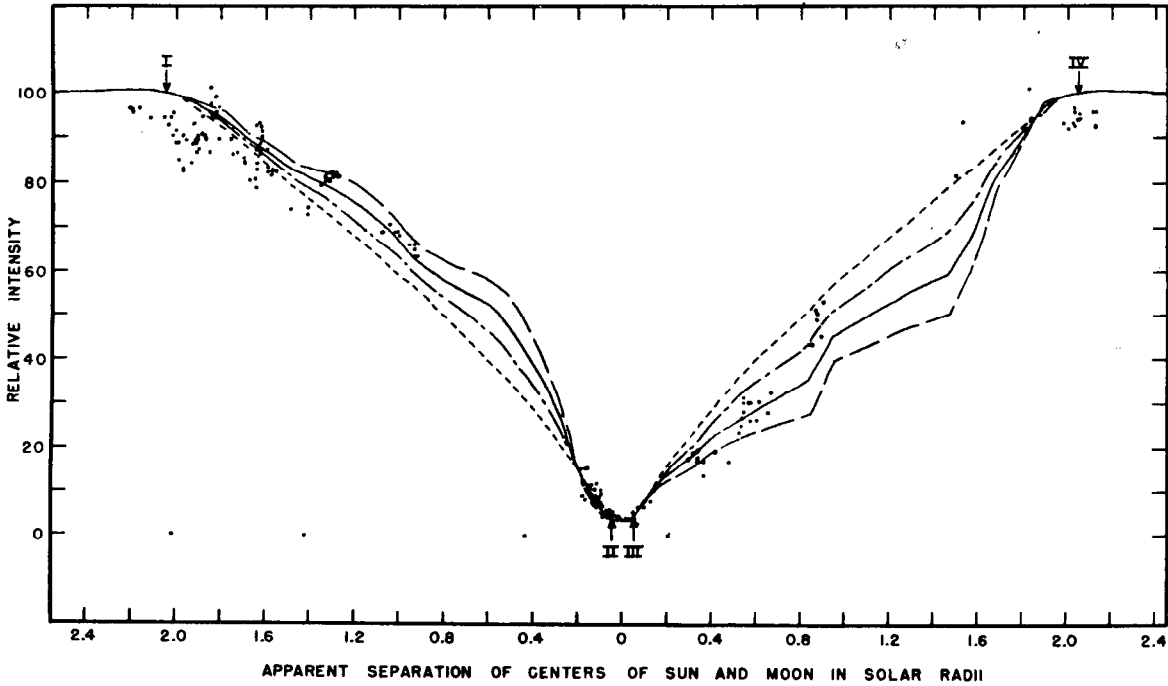


Figure 44 - Trial eclipse functions using the distribution of Figure 40

with : ..... no spots, ----- 20%, ——— 30% and  
 ——— 40% spot contribution.

The measurement of the residual radiation at the time of totality offers an excellent opportunity to evaluate the equivalent temperature and electron concentration in the chromosphere and corona, especially if the measurement is made on a few selected wavelengths. Data of this sort for several eclipses of different magnitude would yield valuable information, and it is important to bear this in mind and arrange if possible to conduct such experiments at future eclipses. While the analysis of the form of the eclipse curve does not lead to a precise determination of the temperatures and concentrations of the various layers of the atmosphere, it can, nevertheless, yield data which would serve to corroborate an analysis based upon data such as that presented in this report.

CONCLUSION

Penetration for Rays of Different Wavelengths

The rate of emission of radio-frequency radiation from the sun has been shown to be dependent entirely upon the physical conditions in

the atmosphere of the sun. The effective depth of penetration for various wavelengths is shown in Figure 45. It is seen from the figure that very much shorter wavelengths must be used in order to apply this method to the really deep layers of the atmosphere. If this is done then the disturbing effects of the increased concentration of the elements, other than hydrogen, must be taken into consideration. The data used to obtain Figure 45 are taken from Tables 10 to 17, where the equivalent temperature at the several wavelengths is computed on the basis of the assumed temperatures and electron distributions. The depth of penetration is determined by the electron densities and temperature, and in general the penetration is less for

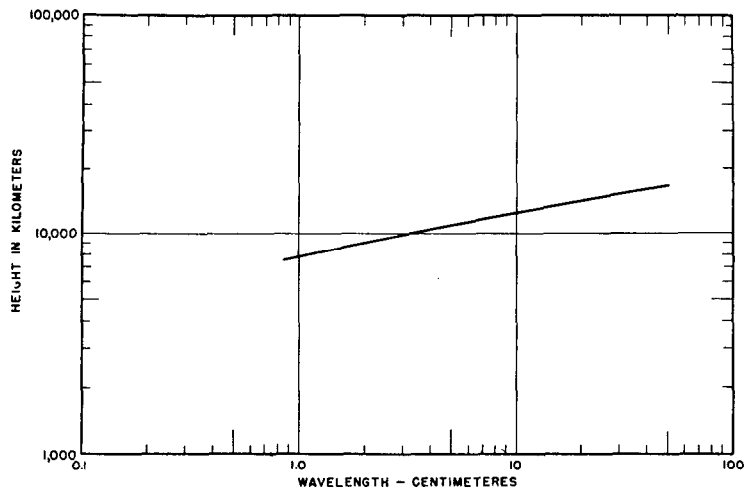


Figure 45 - The effective depth of penetration for radiation in the wavelength range 8 millimeters to 50 centimeters

a ray entering at the limb than for the central ray. The data shown in Figure 45 are computed for the central ray. The calculations of the opacity of the sun's atmosphere in this report are based upon electron densities obtained by two quite different means for the corona and for the chromosphere. Those for the corona are based upon the intensity of scattered light; whereas those for the chromosphere are based upon the relative intensity of spectral lines. Both sets of data arise from the analysis of eclipse observations. An inspection of Figure 18, where the electron density is plotted as a function of the height above the photosphere, reveals that there is a marked discontinuity at the junction of these two sets of data. Whether this discontinuity exists in fact is a fit subject for further investigation. The adoption of this density distribution of electrons necessitates the choice of a peculiar temperature distribution in the chromosphere in order to reconcile the observed temperature of the sun with the assumed conditions in the chromosphere.

The results of the present work reveal that there is sensibly no limb brightening at 8.5 millimeters and that the equivalent temperature of the sun at this wavelength is  $6740^{\circ}$  Kelvin. As was shown earlier, the temperature distribution in the sun's atmosphere that is consistent with the observed data is one in which the temperature remains close to the photospheric temperature out to about 8,000 or 10,000 kilometers and then rises abruptly and rapidly to the elevated temperature of the corona at about 25,000 kilometers. With the temperature indicated as nearly uniform over a large part of the chromosphere it is implied that turbulent conditions prevail and that the situation there is very similar to that in our own atmosphere, where the lower strata are maintained at a reasonably uniform temperature because there are extensive mass motions of gas.

### Use of Results for Determining Conditions in the Sun's Atmosphere

With the exception of the eclipse data at 3.14 centimeters, the only radio data which gives detailed information on the temperature distribution for the sun is the work reported here. In order to obtain a more complete solution to the problem of the distribution of electrons through the sun's atmosphere and the equivalent temperature through the atmosphere, it will be necessary to take data over a wide range of wavelengths with high resolution. The curve showing that temperature distribution in the corona and chromosphere which best fits the present observational data is drawn in curve B in Figure 23. It seems more probable that the actual temperature distribution in the chromosphere might be more closely represented by the dotted curve since no sharp discontinuity is postulated at the limb or at the top of the chromosphere. This seems reasonable since there exists no sharp discontinuity in any of the other factors. A definitive answer to the question of the temperature distribution in the sun's atmosphere can be obtained by repeating the work done at 8.5 millimeters at two or three longer wavelengths such as 3, 10, and 50 centimeters. This will be possible only with large antennas. A consideration of Figure 1 shows that, at a wavelength of 3 centimeters, the fifty-foot reflector will provide a beamwidth of about 0.15 degrees and about 0.45 degrees at 10 centimeters. It will thus be possible to measure the central temperature independent of limb brightening at 3 centimeters but not at 10 centimeters. The 3-centimeter measurement will serve to determine the slope of the temperature curve in the chromosphere. To obtain data relevant to a height as low as 4000 kilometers would require the use of a wavelength of 1 millimeter. This may be technically feasible soon, but even then absorption in the earth's atmosphere will be extremely troublesome. It is known from theoretical considerations that in this region there are many closely spaced atmospheric absorption lines

caused principally by water vapor and oxygen. There are no laboratory measurements to ascertain the frequencies of the lines nor the magnitude of the attenuation to be expected. It is possible that measurements at 2.5 millimeters will soon be made. At this wavelength the crowding of the absorption lines is not so severe, but again the attenuation to be expected is known only theoretically. With this comment on limitations it is recommended that a study be made.

It is entirely possible that out of this entire investigation a further benefit may be derived. Not only will there be a measure of equivalent temperature across the disc through the taking of radio data, but computations can be made on effective depth of penetration and equivalent temperature across the disc based on the assumed distribution of temperature and electron density. In order to make the observed equivalent temperature and its distribution across the disc agree with the calculated values for several wavelengths, it will be necessary to adjust both the temperature and the electron density distribution for the best fit. This procedure will then lead to a distribution in electron density and temperature which is compatible with the radio measurements. Since for the shorter wavelengths the absorption is negligible in the outer atmosphere of the sun and rises very abruptly in the region where the optical depth approaches unity, the atmosphere can be probed with fair accuracy—perhaps as close as one kilometer. The exact location of this atmosphere with respect to the visual surface of the sun will still depend on the correlation of the radio work with visual eclipse data and with further radio data taken at future solar eclipses.

The presence of the large concentration of neutral hydrogen in the lower chromosphere has been neglected here since the collision cross section of the neutral atom is very much less than that of the proton, and even though neutral hydrogen exists in an abundance of say 400 to 1, its effect on  $V$  and  $K$  would be negligible. The question of the negative hydrogen ion is different. Here we are dealing with the collision of two charged particles,  $e^-$  and  $H^-$ , and so the collision cross section will be large. Where  $H^-$  is abundant, then its presence will be felt.

The importance of the eclipse data in determining the electron density and temperature of the corona was pointed out. Observations of the intensity of the radio signal received at totality for total eclipses of various magnitudes would help to determine the physical

conditions of the corona. This is perhaps the only method which will be feasible for exploring in detail the sun's atmosphere at wavelengths above 10 centimeters, since the size of antenna required to provide a beamwidth less than  $0.2^\circ$  at these wavelengths is prohibitive.

The effect of the general magnetic field of the sun has been omitted here, since the magnitude of the field is so low that it would have negligible effect on the refractive index and the absorption in the sun's atmosphere at a wavelength of 8.5 millimeters. For very much longer wavelengths, though, the effect of the general magnetic field could become appreciable, and if the disturbing effects of the fields due to sunspots could be eliminated, then the magnitude of the general magnetic field might well be determined by radio means. To do so, however, would be a very difficult experimental problem inasmuch as the indicated wavelength is quite long, and therefore the antenna size required to obtain the necessary resolution would be quite large. An interferometer-type technique similar to those proposed earlier could be used, but this provides resolution in only one plane and, in addition, makes absolute calibration difficult.

Earlier some of the effects of the disturbed sun were pointed out. At radio wavelengths the sun is a variable star, the variability increasing markedly with wavelength, with the possible exception of the disturbance due to flares. At 8.5 millimeters the intensity of the sun varies by only a few percent; whereas at a wavelength of 5 meters the variation in intensity can be a hundred or a thousand fold. This indicates that to study the nature of the sun as a variable star one should use as long a wavelength as is compatible with good resolution. The present indication is that with the fifty-foot diameter antenna an investigation at a wavelength of 3 or perhaps 10 centimeters should lead to interesting information concerning the variability of the emission of the sun. At a wavelength of 8.5 millimeters the equivalent temperature of a disturbed area, when the area of the disturbance is taken to be commensurate with the area of the associate spot, is found to be about  $100,000^\circ$  Kelvin. This is a value that is not difficult to explain away if one postulates that during times of solar activity large clouds of electrons rise from the lower chromosphere or photosphere to heights of at least 20,000 or 30,000 km. Then the region will have a prevailing condition in which the opacity increases to the point where the optical depth becomes unity in the presence of a temperature which is in the hundreds of thousands. This may well be the explanation of the increase in the equivalent temperature of the sun at the shorter

wavelengths. On the other hand, when the longer wavelengths are considered, the equivalent temperature of the sun at times of great activity rises to millions of degrees and the temperature of selected regions rises to billions of degrees. These effects are decidedly not thermal in origin, and some different mechanism must be found for their explanation.

### Suggested Study of the Disturbed Sun

When the distribution of radiation across the surface of the sun can be determined for the longer wavelengths as it has been for the 8.5 millimeters, a much better understanding of the emission from the disturbed sun will be had, for then it will be possible to correlate directly the enhanced emission with the characteristics of the responsible individual spot or spot group. There are two approaches to the analysis of the effect of the spot on the radio emission. Firstly suppose that in the region of an active spot, the electron concentration is markedly increased. If this occurs then the opacity is increased and the depth of penetration will be decreased. Referring to the temperature curve it is seen that for the shorter wavelengths the increase in height of emission will increase the temperature only slightly unless the increase is greater than several thousand kilometers, which could correspond to a change in electron concentration of about a factor of 10. Since in the case cited earlier the equivalent temperature near the spot was approximately  $100,000^{\circ}$  Kelvin at 8.5 millimeters, then the electron density would have to increase almost a hundred fold. The second approach is to consider the effect of the magnetic field associated with a spot on an electron moving with the thermal velocity corresponding to its position in the atmosphere. The wavelength of oscillation is a well known function of the magnetic field and is  $\lambda = 10,600/H$ . Thus for 8.5 millimeters a field of greater than 11,000 gauss is required. If a field of this magnitude exists it is deep in the sun, and a glance at Table 10 will show that any 8.5 millimeter radiation generated there cannot escape. As the wavelength becomes longer the required field falls until, for example, at 10 centimeters a 1000 gauss field is required. Such a field might well exist near the top of the chromosphere, where the radiation will escape. Denisse has made an analysis of this effect, but results have not as yet been published.

Another possibility that suggests itself is that highly radioactive clouds may be ejected from the sun's interior. The effect of

such a cloud would be to exchange energy with the ambient electrons and thereby enhance their emission.

Observations of the active sun with very high resolution will serve to locate these effects and help to assign quantitative values to the specific intensity of the enhanced radiation. A correlation with the known circumstances, such as the parameters of the spot, will help to describe the conditions under which this enhanced radiation occurs, and then speculation will be more fitting.

The observations on galactic noise have all been made at long wavelengths where the resolution of the antenna is poor but where the intensity of the signal is high due to the nature of galactic noise and the characteristics of receivers. With the advent of larger antennas, it should be possible to extend toward shorter wavelength the range over which the measurements of galactic noise have been made, and if this is done, then the consequent higher resolution will tell much about the structure of the source of the radiation. A further point of interest is that a careful measurement of the variation in the intensity of the noise with wavelength combined with information on the spatial distribution of noise would reveal the mechanism with which the noise is generated.

The solution to the problem of the disturbed sun will have a greater bearing upon the relation between solar activity and variations in the earth's upper atmosphere and magnetic field. Since this is one of the important reasons for continuing work on the radio emission of the sun, it is important to attempt to gain a better understanding of the effect. It has been shown that the radiation from the quiet sun is thermal in origin and may be explained by assigning proper electron and temperature distributions in the sun's atmosphere. On the other hand the radiation from the disturbed sun does not appear to be thermal in origin since the energy involved is too high for any reasonable assumed temperature. An explanation for these strong emissions must arise in some mechanism which depends not on the completely disordered thermal motion of particles but on an ordered movement of ions caused by large gradients of density, temperature, or electric field in the vicinity of a disturbed region. Plasma oscillations of this sort were suggested by Schkloosky<sup>27</sup> as the source of enhanced radio emission and have recently been discussed by Bailey,<sup>60</sup> Pierce,<sup>61</sup> Bohm and Gross,<sup>62</sup> Nergaard<sup>63</sup> and Haeff.<sup>64,65</sup> The latter papers discuss the amplification of radio signals along beams of electrons and show that the magnitude of this effect is such that it must be considered in the analysis of the disturbed sun.

UNCLASSIFIED

Today most of the information about the disturbed sun is obtained by means of radio receivers having beamwidths larger than the sun's diameter so that it is impossible directly to associate variations in the radio signal with specific activities on the surface of the sun. The use of higher resolving power, especially at 3 and 10 centimeters, will materially aid in analyzing this problem for then variations in the sun's emission will be correlated directly with specific areas on the sun where information on solar conditions derived from visual observation will be available.

#### ACKNOWLEDGMENTS

Appreciation is expressed for the guidance and encouragement of Dr. John M. Miller and Dr. E. O. Hulburt of the Naval Research Laboratory and Francis J. Heyden, S.J., of the Georgetown University Observatory. Also there was assistance from many of the members of the R. F. Research Branch of the Naval Research Laboratory in constructing and mounting the equipment. In gathering data on the eclipse, contributory work was done by Messrs. R. J. McEwan, T. B. Jackson, and C. B. Strang, while F. T. Haddock helped in analyzing the results.

\* \* \*

UNCLASSIFIED

REFERENCES

1. Jansky, K. G., "Directional Studies of Atmospherics at High Frequencies," Proc. I.R.E., 20:1920-1932 (1932)
2. Jansky, K. G., "Electrical Disturbances Apparently of Extra-Terrestrial Origin," Proc. I.R.E., 21:1387-1398 (1933)
3. Jansky, K. G., "A Note on the Source of Interstellar Interference," Proc. I.R.E., 23:1158-1163 (1935)
4. Southworth, G. C., "Microwave Radiation from the Sun," Journal of the Franklin Institute, 239:285-297 (1945), and Erratum issued with 241: No. 3 (1946)
5. Reber, Grote, and Greenstein, Jesse L., "Radio-Frequency Investigations of Astronomical Interest," Observatory, 67:15-26 (1947)
6. Williamson, R. E., "The Present Status of Microwave Astronomy," Journal of the Royal Astronomical Society of Canada, 42:9-32 (1948)
7. Burgess, R. E., "Noise in Receiving Aerial Systems," Proceedings of the Physical Society of London, 53:293-304 (1941)
8. Reber, G., "Cosmic Static," Ap. J., 91:621-624 (1940)
9. Reber, G., "Cosmic Static," Ap. J., 100:279-287 (1944)
10. Northcott, R. J. and Williamson, R. E., "Galactic Noise and the Plane of the Galaxy." J.R.A.S. Can. 42:269-279 (1948)
11. Johnson, J. B., "Thermal Agitation of Electricity in Conductors," Phys. Rev. 32:97-109 (1928)
12. Nyquist, H., "Thermal Agitation of Electric Charge in Conductors," Phys. Rev. 32:110-113 (1928)
13. Appleton, E. V. and Hey, J. S., "Circular Polarization of Solar Radio Noise," Nature, 158:339 (1946)
14. Covington, A. E., "Circularly Polarized Solar Radiation on 10.7 Centimeters," Proc. I.R.E., 37:407 (1949)
15. Mayer, C. H., Unpublished Naval Research Laboratory report
16. Schulkin, M., Haddock, F. T., Decker, K. M., Mayer, C. H., and Hagen, J. P., "Observation of a Solar Noise Burst at 9500 Mc/s and a Coincident Solar Flare," Phys. Rev. Series II, 74:840 (1948)

## REFERENCES (Cont.)

17. Ryle, M. and Vonberg, D. D., "An Investigation of Radio Frequency Radiation from the Sun," Proc. Roy. Soc. 193; Series A:98-120 (1948)
18. McCready, L. L., Pawsey, J. L., and Payne-Scott, Ruby., "Solar Radiation at Radio Frequencies and Its Relation to Sunspots," Proc. Roy. Soc. A, 190:357-375 (1947)
19. Hagen, J. P., Jackson, T. B., McEwan, R. J., and Strang, C. B., "Observations on the May 20, 1947 Total Eclipse of the Sun," Naval Research Laboratory Reprint, March 1948
20. Haikin, S.E. and Chikhachev, B. M., "Investigation of Radio Emission from the Sun During the Solar Eclipse of May 20, 1947," Bulletin (Izvestiya) of the Academy of Science, Phys. Ser. XII, No. 1, 38-43 (1948). Available in English as Nav. Res. Lab. Trans. 183
21. Martyn, D. F., "Solar Radiation in the Radio Spectrum. I. Radiation from the Quiet Sun," Proc. Roy. Soc. A, 193:44-59 (1948)
22. Kiepenheuer, K. O., "Origin of Solar Radiation in the 1-6 Metre Radio Wave-Length Band," Nature, 158:340 (1946)
23. Ginsburg, V. L., "On Solar Radiation in the Radio-Spectrum," Comptes rendus (Doklady) de l'Académie des Sciences de l'URSS, 52:487-490 (1946)
24. Denisse, Jean., "Études des Conditions d'Émission par l'Atmosphère Solaire d'Ondes Radioélectriques Métriques," Revue Scientifique No. 84:259-262 (1946)
25. Waldmeier, M., "Radiofrequente Strahlung und Elektronentemperatur der Sonnenkorona," Zurich Publication No. 154 (1948)
26. Waldmeier, M., Müller, H., "Spektrale Energieverteilung und Mittele-Rand-Variation der radiofrequenten Koronastrahlung," Zurich Publication No. 155 (1948)
27. Schklovsky, I. S., "Emission of Radio-Waves by the Galaxy and the Sun. (In Russian), Astronomical Journal of the Soviet Union, 23:333-347 (1946). Available in English as Nav. Res. Lab. Trans. 181
28. Kramers, H. A., "On the Theory of X-Ray Absorption and of the Continuous X-Ray Spectrum," Phil Mag. 46:836-871 (1923)
29. Gaunt, J. A., "Continuous Absorption," Phil. Trans. (A) 229:163-204 (1930)

## REFERENCES (Cont.)

30. Menzel, D. H. and Pekeris, C. L., "Absorption Coefficients and Hydrogen Line Intensities," M. N. Roy. Astro. Soc. 96:77-111 (1935)
31. Hey, J. S., Phillips, J. W., and Parsons, S. J., "Cosmic Radiations at 5 Metres Wave-Length," Nature, 157:296-297 (1946)
32. Hey, J. S., Parsons, S. J., and Phillips, J. W., "An Investigation of Galactic Radiation in the Radio Spectrum," Proc. Roy. Soc. A, 192:425-445 (1948)
33. Reber, G., "Cosmic Static," Proc. I.R.E., 36:1215-1218 (1948)
34. Henyey, L. G., and Keenan, Phillip C., "Interstellar Radiation from Free Electrons and Hydrogen Atoms," Ap. J., 91:625-630 (1940)
35. Greenstein, J. L., Henyey, L. G., and Keenan, P. C., "Interstellar Origin of Cosmic Radiation at Radio-Frequencies," Nature, 157: 805-806 (1946)
36. Townes, Charles H., "Interpretation of Radio Radiation from the Milky Way," Ap. J., 105:235-240 (1947)
37. Preston, T., "The Theory of Heat," Fourth Edition, McMillan Co. (1929)
38. Richtmyer, F.K. and Kennard, E. H., "Introduction to Modern Physics," Third Edition, McGraw-Hill Book Co. (1942)
39. Slater, J. C., "Microwave Transmission," McGraw-Hill Book Co. (1942)
40. Friis, H. T., "Noise Figures of Radio Receivers," Proc. I.R.E., 32:419-422 (July 1944)
41. Dicke, R. H., "The Measurement of Thermal Radiation at Microwave Frequencies," Review of Scientific Instruments, 17:268-275 (1946)
42. "The Observatory," 68:486 (October, 1948). See pages 164-5.
43. Babcock, H. D., "A Study of the Sun's General Magnetic Field," Pub. Ast. Soc. Pac. 60: No. 355, 244 (1948)
44. Wildt, K., "An Interpretation of the Heights of Lines in the Solar Chromosphere," Ap. J., 105:36-84 (1947)
45. Milne, E. A., "Handbuch der Astrophysik," Vol. 1, Part 3, Julius Springer (1930)

## REFERENCES (Cont.)

46. Baumbach, S., "Strahlung, Ergiebigkeit und Elektronendichte der Sonnenkorona," *Astron. Nachr.*, 263, 121 (1937)
47. Allen, C. W., "Interpretation of Electron Densities from Corona Brightness," *M.N.R.A.S.*, 107:426-432 (1947)
48. van de Hulst, H. C., "Zodiacal Light in the Solar Corona," *Ap. J.*, 105:471-488 (1947)
49. Alfven, H., "On the Solar Corona," *Arkiv for Matematik, Astronomi Och Fysik, Band 27A*, 25, 1-23 (1941)
50. Mimno, H. R., "The Physics of the Ionosphere," *Rev. Mod. Phys.*, 9:1-43 (1937)
51. Cowling, T. G., "The Electrical Conductivity of an Ionized Gas in a Magnetic Field with Applications to the Solar Atmosphere and the Ionosphere," *Proc. Roy. Soc. Lond.*, 183A:453-479 (1945)
52. Chapman, S. and Cowling, T. G., *The Mathematic Theory of Non-Uniform Gases*, Cambridge Univ. Press (1939)
53. Van Vleck, J. H., "Absorption of Microwaves by Oxygen," *Phys. Rev.*, 71:413-424 (1947)
54. Van Vleck, J. H. "The Absorption of Microwaves by Uncondensed Water Vapor," *Phys. Rev.* 71:424-433 (1947)
55. Sander, K. F., "Radio Noise from the Sun at 3.2 cm.," *Nature*, 159: 506-507 (1947)
56. Dicke, R. H. and Beringer, R., "Microwave Radiation from the Sun and Moon," *Ap. J.*, 103:375-376 (1946)
57. Covington, A. E., "Micro-Wave Solar Noise Observations During the Partial Eclipse of November 23, 1946," *Nature*, 159:405-406 (1947)
58. Beard, D. B., "Eclipse Area and Eclipse Function Calculation," *Naval Research Laboratory Report N-3212* (1948)
59. Letter from McMath-Hulburt Observatory enclosing a photograph of the sun in calcium light.  
Letter from L. d'Azambuja enclosing a spectroheliograph of the sun.  
Letter from the Naval Observatory enclosing a photograph of the sun.

## REFERENCES (Cont.)

60. Bailey, V. A., "Spontaneous Waves in Discharge Tubes and in the Solar Atmosphere," *Nature* 161, 599, 1948
61. Pierce, J. R., "Possible Fluctuations in Electron Streams due to Ions," *Jour. App. Phys.* 19 231, 1948
62. Bohn, D. and Gross, E. P., "Theory of Plasma Oscillation. A and B," *Phys. Rev.* 75, 1851, 1949
63. Nergaard, L. S., "Analysis of a Simple Model of a Two-Beam Growing Wave Tube," *RCA Review* 9, No. 4, 585, 1948
64. Haeff, A. V., "The Electron Wave Tube - A Novel Method of Generation and Amplification of Microwave Energy," *Proc. IRE.* 37, 4, 1949
65. Haeff, A. V., "Space Charge Wave Amplification Effects," *Phys. Rev.* 74, 1532, 1948